REAL−TIME MEASUREMENT OF THE WATER−INSOLUBLE AEROSOL SIZE DISTRIBUTION: INSTRUMENT DEVELOPMENT AND IMPLEMENTATION

A Thesis

Presented to

The Academic Faculty

By

Roby Greenwald

In Partial Fulfillment

Of the Requirements of the Degree

Doctor of Philosophy in Environmental Engineering

Georgia Institute of Technology

August 2005

REAL−TIME MEASUREMENT OF THE WATER−INSOLUBLE AEROSOL SIZE DISTRIBUTION: INSTRUMENT DEVELOPMENT AND IMPLEMENTATION

Approved by:

Dr. Michael H. Bergin, advisor
School of Civil and Environmental Engineering
Georgia Institute of Technology

Dr. James A. Mulholland
School of Civil and Environmental Engineering
Georgia Institute of Technology

Dr. Rodney J. Weber
School of Earth and Atmospheric Sciences
Georgia Institute of Technology

Dr. Jean-Luc Jaffrezo
Laboratoire de Glaciologie et Géophysique de l'Environnement
Université de Joseph Fourier

Dr. Armistead G. Russell
School of Civil and Environmental Engineering
Georgia Institute of Technology

Date Approved:

July 7, 2005

ACKNOWLEDGEMENT

Acknowledgement is given to the National Science Foundation Atmospheric Chemistry Program for their financial support of this work.

I would also like to acknowledge the following individuals for their collaborative assistance:

Dr. Gerrit Hoogenboom

Dr. William L. Chameides

Dr. Jin Xu

Dr. Daniel Cohan

Dr. Gilles Aymoz

Finally, I would like to express my appreciation to the thesis committee members for their participation in the preparation of this work:

Dr. Michael H.Bergin

Dr. Rodney J. Weber

Dr. Jean-Luc Jaffrezo

Dr. Armistead G. Russell

Dr. James A. Mulholland

TABLE OF CONTENTS

LIST OF TABLES

LIST OF FIGURES

LIST OF SYMBOLS AND ABBREVIATIONS

AOD or τ ..... aerosol optical depth

APS ..... aerodynamic particle sizer

BC ..... black carbon

CCN ..... cloud condensation nuclei

COD ..... cloud optical depth

CPC ..... condensation particle counter

DMA ..... differential mobility analyzer

EC ..... elemental carbon

Γ ..... adiabatic lapse rate

IN ..... ice nuclei

k ..... imaginary part of the refractive index

Λ ..... actual lapse rate

LAI ..... leaf area index

$m = n + k \cdot i$ ..... complex refractive index

n ..... real part of the refractive index

NPP ..... net primary production

OC ..... organic carbon

OPC ..... optical particle counter

PAR ..... photosynthetically active radiation

PSL ..... polystyrene latex

Q_{abs} ..... aerosol absorption efficiency

Q_{ext} ..... aerosol extinction efficiency

Q_{sca} ..... aerosol scattering efficiency

RUE ..... radiation use efficiency

σ_{ap} ..... aerosol absorption coefficient

σ_{ep} ..... aerosol extinction coefficient

σ_{sp} ..... aerosol scattering coefficient

SOA ..... secondary organic aerosol

TOT ..... thermal optical transmittance

VOC ..... volatile organic compound

ω ..... single scattering albedo

WIA ..... water-insoluble aerosol

SUMMARY

This thesis addresses various aspects of the influence of atmospheric particulate matter on the terrestrial system. In Part I, the radiative influence of particulate matter on the production of crops is explored using the CERES crop model. It is known that the presence of aerosols in the atmosphere simultaneously reduces the amount of sunlight reaching the surface and increases the fraction of that light which is diffuse. Reduction of the total amount of sunlight tends to slow the rate of photosynthesis occurring in plants while increasing the fraction which is diffuse tends to increase the net rate of photosynthesis by more evenly distributing sunlight throughout all layers of a plant canopy. Thus the radiative influence of aerosols on photosynthesis may theoretically be either positive or negative. The CERES crop model was modified to estimate the influence of both a reduction in total sunlight and an increase in the diffuse fraction. Model simulations were performed for rice, maize and wheat at a variety of locations and found the likely influence of aerosols on crop production to be a 0-10% reduction in yield compared to the base case of crops grown under a clean atmosphere. The magnitude of the aerosol influence depended on such factors as the prevalence of clouds during the growing season and specific properties of the crops such as the radiation use efficiency (RUE).

In Part II, the concentration and size distribution of water-insoluble aerosols (WIA) is explored. It has been well-established that atmospheric particulate matter influences the planetary radiation budget by scattering and absorbing solar radiation and by modifying the albedo and lifetime of clouds. The magnitude of these influences is related to particle

solubility; however, very few measurements of the concentration of WIA have been to date, and even fewer have been size-resolved. To address this concern, a new technique was developed to provide these measurements in real-time. This instrumentation was evaluated in a laboratory setting and implemented into several field studies. Results from these sampling campaigns indicate that 5-10% (by number) of ambient aerosols between 0.25-2.0 μm are water-insoluble, though this value may vary drastically on time scales as brief as a few minutes and has been observed to be as high as 40% for hours at a time. In areas heavily influenced by motor vehicle traffic, the WIA concentration was highly correlated with both the elemental carbon mass concentration and the absorption coefficient at 530 nm. This implies that WIA is dominated by particulate soot. Many episodes of high levels of crustal dust were also observed. At these times, the WIA size distribution shifted toward larger sizes in a characteristic manner. This suggests that this method is useful for detecting insoluble mineral aerosols as well as particulate soot and that examination of the WIA size-distribution may provide a basis to distinguish between the two.

Publications resulting from this thesis:

Greenwald, R., M.H. Bergin, J. Xu, D. Cohan, G. Hoogenboom and W.L. Chameides, 2005. The influence of aerosols on crop production: a study using the CERES crop model. *Agriculture Systems*, in press.

Greenwald, R., M. H. Bergin, C. M. Carrico and D. Grant, 2005. A new real-time technique to measure the size-distribution of water-insoluble aerosols. *Environmental Science & Technology,* in press.

Greenwald, R., M. H. Bergin, J.-L. Jaffrezo, J.-L. Besombes and G. Aymoz, 2005. Size-resolved, real-time measurement of water-insoluble aerosols in the Chamonix and Maurienne Valleys of alpine France. *Journal of Geophysical Research,* in review.

Greenwald, Roby, M.H. Bergin, R. Weber, and A. Sullivan, 2005. Real-time measurement of water-insoluble aerosol in urban Atlanta. *Atmospheric Environment*, in review.

INTRODUCTION

1.1 Importance of examining atmospheric aerosols

The presence of particulate matter in the atmosphere influences the global climate both directly and indirectly [*Charlson et al.*, 1992]. The direct influence of aerosols results from their perturbation of the planetary radiation balance by scattering [*Ångström*, 1929] and absorbing [*Lindberg*, 1975] incoming solar radiation. The magnitude of this radiative forcing is critically dependent on aerosol size. Particle diameter is itself a function of the amount of hygroscopic growth an aerosol undergoes in the presence of water vapor [*Hobbs et al*., 1974] which is in turn influenced by particle solubility [*Saxena et al*., 1995]. The indirect influence of aerosols on climate arises from the effect particles exert upon the albedo [*Twomey*, 1974] and lifetime [*Albrecht*, 1989] of clouds. Aerosols influence these cloud properties through their role as cloud condensation nuclei (CCN). The effectiveness with which a particle may serve as a CCN is dependent upon its affinity for water [*Saxena et al*., 1995] and is therefore related to particle solubility.

An additional indirect climatic effect of aerosols is via their influence on global biogeochemical cycles. The attenuation of light by aerosols alters the amount and nature of the radiation available for photosynthetic organisms. As incoming sunlight passes through the atmosphere and is scattered and absorbed by aerosols, the total amount of radiation reaching the surface is decreased while the fraction of light which is diffuse is simultaneously increased. A reduction in total radiation tends to slow the rate of plant photosynthesis while an increase in the diffuse fraction can have a net positive effect on photosynthesis by more efficiently distributing radiation through a plant canopy [*Sinclair*

et al., 1992]. The deposition of aerosols to leaf surfaces may also influence the photosynthetic rate [*Bergin et al.* 2001], although this effect can only be negative since there is no increase in the distribution of diffuse radiation through the canopy. The deposition of iron-rich mineral aerosols into nutrient-poor regions of the oceans may enhance the productivity of phytoplankton and provide a net removal of CO_2 from the atmosphere [*Martin*, 1990]. These influences of aerosols on photosynthesis have an indirect effect on climate by altering the global carbon and hydrological cycles. In addition, in the case of agricultural plant species, the photosynthetic influence of aerosols may affect the amount of food available for human consumption [*Chameides et al.,* 1999].

In addition to the climatic effects described above, aerosols have also been observed to influence the health of air-breathing organisms. The inhalation of particles with diameters less than 2.5 μm has been repeatedly documented as having a deleterious effect on human health [*Peel et al*., 2005; *Metzger et al*., 2004; *Brook et al*., 2002; *Peters et al*., 2001]. Aerosols may influence both the respiratory and the cardiovascular systems in humans. Determination of the specific mechanisms by which particles influence the body is the subject of intense study within the medical community. Although precise mechanisms or the specific aerosol species responsible for triggering health responses are generally not known at this time, many epidemiological studies have observed correlations between the concentration of certain types of aerosols and emergency department visits [*Peel et al*., 2005; *Metzger et al*., 2004; *Le Tertre et al*., 2002]. Specifically, elemental carbon in the form of soot has been observed to be correlated with cardiovascular emergency department visits [*Metzger et al*., 2004; *Le Tertre et al*., 2002]. Elemental carbon has also been observed to have specific properties harmful to lung tissue [*Sosnowski et al*., 2000].

1.2 Types of aerosols

Aerosols may be broadly classified based on their constituent components. However, it is possible and in fact quite common for an individual particle to be composed of more than one of these categories. In addition, any particle may contain water condensed from atmospheric water vapor, although the amount of condensed water present is a function of a particle's affinity for water which in turn depends on its composition.

1.2.1 Carbonaceous aerosols

Carbonaceous aerosols may be composed of organic carbon (OC) or elemental carbon (EC). Although OC particles do not necessarily contain EC, most EC particles contain some amount of OC. OC may either be primary or secondary (primary aerosols are emitted as particles at their source whereas secondary aerosols are emitted in the gas-phase). An example of a primary OC particle would be pollen released by plants or cellular detritus entrained by the wind. This latter type of primary OC can contribute substantially to the total aerosol loading [*Jaenicke*, 2005]. Much OC though is secondary in nature and is frequently referred to as secondary organic aerosol or SOA. Biogenic OC sources include such compounds as isoprenes and terpenes emitted by trees, and anthropogenic sources include volatile organic compounds (VOCs) from fuels or industrial emissions. Although the amount of OC present in the atmosphere varies widely by region, time of year, and other environmental conditions, it has been estimated that on average, OC comprises 20-50% of fine particulate mass at mid-latitudes [*Saxena and Hildemann,* 1996]. Size-resolved measurements of OC using cascade impactors have found the peak in OC mass concentration at particle sizes less than 1.0 μm [*Jaffrezo et al.*, 2005c; *Turpin et al.,* 2000; *Chen et al.*, 1997].

Although elemental carbon may appear in a wide variety of forms (graphite, diamond, fullerene), by far the most abundant type found in the atmosphere is combustion derived soot. Soot particles are formed in high temperatures from incompletely combusted organic compounds and radicals and are organized into spherules 20-60 nm in diameter [*Medalia and Rivin*, 1982]. The spherules themselves quickly coagulate into chain agglomerates with fractal-like structures which may become as large as 10 μm or more. Although soot particles are mostly carbon, approximately 10% of their mass is typically composed of hydrogen, and they readily absorb organic vapors. Due to their fractal-like structure, soot particles display a wide variety of morphologies from nearly spherical to highly non-spherical. Other physical properties such as density and refractive index are also highly-variable depending on the amount of open space contained with the agglomerate. EC measurements using cascade impactors have observed that the peak in mass of ambient soot particles is frequently between 0.4-1.0 μm [*Jaffrezo et al.*, 2005c; *Carrico et al.,* 2003; *Venkataraman et al.*, 1994b], although a significant amount of mass has also been observed at aerodynamic diameters less than 0.2 μm [*Venkataraman et al.*, 1994b]. Absorption of solar wavelengths in the atmosphere is dominated by elemental carbon [*Lindberg*, 1975; *Rosen et al*., 1979], although recent evidence has suggested that some organic aerosols may also be capable of absorbing visible light [*Kirchstetter et al.,* 2004]. In addition, some iron-containing mineral aerosols such as hematite also absorb in the visible range [*Sokolik,* 1999].

1.2.2 Inorganic aerosols

Inorganic aerosols are composed of non-carbonaceous material and may be loosely sub-divided into ionic aerosols and mineral aerosols (although some minerals are also

ionic). The predominant ionic species are sulfate, nitrate, ammonium, and in areas near oceans, sea salt. Sulfate is a secondary aerosol derived from sulfur dioxide emissions from coal-fired plants burning sulfur-containing fuel. In regions near the ocean, biological processes of marine micro-organisms may also contribute substantially to sulfate concentration. Nitrate is an oxidation product of natural and anthropogenic emissions of NO_x. Ammonium is a product of various biological processes including biomass decay and the digestive processes of certain animal species. Anthropogenic ammonium sources include the application of ammonia containing fertilizers to agricultural fields, emissions from certain industrial processes, and emissions from vehicle catalysts. Ca^{2+} and CO_3^{2-} from crustal sources and K^+ from biomass burning are also important ionic aerosol species. Ionic species are the most hygroscopic of all types of aerosols and will readily absorb water vapor when the relative humidity is above 30-50%.

Mineral aerosols are composed of crustal elements entrained by wind blowing over exposed soils or by agricultural- or construction-related perturbation of soil. Arid regions are the dominant source regions, although exposed soils in all parts of the world can create mineral aerosols. Principal species include silica (SiO_2), alumina (Al_2O_3) and various iron-containing minerals. The size distribution of mineral aerosols is to some extent dependent on distance from the source region since larger particles are removed by gravity more quickly than small particles. Near the source region, mineral aerosols may be on the order of 1 mm or as large as grains of sand. In areas distant from the source, the size of mineral aerosols is still quite large compared to other types of particles and the peak in the size distribution is frequently at observed at sizes larger than 1 μm [*Chun et al*., 2001].

1.3 Important properties of particulate matter

1.3.1 Particle size

The size of particles found in the atmosphere spans six orders of magnitude from nanometer scale to millimeter scale. The peak in the number size distribution is typically observed at 10-20 nm [*Jaenicke,* 1993] while the mass size distribution is often bi-modal with a peak between 0.2 and 1.0 μm and another around 10 μm [*ibid.*]. Since no one single method is able to measure the size distribution across the entire range of sizes, many different techniques have been developed. A common filter-based method to measure the aerosol size distribution is the cascade impactor. This device segregates particles onto a series of impaction plates according to their inertia. For a given flow velocity, there is a size of particle which will have too much inertia to avoid impaction and will be retained by the collection plate. Particles smaller than this cut size will remain in the gas stream and continue with the flow. Cascade impactors use a succession of different size jets such that at each stage, the flow velocity is increased so that progressively smaller particles are retained. The filters may subsequently be analyzed gravimetrically for size-resolved particle mass or used in conjunction with various analytical tools to determine particle speciation. The chief disadvantages of cascade impactors are the fact that filter analysis is time consuming and labor-intensive and that the sampling process itself has very poor time resolution. Since the aerosol population is divided over many stages, an impactor must typically be run for 24 hours or more to collect enough particles for analysis.

Optical particle counters (OPCs) measure the aerosol size distribution based on the amount of light scattered by a particle as it passes through a light source of known intensity. OPCs contain a sample cell in which the sample intercepts the light source and the scattered light is directed by various optical appliances to photodetectors which

quantify this light as a voltage peak. Most OPCs use a gas (typically the ambient air) as the scattering medium, though instruments exist which use a liquid medium. OPCs are calibrated using particles of known size and refractive index. The most common calibration particle is polystyrene latex (PSL). Aerosol light scattering is a function of particle diameter, shape, and refractive index and the wavelength of the incident light. Uncertainty in particle size arises from the fact that ambient particles typically differ significantly in shape and refractive index from PSL [*Whitby,* 1967; *Quenzel*, 1969]. Light scattering is a function of particle size and light wavelength and is maximized when the magnitude of these two quantities are close to one another. For each instrument design, there is a particle size for which the amount of scattered light is too small to be accurately measured by photodetectors. This lower limit of detectable particle size depends on both the wavelength of the light source and the sensitivity of the photodetectors. As a general rule, OPCs which use shorter wavelengths are able to detect smaller particles than those which use long wavelengths. In general however, OPCs are not able to detect particles smaller than about 100 nm. Even though there is significant uncertainty in the particle size reported by an OPC, the concentration is generally accurate provided that the concentration is sufficiently low that only one particle intercepts the light source at a time [*Jaenicke*, 1972]. This concentration is referred to as the coincidence limit. OPCs operate in real-time and consequently are able to detect changes in particle concentrations on time scales much shorter than filter-based measurements. While filter methods measure mass concentration, OPCs measure number concentration. Conversion between these two quantities requires information concerning particle shape and density and as a consequence, is often imprecise.

Other techniques to measure the aerosol size distribution include the differential mobility analyzer (DMA) and the aerodynamic particle sizer (APS). The DMA is able to

select a specific size of particle from the aerosol population based on the size-dependent mobility of a charged particle in an electric field. DMAs are frequently used in conjunction with a condensation particle counter (CPC) to grow particles to easily detectable sizes and measure the size-resolved number concentration. The DMA is useful for particles smaller than 0.5 μm. The APS accelerates particles through a nozzle and measures the time-of-flight between two lasers. Large particles do not accelerate as quickly as small particles due to their increased drag force; hence a relationship may be established between particle size and time of flight. The APS is most useful for particles from 0.5-20 μm. Both of these techniques measure the number concentration. Since the size reported by each of these techniques is based upon a different particle property, the reported diameter may be different even for identical particles.

1.3.2 Radiative properties

In order to correctly predict the influence of particulate matter on climate, it is important to accurately characterize the radiative properties of aerosols. It is useful to sub-divide aerosol radiative properties into *intensive* properties (those which are dependent on the physical characteristics of an individual particle) and *extensive* properties (those which are dependent on concentration).

1.3.2.1 *Intensive radiative properties.* In addition to such traits as size and shape, this category includes properties related to the interactions between the electromagnetic field of the electrons within a particle and that of an incident photon. The extent to which this interaction alters the speed of light is quantified by the refractive index, *m*, defined as the speed of light through the material in question divided by the speed of light in a vacuum. The refractive index is a wavelength-dependent complex number usually denoted

$m = n + k \cdot i$. The real part of the refractive index is related to the scattering of photons while the imaginary part is related to absorption. The scattering effect is actually the sum of three processes: reflection, refraction, and diffraction. Reflection refers to the scattering of photons which strike the surface of a particle, refraction is due to the deflection of a photon as it passes through the material of a particle, and diffraction is the result of the influence of the electromagnetic field generated by the particle. Since this field extends beyond the physical limits of the particle, the cross-sectional area through which a particle may influence light is actually larger than the particle's physical cross-section. Mathematical descriptions of these interactions based on Maxwell's equations were independently proposed by Gustav Mie [*Mie,* 1908] and Ludvig Lorenz and are commonly referred to as either Mie theory or Lorenz-Mie theory.

An important derived intensive property is the aerosol extinction efficiency, Q_{ext}, which is defined as the amount of light extinguished by a particle divided by the amount of incident light. This value is the summation of the aerosol scattering efficiency, Q_{sca} and the aerosol absorption efficiency, Q_{abs}. Since a particle may diffract photons not incident on its surface, Q_{sca} (and thus Q_{ext}) may be greater than one. Q_{sca} is dependent on the relationship between particle size and the wavelength of light and for a given refractive index, it is maximized when the two quantities are similar to one another.

The aerosol phase function describes the angular dependence of the scattered light. For particles much smaller than the wavelength of incident light, scattering is somewhat evenly distributed between the forward and backward directions. As particle size increases, the distribution becomes more heavily weighted in the forward direction. The asymmetry parameter, g, is related to the phase function and describes the relative amount of scattering in the forward or backward direction. For g = +1, all scattering is in the forward direction, g = -1, all scattering is in the backward direction, and g = 0,

scattering is equal in both directions. For atmospheric aerosols (at least those that are efficient scatterers), g > 0.5.

1.3.2.2 *Extensive radiative properties.* These properties are the result of the action of an entire population of particles and thus include the influence of particles of different size, shape and refractive index. The aerosol extinction coefficient, σ_{ep}, is the integration of Q_{ext} over all particle sizes of the aerosol population and is the sum of the aerosol scattering (σ_{sp}) and absorption (σ_{ap}) coefficients. The units of these coefficients are inverse length and are most commonly expressed as Mm^{-1}. The aerosol optical depth, τ, is a dimensionless parameter defined as the integral of σ_{ep} over a vertical atmospheric column and ranges from approximately 0.05 for the background troposphere to over 1.0 for heavily perturbed environments. The single scattering albedo, ω, is the ratio of the scattering coefficient to the extinction coefficient. For aerosol populations without a significant amount of EC, the single scattering albedo is close to 1.0 (although some mineral aerosols also absorb radiation at visible wavelengths, namely hematite). The Ångström exponent, å, describes the wavelength dependence of aerosol radiative forcing and may be defined either in terms of σ_{ep} or τ. A large value of å generally implies a small average particle size in the atmospheric column.

1.4 Atmospheric characteristics which influence aerosol concentration

The temperature structure of the atmosphere with respect to height influences the concentration of gas- and aerosol-phase species emitted at the surface. In the lower atmosphere, temperature decreases with height. The rate of this decrease is termed the lapse rate, Λ. For the special case of dry adiabatic conditions, this is called the adiabatic

lapse rate, Γ, and is roughly equal to a 1° C decrease in temperature per 100 m increase in height. If $\Lambda = \Gamma$, then an air parcel released at the ground will be neutrally buoyant relative to its surroundings and neither rise nor fall. If $\Lambda > \Gamma$, then this air parcel will have a tendency to rise, and the atmosphere is said to be unstable. If $\Lambda < \Gamma$, a rising air parcel will lose temperature more quickly than its surroundings until the temperatures are equal at which point the parcel will cease to rise. Under these conditions, the atmosphere is said to be stable. In a stable atmosphere, vertical mixing is suppressed while in an unstable atmosphere, vertical mixing is rapid.

The layer of the troposphere just above the surface is called the planetary boundary layer. The depth of this layer (called the mixing depth or mixing height) averages approximately 1000 m, but varies with time of year and is generally lower in the winter season. At the top of this layer, the temperature profile reverses limiting the upward motion of rising air parcels. This temperature inversion also acts to constrain wind to horizontal directions. Since emissions at the surface do not rapidly mix with the atmosphere above the temperature inversion, they accumulate within the boundary layer. This layer becomes locally well-mixed on time scales of less than one day due to the turbulent action of wind and in the case of an unstable atmosphere, to vertical motion as well. For this reason, the boundary layer is sometimes referred to as the mixing layer or the well-mixed layer. Since the mixing height determines the volume over which emissions are mixed, atmospheric concentrations of species emitted at the surface will be higher if the mixing height is lower. A ground-level inversion level is also common in the atmosphere depending on time of day and follows a diurnal pattern. Overnight, the earth radiates heat to the atmosphere and becomes cooler than the air. This leads to the formation of an inversion layer at the ground. In the morning, as sunlight begins to warm the surface, this layer deepens and is typically broken by the early afternoon.

1.5 Research objectives

The overall motivation for the research described in this thesis is to further elucidate the influence of atmospheric particulate matter on the global climate and human health. Two specific influences of aerosols are addressed separately in Parts I and II. Since the radiative properties of aerosols present in the atmosphere alter the amount of solar radiation which reached the earth's surface, the growth of plants which depend upon this energy source will be influenced by the atmospheric concentration of particles. In order to estimate this influence on the supply of food produced agriculturally, it is useful to mathematically examine the relationship between specific plant species and the amount of solar radiation available for photosynthesis. Such an examination is discussed in Part I. Given that particle solubility influences the planetary radiation balance both directly and indirectly, it is important for aerosol scientists to have access to tools which are able to efficiently assess this important property. The development of such a tool is described in Part II. In addition, an important objective of this second part is to demonstrate the usefulness of the data resulting from the field implementation of this tool to measure the concentration of water-insoluble aerosols and to compare these results to those obtained from existing technologies.

PART I.

THE INFLUENCE OF AEROSOLS ON CROP PRODUCTION

THE INFLUENCE OF AEROSOLS ON CROP PRODUCTION: A STUDY USING THE CERES CROP MODEL

Abstract

The attenuation of solar radiation by atmospheric aerosols simultaneously decreases the amount of radiation reaching the surface and increases the fraction of radiation which is diffuse. Decreasing the total amount of photosynthetically active radiation (PAR, 400-700 nm) tends to decrease the amount of photosynthesis occurring in plant leaves. Increasing the fraction of PAR which is diffuse allows more PAR to reach shaded leaves and can thus increase the total amount of photosynthesis occurring in a plant canopy. In an attempt to quantify these two radiative influences of aerosols, the CERES crop model [*Ritchie et al.*, 1998] was modified to estimate the impact on yield for maize, wheat, and rice under varying atmospheric conditions. The influence of aerosols on total and diffuse PAR was modeled using the National Center for Atmospheric Research (NCAR) Tropospheric Ultraviolet Visible (TUV) radiation model [*Madronich et al.*, 1993] under both clear skies and overcast skies and again when cloudiness conditions were allowed to vary to reflect actual meteorological conditions. Results from the radiation model were applied to existing meteorological data sets. The weather data were then used as input for the CERES model, and the impact of atmospheric aerosol loading on crop yield was estimated for several different locations around the world. The change in crop yield due to the influence of aerosols was found to be extremely dependent on the magnitude of the increase in radiation use efficiency (RUE) incurred by increasing the diffuse fraction. However, the exact relationship between the diffuse fraction and RUE has not been definitively measured for most crops. The influence of aerosols was found to be more negative on overcast days since the diffuse fraction is already quite high even in a clean

atmosphere. Consequently, the more overcast days there are in a growing season, the more negative is the influence of aerosols. For what is believed to be the most realistic set of model results based on location-specific aerosol loadings and crop-specific RUE change, the influence of aerosols is predicted to decrease maize and wheat yields by 5-10% and rice yields by 0-10%. Aerosols also tend to decrease plant water stress by reducing soil evaporation and transpiration. When crops are grown under rainfed conditions, this reduction in water loss from evapotranspiration may offset the decrease in the photosynthetic rate and cause aerosols to have a positive influence on final grain yields.

2.1 Introduction

The tremendous importance of agricultural production cannot be underestimated in an era in which the earth's population is over six billion and growing. In order to ensure that food supplies keep pace with population growth, a complete understanding of the processes involved in crop growth and development is a necessity. Non-agricultural plant species are also extremely important to the earth's ecosystem in that they influence climate through transpirative effects on the hydrological cycle and by sequestering carbon as biomass. Plant growth depends on temperature, solar radiation, water and nutrients. Atmospheric aerosols influence all of these factors to some extent [*Charlson et al*., 1992; *Schwartz*, 1996]. In order to accurately determine the influence of aerosols on plant growth, it is necessary to understand the relationships between aerosols and radiation, temperature, and precipitation formation, and to understand how changes of these parameters influence plant growth.

Atmospheric aerosols directly influence the amount of solar radiation reaching the surface by scattering and absorbing light as it passes through the atmosphere. Recent

field studies have shown that anthropogenic aerosols can reduce solar radiation by as much as 30% on clear days in the agriculturally important Yangtze delta region of China [*Chameides et al*., 1999; *Xu et al*., 2001]. In addition to reducing the total amount of radiation, aerosol light scattering also tends to increase the fraction of radiation which is diffuse. Diffuse fractions as high as 0.5-0.7 have been observed on cloudless days in areas with high aerosol loadings [*Lorente et al*., 1994]. Aerosols also indirectly alter the amount of solar irradiance incident on the earth's surface by modifying the albedo, frequency, and lifetime of clouds [*Hobbs*, 1993].

Plants utilize solar radiation in the wavelength band extending from 400 to 700 nm known as photosynthetically active radiation or PAR. Most types of plants (i.e. C3 plants) become light saturated at about $^1/_3$ to $^1/_2$ full sunlight. Or put another way, instantaneous CO_2 uptake becomes constant with increasing PAR. On the other hand, C4 plants such as grasses do not become light saturated under most natural conditions. However, their rate of increase of photosynthesis with increasing radiation slows at intense levels of radiation [*Nobel*, 1999]. Direct beam radiation is intercepted only by sunlit leaves. Diffuse radiation, however, is quite evenly distributed amongst leaves in a canopy layer. Reducing the direct portion of PAR will typically only have a slight effect on photosynthesis occurring in sunlit leaves (since they are likely to be near or beyond the saturation point) and no effect on shaded leaves (since they do not intercept direct radiation). Increasing the fraction of PAR that is diffuse will not significantly change the amount of radiation reaching sunlit leaves but will increase the amount of radiation reaching shaded leaves. Since shaded leaves are typically at low light levels (where small increases in radiation result in relatively large increases in photosynthesis), the increase in PAR reaching shaded leaves due to increasing the diffuse fraction will significantly increase the amount of photosynthesis occurring in those leaves. Since aerosols reduce the total (direct plus diffuse) amount of PAR reaching the surface but

simultaneously increase the fraction which is diffuse, it is theoretically possible for the radiative influence of aerosols on plant growth to be either positive or negative.

Recent work has suggested that aerosol light attenuation may be having a significant influence on crop yield. *Chameides et al*. [1999] estimated the reduction in rice and wheat yields in the Yangtze delta region of China under several different aerosol loadings using the CERES crop model. However, the CERES crop model considers only the total amount of radiation incident on the surface and does not account for the effect of increasing the diffuse fraction. Several agricultural studies have indicated that the influence of the diffuse fraction (henceforth, the term diffuse fraction will be used to refer to diffuse PAR divided by total PAR) is extremely important in estimating plant growth. It has been suggested that increasing the diffuse fraction may allow plants to more efficiently utilize solar radiation and grow at a faster rate [*Gu et al*., 2000; *Rochette et al*., 1996; *Sinclair et al*., 1992]. *Sinclair et al*. [1992] predicted that radiation use efficiency (RUE; g C fixed per MJ PAR absorbed) for soybeans, a C3 crop, increases by about 53% between diffuse fractions of 0.1 and 0.5 with little additional increase at higher diffuse fractions. The corresponding increase for maize, a C4 crop, was estimated to be about 27%. *Rochette et al*. [1996] observed a linear increase in RUE for maize equal to about 90% between diffuse fractions of 0.1 and 1.0. Modeling results from a wide variety of plant species reported by *Choudhury* [2001] suggested that light use efficiency may triple between diffuse fractions of 0.0 and 1.0. Due to the effect of Rayleigh scattering, the diffuse fraction is typically at least ~0.13 under clear skies with low aerosol concentrations; the average increase in RUE reported by *Choudhury* [2001] is ~140% between 0.13 and 1.0. *Roderick et al*. [2001] acknowledge the importance of the diffuse fraction in estimating global CO_2 uptake and predict a quadratic relationship between net primary production (NPP; photosynthetic production minus respiration) and the diffuse fraction with a maximum occurring at a diffuse fraction of 0.4 or higher, depending on the

type of plant community involved. Recent modeling work by *Cohan et al*.[2002] estimated instantaneous NPP in a spruce forest and a soybean field. *Cohan et al*.[2002] suggested that the increase in RUE caused by high diffuse fractions may offset the reduction in total PAR caused by aerosols and allow plant growth to actually increase under moderate aerosol loadings and light cloud conditions, although under heavy aerosol loadings, aerosols were found to have a negative effect on NPP. The instantaneous change in NPP however is not necessarily a good predictor of the influence of aerosols on plant growth over the entire year. The objective of this paper is to build on the work of *Cohan et al*.[2002] and estimate both the direct and diffuse radiative influences of aerosol concentration on final crop yield when the cumulative effect over an entire growing season is examined. The specific crops modeled in this study are maize (*Zea mays*), rice (*Oriza sativa*) and wheat (*Triticum sp*.). This paper is intended to provide insight into the possible upper and lower bounds of the influence of aerosols averaged over years of meteorological data, but it is not intended to provide specific predictions of crop yield under specific aerosol loadings and weather conditions.

2.2 Modeling Approach

2.2.1 Crop Model

The generic grain cereal simulation model CERES Version 3.5 (98.0) was used to estimate the effect of aerosols on final crop yield [*Hoogenboom et al*., 1994; *Ritchie et al*., 1999]. CERES has been integrated in the Decision Support System for Agrotechnology Transfer (DSSAT) [*Tsuji et al*., 1994; *Hoogenboom et al*., 1999, *Jones et al*., 2003] and is a widely accepted model commonly used to predict crop yields around the world for a variety of different applications [*Tsuji et al*., 1998]. *Saarikko* [2000] and *Tubiello et al*. [2001] used the CERES model to estimate wheat yields under changing

climatic conditions. *MacRobert and Savage* [1998] and *Steele et al*. [2000] used CERES to estimate the influence of differing irrigation schedules on maize and wheat production. *Castrignano et al*. [1998] modified CERES to estimate the influence of increased soil salinity on maize production in the Mediterranean region. For this study, the model was modified to estimate the influence of decreasing total PAR and simultaneously increasing the diffuse fraction on crop growth and final yield.

The CERES model has been previously evaluated numerous times by comparing model predictions to field measurements of plant characteristics such as leaf area index, biomass, grain number and grain yield for crops grown under known conditions. *Braga* [2000] used CERES-maize to estimate the influence of varying soil conditions within the same field on maize growth and found that predicted yields were within 10% of the observed yields at 40 locations over two years. *Mall and Aggarwal* [2002] used CERES-rice to estimate the influence of future climate change on rice yield in various locations throughout India and found predicted yields to be within 15% of observed yields when past meteorological conditions were simulated. *Cheyglinted et al*. [2001] used CERES-rice to estimate the influence of the timing of nitrogen applications on several varieties of rice grown in Thailand and found little difference between simulated and observed yields for most varieties. *Ghaffari et al*. [2001] used CERES-wheat to examine the influence of several different management practices on winter wheat grown in England and determined that the model could be used to accurately predict wheat yield. *Heng et al*. [2000] used CERES-wheat to examine the optimization of nitrogen fertilizer application on irrigated wheat fields at many locations around the world and found that simulated wheat yield was within approximately 15% of observed yield.

The CERES model was developed to simulate crop growth and development properties such as yield, leaf area index (LAI; total single-sided leaf area per ground area), and biomass production for different grain cereals including the world's three most

important grain crops: rice, maize, and wheat [*Ritchie et al*., 1998]. These computer simulations are based on inputs of soil properties, including nutrient and water availability, crop and cultivar specific growth parameters, and meteorological information such as daily total radiation, maximum and minimum temperature and precipitation [*Hunt et al*., 2001]. The model computes daily CO_2 uptake based on PAR, RUE, LAI, and various water and nutrient stress levels. Water and nutrient stress are calculated through a dynamic simulation of both the soil and plant water and nitrogen balances [*Godwin and Singh*, 1998; *Ritchie*, 1998]. Biomass is apportioned to different plant components as a function of the phenological stage of development and the level of nutrient and water stress. The standard CERES model assumes that RUE is a constant value for each species of crop and does not change with the diffuse fraction.

Plant development from germination to harvest maturity is based on a nine stage development scheme [*Ritchie*, 1991; *Ritchie et al*., 1998]. Which parts of the plant are actively growing at any time is dependent on the growth stage. During reproductive development, carbohydrates are apportioned to the grains. Final yield for grain cereals is expressed as the dry mass of the grains at the end of the season. The length of each development stage is a function of temperature, photoperiod, and water and nutrient stress. The relationship between temperature and stage advancement is itself a property of both the plant species and cultivar (a cultivar is a specific variety of a particular species). In this study, the cultivar selection was consistent with the environmental requirements of the location where a crop was modeled. For example, at high latitudes with short growing seasons, cultivars were selected which mature within the available amount of time.

Plant growth is also strongly influenced by other environmental factors such as the availability of water and nutrients. The CERES model calculates on a daily basis a water stress factor and a nutrient stress factor. These factors relate the amount of water or

nutrient demanded to the amount available. The purpose of this study was to examine the change in yield caused by the radiative influence of aerosols. In order to isolate the influence of aerosols, it was necessary to make sure that plant growth was not limited by water or nutrient availability. Therefore, the model was configured so that the crops never experienced water or nutrient stress. These are realistic conditions for crops that are fully irrigated and fertilized. However, in many situations crop growth may in fact be limited by water or nutrient stress under actual field conditions, especially for rainfed crops or crops grown in low input systems in developing countries.

2.2.2 Site selection and meteorological data

In order to obtain statistically meaningful results, twenty or more years of meteorological data were collected from the literature for several geographic locations around the globe. These meteorological data sets contain the cumulative amount of total radiation incident at the surface, the maximum and minimum temperature, and the amount of precipitation for each day of the year. The CERES model assumes that PAR is simply $^1/_2$ of the measured total downwelling irradiance. In order to examine the influence of aerosols on crop growth, cumulative daily radiation was estimated for each day of the year at each site using a radiative transfer model that considers the influence of both aerosols and clouds and is described in detail in the next section. The observed daily cumulative radiation in the meteorological files was replaced with the estimated output from the radiation model as described below. Sites were chosen based on the availability of a sufficient amount of observed meteorological data and on the appropriateness for the crop in question to be cultivated at that location. Table 2.1 lists information for each simulation location.

TABLE 2.1. Locations and crops used in the crop simulations

location	Orland, California,USA	Gainesville, Florida, USA	Hyderabad, India	Ames, Iowa, USA	Bangkok, Thailand
lat., long.	39.0N, 121.0W	29.6N, 82.4W	17.5N, 78.3E	42.0N, 93.6W	19.0N, 99.0E
elevation [m]	20	10	300	98	10
crops and cultivars	rice, IR 58	maize, McCurdy 84	maize, long season rice, IR 58 wheat, facultative	maize, med. season wheat, spr., high-lat	rice, IR 58
soil profile	deep silty clay	Millhopper sand	Medium Alfisol	Haynie	Suphan Lowland
planting date	rice, 5 May	maize, 2 Feb	maize, 6 June rice, 6 June wheat, 6 June	maize, 15 April wheat, 10 March	rice, 3 Sept
row spacing [cm]	rice, 20	maize, 61	maize, 61 rice, 20 wheat, 16	maize, 61 wheat, 16	rice, 20
growing season	17 May-14 Sept	2 Feb-4 July	6 June-20 Sept	15 April-31 Aug	3 Sept-7 Dec
percent overcast days	9.5%	43.5%	64.0%	52.0%	68.0%

2.2.3 Radiation Model

In order to estimate the influence of aerosol loadings on crop yields, the recorded cumulative daily radiation values reported in the observed meteorological data sets from each location were substituted with values calculated using the National Center for Atmospheric Research (NCAR) Tropospheric Ultraviolet Visible (TUV) radiation model [*Madronich et al*., 1993]. The 2-stream mode of this model was used to compute diffuse fractions. These radiation levels were computed as a function of latitude, day of year, aerosol optical depth (AOD), and cloud optical depth (COD). AOD is a unitless parameter defined as the integral of the aerosol light extinction coefficient over the entire atmospheric column. AOD is dependent on factors that include the light wavelength,

aerosol concentration, and the physical and chemical properties of the particles. For discussion purposes, we refer to the optical depth at a wavelength of 550 nm since this wavelength is the middle of both the visible and of the PAR wavelength ranges.

For all values of AOD, the same set of assumptions was made concerning the aerosol intensive properties (i.e. the properties that do not depend on concentration). The single scattering albedo (ratio of aerosol light scattering to total aerosol light extinction) was assumed to be 0.9 (i.e. 10% of aerosol light extinction is due to absorption). This value is within the range of values reported in agricultural regions of the U.S. and China [*Sheridan and Ogren*, 1999; *Xu et al*., 2002]. The asymmetry factor (the intensity-weighted average of the cosine of the scattering angle) was assumed to be 0.61 (i.e. most scattering is in the forward direction). According to Mie theory, this value is typical for a region in which most of the aerosol mass is in the fine mode (D_p<2.5μm) [*Xu et al*. 2002]. Clouds were assumed to be between 5 and 6 km altitude. Unlike for climate change simulations, the vertical distribution of aerosols and clouds was not important for this study since only the amount of radiation reaching the surface was examined and not the heating or cooling effect of the clouds on the atmosphere. The single scattering albedo of cloud droplets was assumed to be 1.0 (i.e., no absorption by droplets) with an assumed asymmetry factor of 0.85. For this study, AOD and COD were decoupled. In actuality, cloud formation, lifetime, and optical thickness are dependent on aerosol concentration and composition. Higher aerosol concentrations tend to increase cloud reflectance and lifetime [*Twomey*, 1991]. This indirect radiative influence of aerosol concentration was not examined in this study.

At each location, twelve different atmospheric conditions were modeled: AOD equal to 0.05 (the assumed background value), 0.2, 0.4, 0.6, 0.8, and 1.0 under both clear skies and moderately overcast skies. The clear sky scenario assumes that COD = 0. The overcast sky scenario assumes that COD = 5.0, which is typical for skies containing

thin clouds through which the disk of the sun is barely visible. A COD typical of thin rather than heavy cloud cover was chosen so as to not overestimate the influence of clouds. However, cloud optical depths are frequently thicker than this for extended lengths of time in many agricultural regions. Cloud cover was also assumed to be uniform across the entire sky (the TUV model is not designed for partly cloudy conditions). The radiation model was run for all twelve scenarios for every day of the year at each geographic location. The output from the model was cumulative broad band radiation, cumulative PAR, and the daytime average diffuse fraction for each day of the year.

Figure 2.1 shows the normalized frequency distribution of AOD at a wavelength of 550 nm for three different types of locations. The measurements made at the Southern

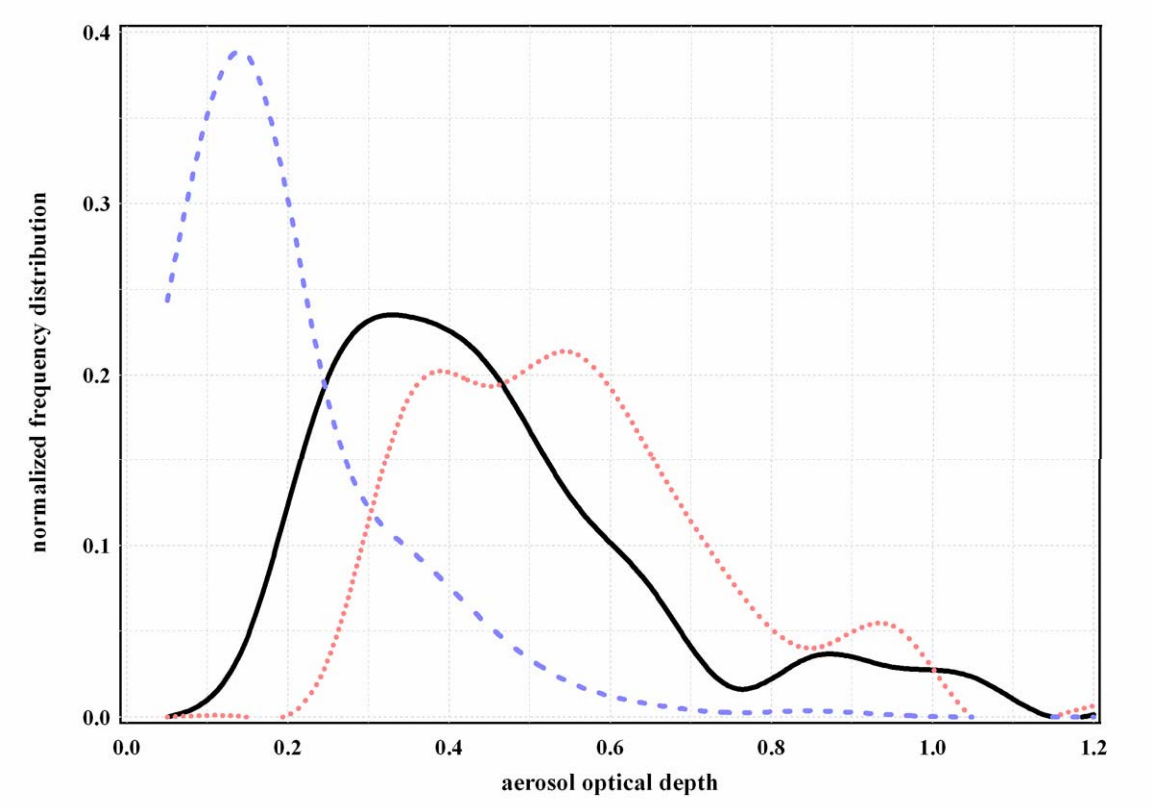

FIGURE 2.1. Normalized frequency distribution of AOD measurements from three diverse locations. (- - - - SGP ARM site, ——— Atlanta Super Site, ····· Linan, China.)

Great Plains Atmospheric Radiation Measurement (SGP ARM) site in Oklahoma are for the entire year 1998 and are from a rural U.S. location [*R.N. Halthore*, personal communication]; the Atlanta Super Site measurements (August 1999) are more typical of an urban U.S. site [*Carrico et al*., 2002]; the Linan, China measurements (November 1999) are from a rural, agricultural site in the Yangtze delta region [*Xu et al*., 2002]. These measurements indicate that in the rural U.S., the AOD is typically around 0.1 and rarely exceeds 0.4. In an urban U.S. region, the AOD is most frequently around 0.3 and occasionally is somewhat higher. In the Yangtze delta, however, the AOD is typically 0.5-0.7 and is frequently much higher than even a polluted urban area of the U.S. This is due to the proximity of the Yangtze delta to urban sources, as well as widespread regional point sources [*Xu et al*., 2002]. It is likely that the modeled sites in Florida and Iowa typically experience AOD~0.1-0.2. The California site is somewhat influenced by urban areas and likely has a typical AOD~0.2-0.4. The modeled sites in Thailand and India are likely to be similar to the Yangtze delta site and have an AOD~0.5-0.7.

For each location, three meteorological files were compiled: continuously clear skies, continuously overcast skies, and variably overcast skies. The continuously clear sky case used the model results calculated using COD = 0.0 while the continuously overcast case used COD = 5.0. The continuously clear and continuously overcast conditions are admittedly not realistic but are intended to establish the upper and lower bounds of the influence of aerosols. Actual cloudiness conditions were not recorded in the meteorological files. In order to overcome this shortcoming, a variably overcast case was developed to more realistically model actual atmospheric conditions. For this case, skies were assumed to be clear except on days receiving precipitation and on days preceding days with precipitation. Days preceding days with precipitation were assumed to be overcast in an attempt to account for days which are cloudy but on which no precipitation occurs. For each of these three scenarios, the calculated cumulative daily PAR and

daytime average diffuse fraction were inserted into the existing meteorological files on the appropriate day of the year. This procedure was performed for all values of AOD. The temperature and precipitation data in the measured meteorological data sets were not changed.

2.2.4 Diffuse fraction and RUE

The CERES model computes the daily photosynthetic rate based on the simplifying assumption that RUE is a species-specific property which does not change as the plant develops or under varying light conditions. In actuality, RUE varies not only by species, but also by cultivar and environment. *Goetz* [1996] showed that the RUE of an individual plant could vary depending on stage of growth and stress level. Although enough work

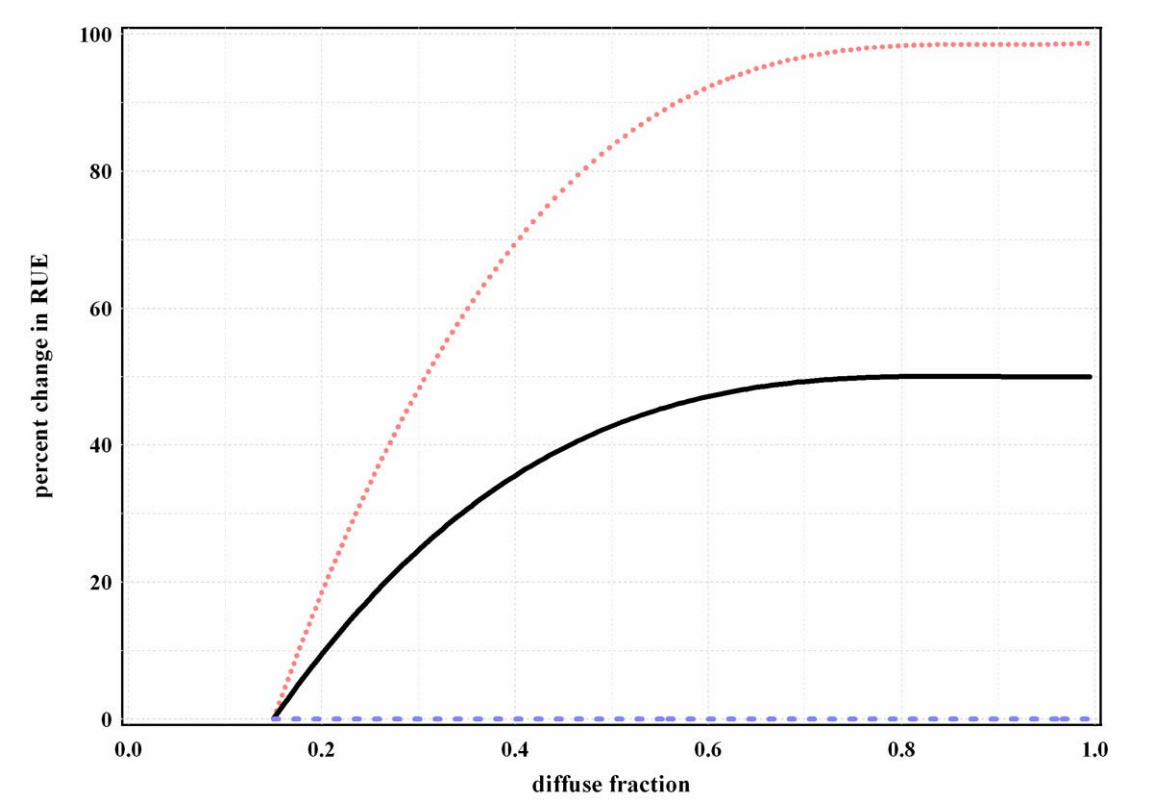

FIGURE 2.2. Response curves used to calculate the percent increase in RUE as a function of diffuse fraction. (no change in RUE, maximum RUE change = 50%, maximum RUE change = 100%.)

has been published to convincingly suggest that instantaneous RUE is dependent on the diffuse fraction, there have not been sufficient measurements made for a variety of different crops to definitively determine the magnitude of this dependence.

Several response curves were used in order to estimate the sensitivity of crop growth to the increase in RUE associated with an increasing diffuse fraction and are shown in Figure 2.2. These curves were chosen simply to span the range of expected possibilities. In actuality, they most likely vary by crop, cultivar, stage of development, LAI, irradiance level, and stress level. The response curves ranged from no change at all in the base RUE to a doubling of RUE at high diffuse fractions. Also used was a response curve which split the difference between the extremes. The percent increase in RUE was assumed to asymptotically approach the maximum change at a diffuse fraction of 0.8. This agrees with the predictions made by *Sinclair et al*. [1992], although *Rochette et al*. [1996] suggested that the increase in RUE is linear with increasing diffuse fraction and *Choudhury* [2001] suggested that the maximum increase may be larger than 100%. For each day in the CERES model runs, RUE is calculated as the base RUE plus a percent increase. The percent increase is a function of that day's diffuse fraction and the applicable response curve. For example, day 210 of year 2 of the Ames, Iowa data set is a non-rainy day. For an AOD = 0.6 and a COD = 0, the TUV model estimates an average diffuse fraction of 0.38. If the 50% increase RUE response curve is used, then the RUE used to compute that day's carbon uptake is the base RUE plus 33%.

For each value of AOD and COD, the CERES model was run for each year for which weather data were available. The yields from each of these years were summarized by calculating an average and a standard deviation. These yields were then compared to the base case of AOD = 0.05, and a percent change was calculated. The standard error of the mean was used to evaluate the variability in the change in mean yield. This process was repeated for each RUE response curve and at each geographic location.

2.2.5 Relationship Between the Diffuse Fraction and Aerosol Optical Depth

The TUV model was used to estimate the change in PAR reaching the surface and the diffuse fraction as AOD increases under both clear and overcast skies. Figure 2.3 shows these changes for Ames, Iowa (a mid-latitude site) as a function of aerosol optical depth. Under clear skies, PAR decreases by ~30% as AOD is increased to 1.0 from the background level of 0.05. At the same time, the diffuse fraction is increased by over 200%. Under overcast skies, PAR is still reduced by ~25% at AOD = 1.0, but the diffuse fraction is only increased by about 5% since it is already quite high due to light scattering by cloud droplets. Therefore, it is expected that the influence of aerosols on plant growth will be quite different on clear days than it is on overcast days. On clear days, aerosols

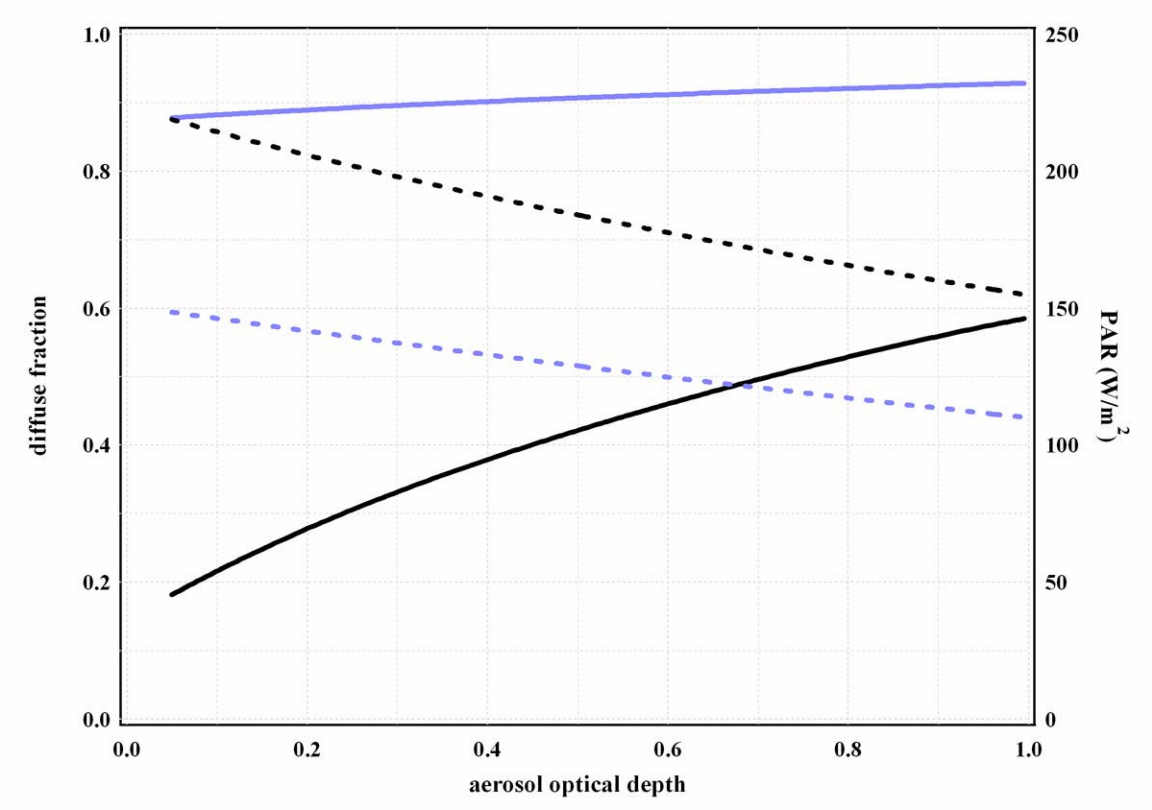

FIGURE 2.3. Change in daytime average diffuse fraction and instantaneous PAR for Ames, Iowa. (clear skies diffuse fraction, cloudy skies diffuse fraction, clear skies PAR, cloudy skies PAR.)

are expected to increase RUE at the same time that they decrease PAR and so could theoretically either increase or decrease the amount of photosynthesis taking place, depending on the concentration. On overcast days on the other hand, aerosols are not expected to significantly change RUE and so are expected to have a negative influence on photosynthesis.

2.3 Results

The change in yield for each of the eight combinations of crop and location for each of the three different cloud cases are summarized in Figures 2.4, 2.5, and 2.6. The 0% lines assume that the crop RUE does not change with the diffuse fraction. This is essentially how yields are computed by the unaltered CERES model (i.e. the version that does not distinguish between direct and diffuse radiation). The 50% and 100% lines assume that RUE asymptotically approaches a 50% and a 100% increase over the base RUE at a diffuse fraction of 0.8. Note that an increase in RUE of 50% or 100% only occurs when the diffuse fraction is higher than 0.8; at diffuse fractions between the background and 0.8, the change in RUE is less than the maximum and is a function of the response curve used. The percent change in yield as compared to the background AOD of 0.05 for each specific condition is shown. The error bars represent the standard error of the mean for approximately 20 years of meteorological data, depending on the location.

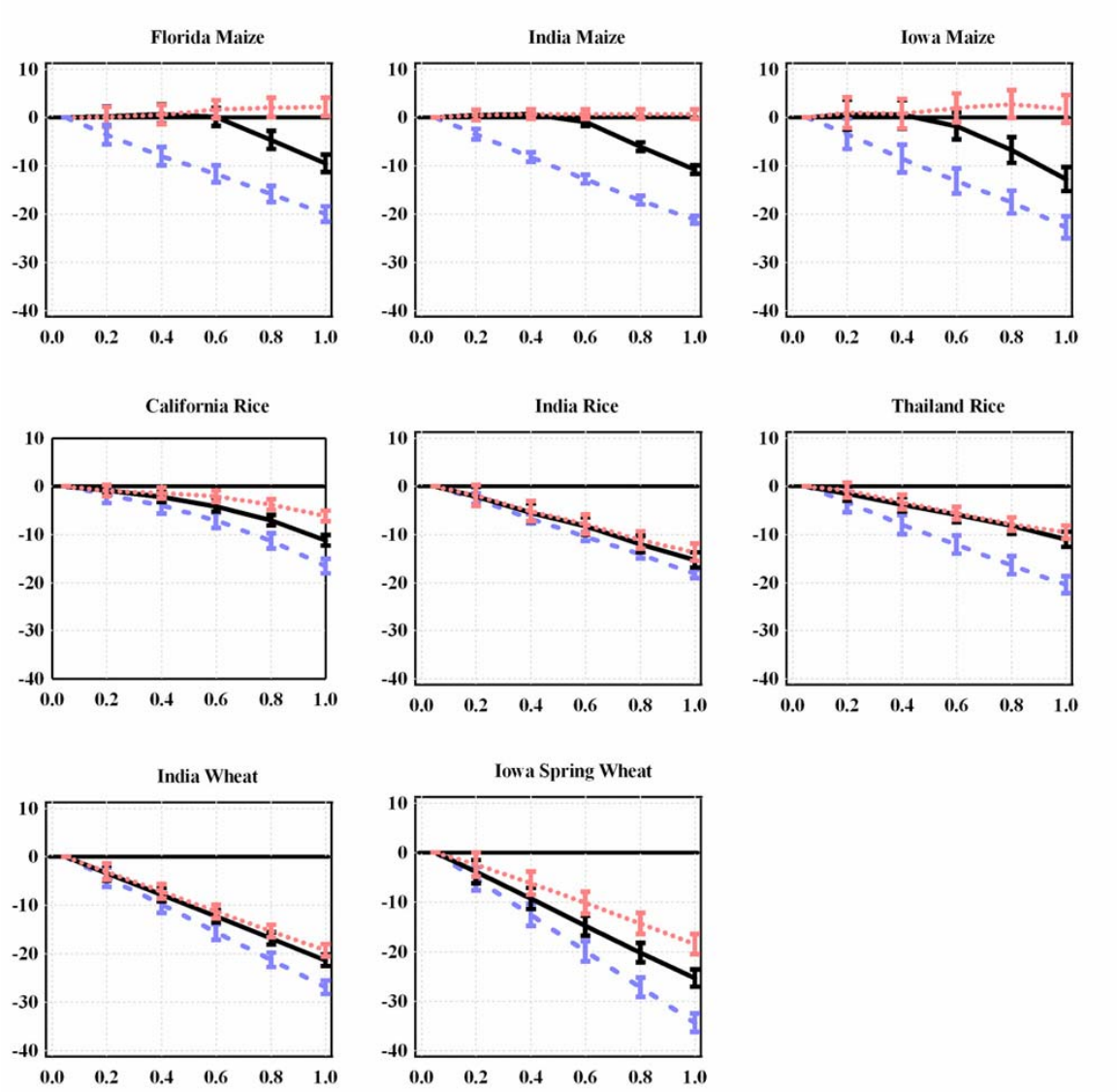

FIGURE 2.4. Percent change in crop yield as a function of AOD under continuously clear skies. (maximum RUE change = 0%, maximum RUE change = 50%, maximum RUE change = 100%.)

2.3.1 Influence of Aerosols on Crop Production for Clear Sky Conditions

Figure 2.4 shows the change in yield assuming that skies are continuously free of clouds. Under these clear sky conditions, the increase in RUE associated with increasing AOD offsets the decrease in PAR, and yields are positively influenced by increasing AOD for the 50% and 100%. If RUE does not change, yields are negatively

influenced. Yield for wheat and rice (C3 crops) is predicted to decrease linearly if RUE does not change with a maximum decrease in yield of about 30% at AOD=1.0. If RUE fluctuates as a function of the diffuse fraction, yields are predicted to increase to a maximum of about 15% (for a maximum RUE change of 50%) to 40% (∆RUE=100%) at AOD=0.6. Yield for maize (a C4 crop) is also predicted to decrease linearly to about 30% if RUE does not change. If RUE fluctuates as a function of the diffuse fraction, yield is predicted to increase to a maximum of about 15% (∆RUE=50%) to 25% (∆RUE=100%). The maximum increase in yield occurs at AOD=0.4, which is slightly lower for maize than for wheat or rice. For all crops, the mean change in yield is only slightly sensitive to location.

2.3.2 Influence of Aerosols on Crop Production for Overcast Sky Conditions

Figure 2.5 shows the change in yield for all crops at all sites assuming that skies are continuously moderately overcast (cloud optical depth = 5.0). Under these conditions, PAR is decreased about 25% and the diffuse fraction is increased by only 5% when AOD increases from 0.05 to 1.0. Consequently, yields for all three crops tend to be significantly diminished by higher aerosol loadings even if RUE is allowed to double from the background value. Wheat yields are predicted to decrease by as much as 60% at AOD=1.0 if RUE does not change and by 25% if RUE is allowed to increase. Rice yields are predicted to decrease between 20-30% at AOD=1.0 regardless of the change in RUE. Maize yields are predicted to decrease by about 20% at AOD=1.0 if ∆RUE<50% and by about 50% if ∆RUE=100%. Since cloudiness conditions are uniform, there is again little variation between sites.

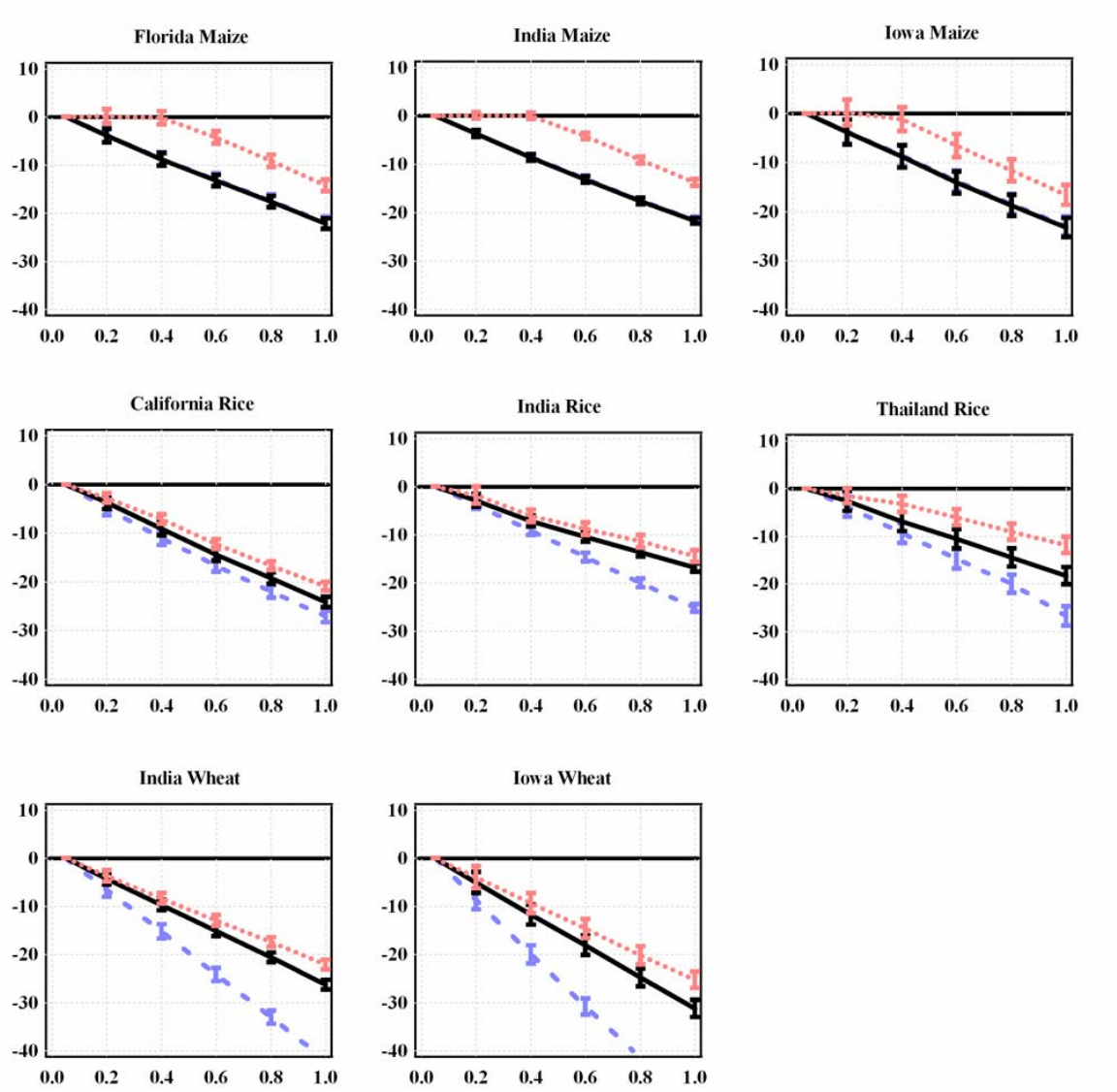

FIGURE 2.5. Percent change in crop yield as a function of AOD under continuously cloudy skies. (maximum RUE change = 0%, maximum RUE change = 50%, maximum RUE change = 100%.)

2.3.3 Influence of Aerosols on Crop Production for Variably Cloudy Skies

Figure 2.6 shows the change in yield for all crops at all sites for the more realistic case of variably overcast skies. As previously described, skies are overcast on days receiving precipitation and days preceding days with precipitation and are clear on all other days. The predictions made for this case lie in between the predictions made for the clear sky and overcast sky cases. Since the cloudiness conditions are no longer

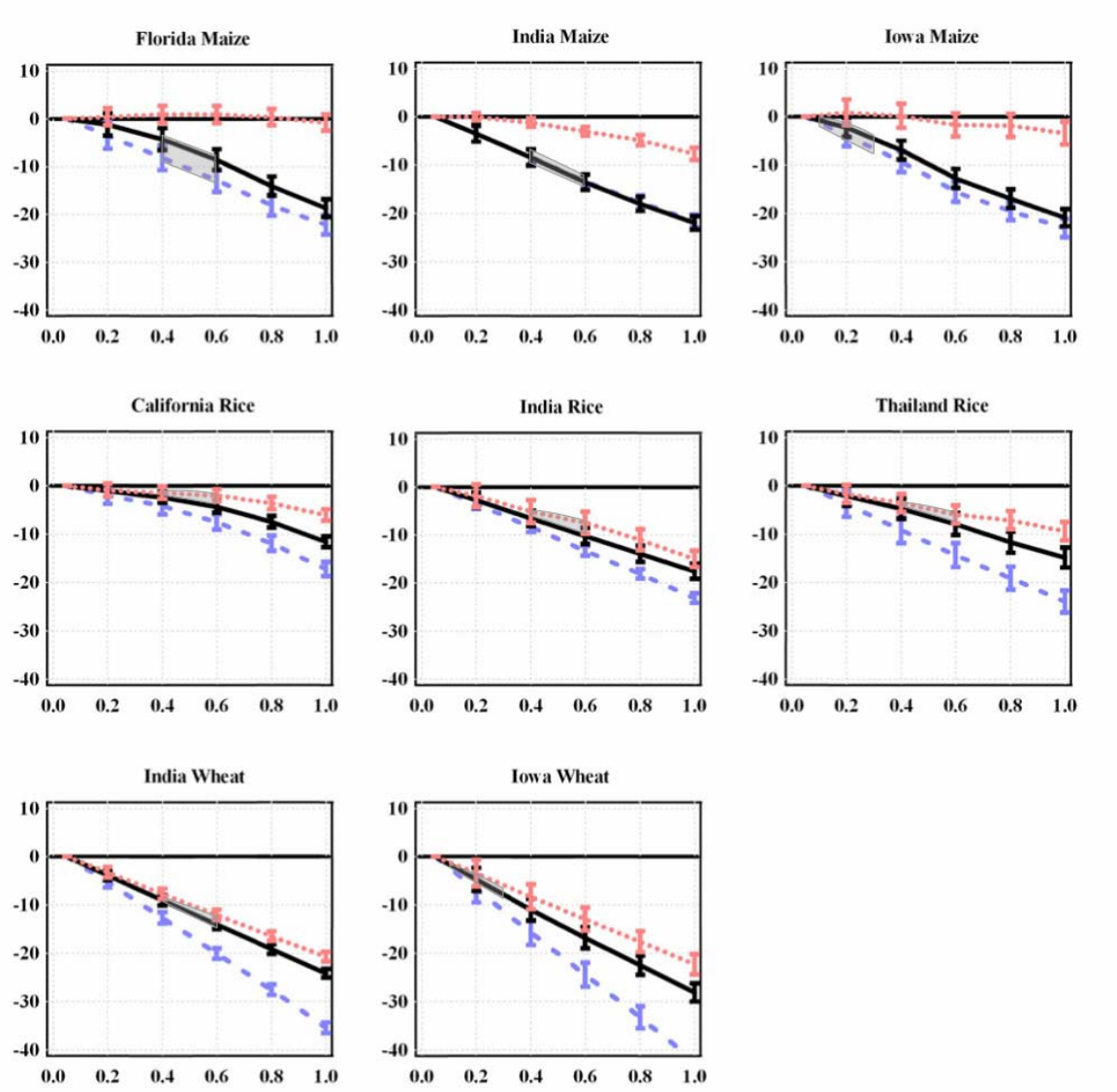

FIGURE 2.6. Percent change in crop yield as a function of AOD under variably cloudy skies. (maximum RUE change = 0%, maximum RUE change = 50%, maximum RUE change = 100%.)

uniform but are instead dependent on the site-specific meteorological files, there is a considerable amount of variability from site to site. Wheat yields are predicted to decrease up to 40% if RUE does not change but are within a few percent of no change at all for most optical depths when RUE is defined as a function of the diffuse fraction. Rice yields are predicted to decrease by 30% at AOD=1.0 if ΔRUE=0. If RUE does change with the diffuse fraction, model predictions vary depending on the number of

overcast days within a typical growing season. In sunny California, rice yields are predicted to increase between 15% (ΔRUE=50%) and 40% (ΔRUE=100%), with the maximum increase occurring at AOD=0.4-0.6. For the India and Thailand simulations, yields are predicted to be within 10% of no change for most optical depths. The maximum increase in yield is predicted to occur when AOD is between 0.2 and 0.4. Maize yields are predicted to decrease linearly at all sites to a maximum of about a 20% reduction if RUE does not change. If RUE does change, yield predictions again vary from site to site depending on cloudiness conditions. For the Florida and Iowa simulations, yield changes are ±10%, whereas for India, yields are predicted to vary from no change to a 20% reduction. The maximum positive effect is predicted to occur at around AOD=0.4 for all three sites.

2.4 Discussion

In order to properly interpret the results from these CERES model simulations, it is very important to accurately understand the relationship between aerosols and RUE. As explained in the introduction, increasing the diffuse fraction can significantly increase the amount of photosynthesis occurring in shaded leaves. Decreasing total PAR likely does not change the photosynthetic rate of sunlit leaves for C3 plants (since they are light saturated for much of the day); however, this will decrease photosynthesis in C4 sunlit leaves since they are not light saturated. Given that aerosol light scattering decreases total PAR at the same time that it increases the diffuse fraction, aerosols are therefore expected to increase RUE of C3 plants (e.g. wheat, rice) more than C4 plants (e.g. maize). This is consistent with both *Rochette et al*. [1996] and *Sinclair et al*. [1992]. This implies that the response of wheat and rice to increasing diffuse fraction is likely to be closer to the high end (i.e. between 50% and 100% response curve) while maize's

response is probably closer to the low end (i.e. between the 0% and 50% curves). Since the increase in RUE is associated with the amount of photosynthesis occurring in shaded leaves, the ratio of shaded leaves to sunlit leaves is very important. When plants have just emerged and have low LAI, this ratio is quite low. This implies the increase in RUE is likely to be less at low LAI than in mid-growing season when a crop is fully developed and has multiple canopy layers and a high LAI. The model as altered for this study does not account for this and defines the increase in RUE as a function of the diffuse fraction regardless of LAI. There is evidence that plants are able to physiologically adapt to the light conditions. *Kasim and Dennett*, [1986] observed an increase in leaf size and a decrease in the rate of leaf senescence when beans are grown under shade. This response was observed to be more pronounced if the shading occurred early in the growing season rather than after the plant had already flowered.

Under overcast skies, CERES suggests that aerosols exert a significantly more negative influence on wheat yields than on maize or rice yields when RUE does not change. This can be explained by the fact that wheat's maximum leaf area index tends to be lower than maize or rice's and that it takes longer to achieve full canopy coverage. Figure 2.7 shows model predictions of LAI vs. crop age for all three crops grown in India under variably cloudy skies. The fraction of PAR which is intercepted by the plant canopy directly depends on LAI. At low LAI, much of the sunlight is absorbed by the ground rather than by leaves. At LAI>~3, however, over 90% of the incident PAR is absorbed by the canopy. Given that CO_2 uptake is directly related to the amount of PAR absorbed, the longer it takes a plant to develop a canopy with a LAI>~3, the less carbon is available for growth. This creates a positive feedback cycle: the less PAR the plants absorb, the slower they grow, and the slower they grow, the less PAR they absorb. If RUE does not change, the reduction in PAR associated with aerosols has a more pronounced negative influence on wheat yield. As explained in the previous paragraph,

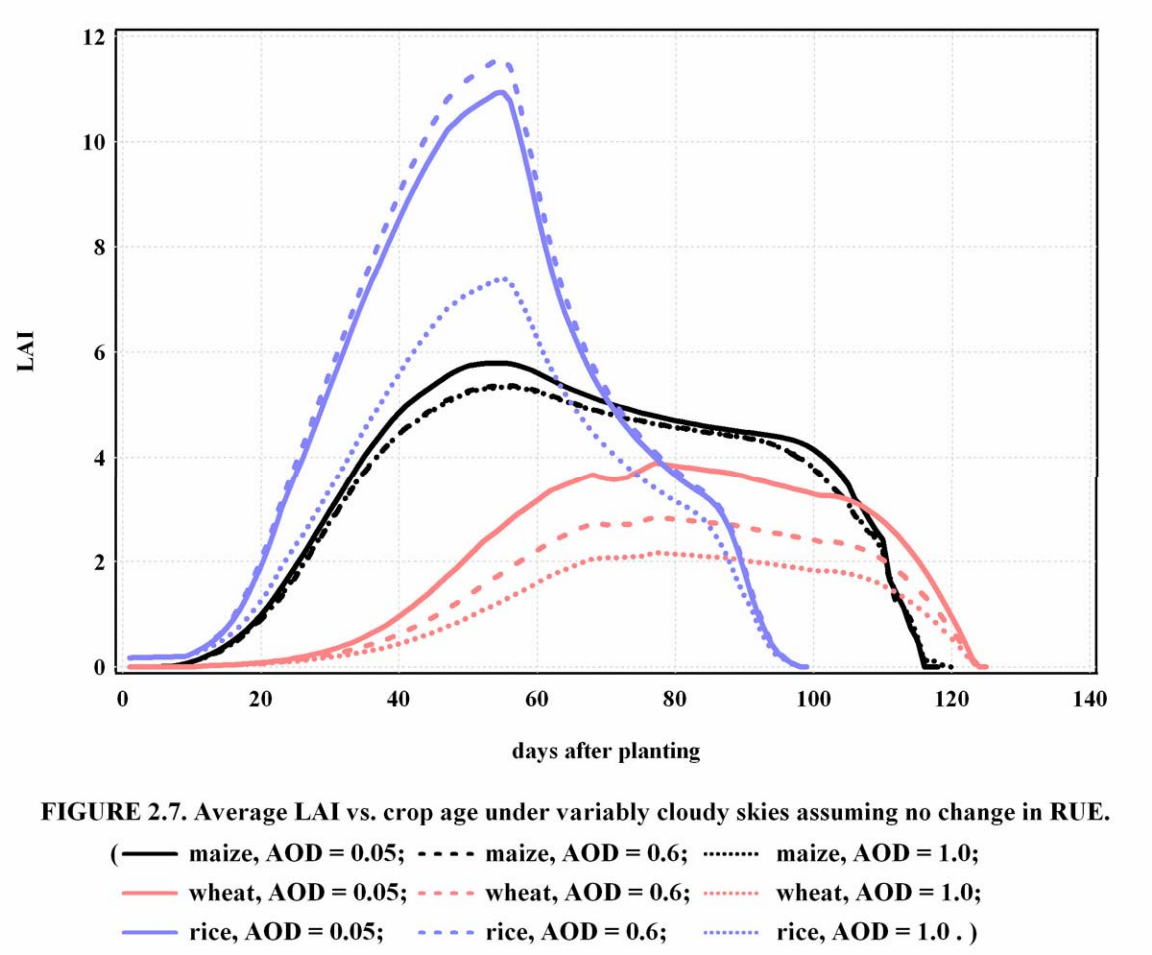

FIGURE 2.7. Average LAI vs. crop age under variably cloudy skies assuming no change in RUE.
(maize, AOD = 0.05; maize, AOD = 0.6; maize, AOD = 1.0;
wheat, AOD = 0.05; wheat, AOD = 0.6; wheat, AOD = 1.0;
rice, AOD = 0.05; rice, AOD = 0.6; rice, AOD = 1.0 .)

RUE for wheat likely increases significantly under high diffuse fractions. When this happens, wheat is able to grow to full canopy coverage, and yield is not nearly as negatively influenced as when RUE does not change.

It is interesting to note that the difference in yield predictions from location to location are much more pronounced when sky cloudiness conditions are allowed to vary than when conditions are uniform. This can be explained by the fact that on overcast days, the diffuse fraction is already quite high, and increasing AOD simply decreases PAR without changing RUE. Therefore, on overcast days, high aerosol loadings exhibit a more negative influence on photosynthesis than on sunny days. As a result, it is the overcast days which are chiefly responsible for the decreases in mean yield. It stands to reason then that the more overcast days there are during a growing season, the more

negative the influence of aerosols on crop production will be. Table 2.1 lists the average percent of the days during the growing seasons used for this study which have overcast skies (as determined by the previously described method). For all crops, there is a correlation between average yield reduction and the percentage of overcast days in a growing season. Locations with fewer overcast days in a growing season (such as the central valley of California) tend to exhibit a more positive influence of aerosols than locations with more overcast days during a growing season. This observation may be of future significance as the amount of global cloud-cover is increased or decreased due to climate change.

When sky conditions are uniform (either continuously overcast or continuously clear), the model still predicts slight variations in yield reductions for the same crop from location to location. This is due to a combination of several factors, namely the differences in the cultivars grown at each location and the differences in latitude for the sites. Even within the same species, there are significant differences in plant properties governing growth, development, and final grain yield. In particular, the maximum number of grains per plant, the grain filling rate, and the phyllocron interval (the interval in degree days between successive leaf tip appearances) can vary significantly from variety to variety. The very different temperatures between sites can significantly influence plant growth and development even in the absence of water or nutrient stresses. Latitude also plays a role in the influence of aerosols on crop production. Figure 2.8 shows the percent reduction in PAR reaching the surface averaged over the entire year as a function of AOD for all locations examined in this study. It is evident from this figure that the reduction in PAR is greater at higher latitudes (i.e. closer to the poles), or put in more general terms, the reduction is higher when the sun is lower in the sky. This is in spite of the fact that AOD is normalized to solar zenith angle. The reason for this is that the fraction of light scattered upward by aerosols is higher when the sun is lower in the sky.

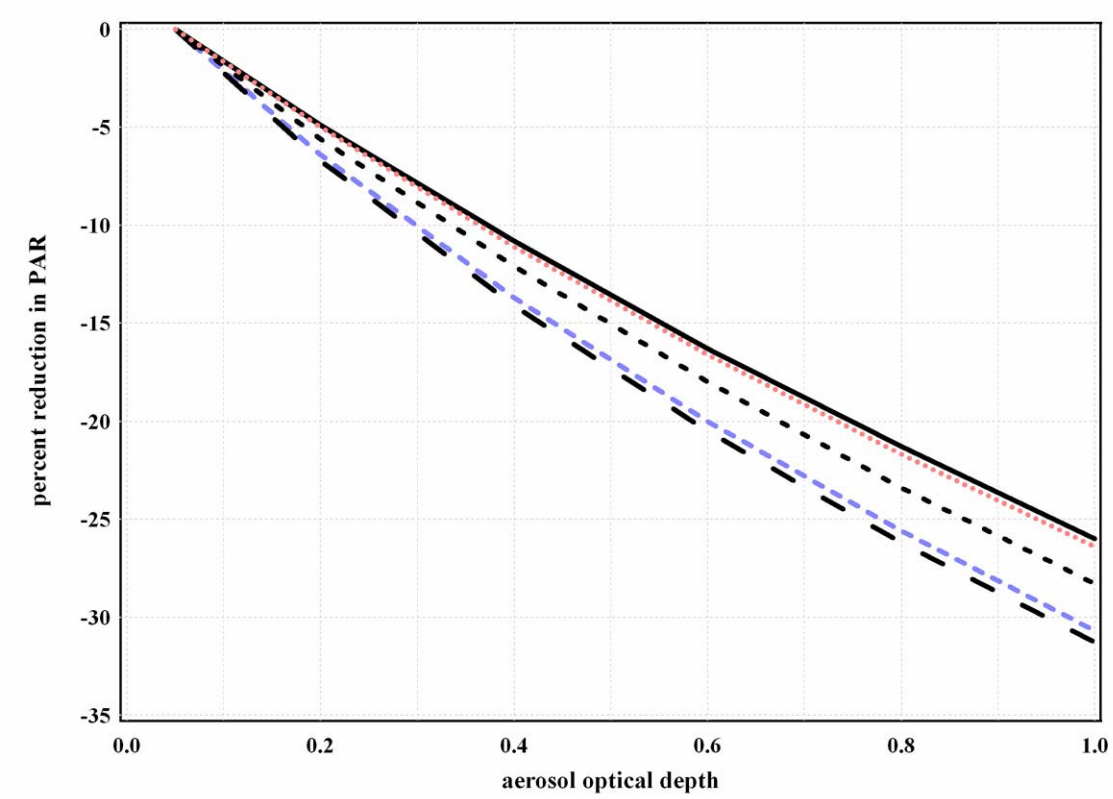

FIGURE 2.8. Percent reduction in PAR vs. AOD for a variety of latitudes.
(India, 17.5 degrees N; Thailand, 19 degrees N;
Florida, 29.6 degrees N; California, 39 degrees N;
Iowa, 42 degrees N.)

It was assumed for this study that the asymmetry parameter was 0.61 for particles and 0.85 for cloud droplets (i.e. most scattering is in the forward direction for both). When the sun is low in the sky, some of the forward-scattered radiation is lost to space and thus a disproportionately smaller amount of PAR reaches the surface at high latitudes than at lower latitudes for the same AOD. This same argument suggests that crops grown at times of year when the sun is lower in the sky would also experience a greater reduction in PAR for the same AOD as crops grown in mid-summer.

Model simulations were performed assuming that AOD was constant for the entire growing season. This is obviously not realistic. Aerosol concentrations vary widely throughout the year depending on meteorological conditions, the existence of upwind

sources, atmospheric chemistry, and many other influences. Although AOD can frequently be quite high in many important agricultural areas (see Figure 2.1), being maintained as high as 1.0 for an entire growing season is not likely. *Kasim and Dennett* [1986] report that the timing of shading is very important to the development of a plant canopy. If a field is shaded while the plants are young and still growing, they can increase the size of their leaves and slow the rate at which old leaves are lost. This suggests that high aerosol concentrations early in the growing season are less likely to have a negative effect on plant growth than high concentrations late in the season.

Aerosols also have a number of indirect effects that were not specifically examined in this study but which deserve mentioning. Aerosol radiative forcing usually (though not always) has a negative influence on temperature. This can have either a positive or negative influence on plant growth and development depending on the stage of development and if the temperature is above or below the optimum. The decrease in radiation associated with increasing aerosol concentrations also results in less water loss due to soil evaporation and leaf transpiration. On model runs without sufficient irrigation, this reduction in water loss at increased aerosol concentrations resulted in significantly less water stress. Although the results of these rainfed simulations are not reported in this paper, it is worthwhile to point out that in times of drought or in areas where adequate irrigation is not a possibility, the radiative influence of aerosols on evapotranspiration is negative (meaning less water loss) and may be sufficiently larger than their negative influence on the rate of photosynthesis so that the overall influence of aerosols may be an increase in final grain yields.

Perhaps the most immediate observation which can be made from these results is that the change in mean yield as a function of aerosol optical depth is highly dependent on the radiation use efficiency of the crop. RUE itself is dependent on the fraction of radiation that is diffuse. The amount of increase in RUE seems to be the most important

factor in determining the magnitude and in a few cases even the sign of the change in yield. If RUE increases more than 50% over the base value at high diffuse fractions, this increased efficiency frequently offsets the reduction in PAR due to the influence of aerosols, and consequently, yields are predicted to either increase or decrease by much less than if the RUE does not change. Since the amount of the increase induced in RUE by aerosols is not definitively known, it is not at this time possible to confidently predict the magnitude or in some cases, even the sign of the influence of aerosols on crop yield.

The shaded areas of Figure 2.6 represent the most likely range of model predictions based on information presented in this paper. Figure 2.6 is the variably cloudy case where the number of overcast days in a growing season is based on information in the meteorological files. The maximum change in RUE at high diffuse fractions is assumed to be between 0% and 50% higher than the base RUE for maize (a C4 plant). For wheat (C3), this change is assumed to be between 50% and 75%, and for rice (also C3, but with a much higher LAI), this change is assumed to be between 75% and 100%. A worst-case scenario of AOD over the entire growing season for most of these locations is probably in the range of 0.4-0.6, although a rural site such as Iowa is likely to be a bit lower than that and is probably very similar to the SGP ARM site in Figure 1.2 (i.e. AOD=0.1-0.3). Based on these assumptions, the influence of aerosols is predicted to cause an approximately 10% reduction in maize yields at the Florida and India sites and an approximately 5% reduction at the Iowa site, a 0-10% decrease in rice yield at all modeled sites, an approximately 10% reduction in wheat yield in India, and an approximately 5% reduction in wheat yield grown in the Midwestern United States.

2.5 Conclusion

The atmospheric concentration of anthropogenic aerosols can be significant in many important agricultural areas around the world. The radiative influence of these aerosols is quite likely influencing global crop yields, although the magnitude and even the sign of this influence has not been determined. The presence of aerosols in the atmosphere simultaneously decreases PAR and increases the fraction of PAR which is diffuse. Increasing the diffuse fraction increases the radiation use efficiency of a plant. The magnitude of this increase is not definitively known and most likely varies by species, cultivar, stage of development, irradiance level, LAI, and stress level. On clear sky days, aerosols both significantly decrease the amount of PAR reaching the surface and increase the diffuse fraction. On overcast days, aerosols decrease PAR without significantly changing the diffuse fraction. Therefore, the influence of aerosols on photosynthesis is more negative on overcast days than on clear days. Consequently, the more overcast days there are in a growing season, the more likely aerosols are to negatively influence agricultural production. Model results were found to be extremely sensitive to the initial assumption concerning the magnitude of the change in RUE with an increasing diffuse fraction. The relationship between the diffuse fraction and RUE is not well-known for most species of plant and needs to be determined in order to accurately predict the influence of aerosols on crop production. Using the most likely set of assumptions concerning AOD and ΔRUE, the influence of aerosols is predicted to reduce maize yields by approximately 10% at all examined sites, increase rice yields by 20% in California's central valley, slightly increase rice yields in Thailand, reduce rice and wheat yields by 5-10% India, and cause essentially no change in wheat yield grown in the Midwestern United States. These model simulations were performed by stipulating that the plants experienced no water or nutrient stress. The results from these

simulations strongly suggest the need for a more comprehensive study that will examine the influence of aerosols on temperature and evapotranspiration, the indirect effect of aerosols on clouds and precipitation, and the influence of water and nutrient stress.

PART II.

THE REAL−TIME MEASUREMENT OF THE WATER−INSOLUBLE AEROSOL SIZE DISTRIBUTION

A NEW REAL-TIME TECHNIQUE TO MEASURE THE SIZE-DISTRIBUTION OF WATER-INSOLUBLE AEROSOLS: INSTRUMENT DEVELOPMENT

Abstract

To date, there has been much research into the size distribution of ambient atmospheric aerosols, particularly either the total aerosol population or water-soluble ionic species such as sulfate or nitrate. Meanwhile, there have been virtually no size-resolved measurements of water-insoluble aerosols (WIA). This has been due to a lack of practical measurement technology rather than a reflection of the importance of WIA to climate and health. Particle solubility influences the planetary radiation balance both directly and indirectly: solubility influences both the amount of hygroscopic growth (and thus light scattering) which occurs as a function of relative humidity and the ability of particles to serve as cloud condensation nuclei (and thus the lifetime and albedo of clouds). Also, recent information suggests that WIA may be harmful to human health. To address these concerns, a new real-time technique has been developed to measure the size-resolved concentration of WIA. This technique involves the entrainment of particles into a liquid stream and measurement of the WIA size distribution using a liquid optical particle counter. The time resolution of this instrumentation is approximately four minutes (depending on flow rate) and is capable of sizing and counting insoluble particles with diameters 0.25-2.0 μm at atmospheric concentrations as low as 0.1 cm^{-3}. Laboratory characterization using polystyrene latex spheres shows agreement within ±5% of the liquid stream and air stream particle concentrations when adjusted for flow rate. The instrumentation was field-tested at a rural site on the edge of the metro-Atlanta urban area. During this test, WIA concentration averaged 5% of the total particle concentration between 0.25-2.0 μm but reached as high as 35%.

3.1 Introduction

The scattering and absorption by aerosols of incoming solar radiation alters the energy balance of the atmosphere and consequently directly influences climate on both a local and global scale. The magnitude of aerosol light extinction is critically dependent on particle size [*Mie,* 1908]. The diameter of ambient aerosol particles is a complex function of relative humidity and the hygroscopic growth properties of the aerosol [*Hobbs et al.,* 1974]. Particle water-solubility is a key factor in determining the amount of hygroscopic growth an aerosol will experience in a humid atmosphere [*Saxena et al.,* 1995]. This implies by extension that particle solubility greatly influences light extinction by aerosols. The size- and solubility-dependent attenuation of solar radiation by aerosols also influences atmospheric photochemistry [*Dickerson et al.,* 1997] and visibility [*Malm et al.,* 1994; *Husar et al.,* 1995]. In addition, aerosols have an indirect effect on climate by modifying the lifetime [*Albrecht*, 1989] and albedo [*Twomey,* 1974] of clouds. The extent to which a particle is able to function as a cloud condensation nucleus (CCN) is also dependent on particle water-solubility [*Saxena et al.,* 1995; *Hanel*, 1976; *Laakonsen*, 1998]. Theoretical estimates have shown that the insoluble mass fraction of an aerosol influences the ability of an aerosol to become activated to form a cloud droplet [*Laakonsen,* 1998; *Gorbunov*, 1998]. This suggests that the size-resolved insoluble fraction may play a role in cloud formation, lifetime, and precipitation. The dry deposition of aerosols to leaf surfaces may influence the amount of radiation available for plant growth [*Bergin et al.,*2001]. Scanning electron microscopy analysis of particles deposited onto leaf surfaces suggests that water-insoluble particles adhere more stubbornly and are less likely to be removed by rainfall [*ibid.*]. Both the dry deposition velocity and the scattering and absorption of solar radiation by aerosols deposited on leaf surfaces depend on particle size. This implies a need for size-resolved information

concerning water-insoluble aerosol concentration. The deposition of aerosols into the deep lungs can exert a negative influence on the health of air-breathing organisms. It has been suggested that insoluble soot particles modify the properties of lung surfactants and retard alveolar clearance in humans [*Sosnowski et al.,* 2000]. Examination of hospital admissions for cardiac disease in European cities has found that the pollutant most likely responsible is black carbon diesel exhaust [*Le Tertre et al.*, 2002], a water-insoluble atmospheric aerosol. An epidemiological study in Atlanta, Georgia also found a high correlation between the concentration of elemental carbon and cardiovascular emergency department visits [*Metzger et al.,* 2004]. These results suggest that water-insoluble aerosol (WIA) may be harmful to human health. The processes governing alveolar deposition are functions of particle diameter, again suggesting the importance of size-resolved measurements of WIA.

There is a significant amount of information available in the literature on the size-resolved chemical composition of water-soluble ionic species, in particular sulfate and nitrate [*Milford and Davidson*, 1987]. In addition to water-soluble ions, carbon (elemental carbon and various organic compounds) has been found to be a considerable fraction of the submicron aerosol mass in urban regions [*Gray et al.,* 1986; *Sloane et al.*, 1991; *McInnes et al.,* 1998; *Bergin et al.,* 2001]. Recent work suggests that a portion of the submicron aerosol mass in urban areas can be insoluble in water. A comparison of several sites around the world indicate that the fraction of organic carbon not soluble in water ranges from 30-80% [*Saxena and Hildemann*, 1996]. Insoluble mass fractions for fine mode aerosol at a few sites in Europe have been reported to be 25-35%, with organic compounds being responsible for ~10% of the insoluble mass [*Zappoli et al.,* 1999]. Measurements made by our group in the Yangtze delta region of China in November 1999 indicate that ~40% of the fine mode (D_p<2.5 μm) mass was water-insoluble organic carbon [*Xu et al.,* 2002]. Shipboard measurements made in the East

Atlantic Ocean during the second Aerosol Characterization Experiment in 1997 found that 30-60% of the submicron organic carbon aerosol was insoluble in water [*Novakov et al.,* 2000]. Although it is expected that the submicron mode may contain a fraction of water-insoluble windblown dust, depending on the specific location, these recent results suggest the submicron mass also contains water-insoluble organic compounds. Supermicron aerosol mass frequently contains significant quantities of insoluble mineral dust. The measurements discussed above are filter-based (and thus have very poor time-resolution) and are not size-resolved. Consequently, it should be pointed out that there is not a great deal of information in the literature concerning the size-distribution of water-insoluble aerosol.

It is also likely that the size-resolution of WIA will yield information on the atmospheric processing to which ambient particles have been subjected. The ratio of water soluble to insoluble mass in the coarse mode may give an indication of the degree to which heterogeneous reactions have occurred on aerosol surfaces (e.g. the reaction of nitric acid with calcium containing crustal particles). In addition, the relative amount of insoluble to total aerosol carbon in the accumulation mode may indicate the extent to which aerosols have been oxidized to more polar, water-soluble compounds during transport.

3.2 Experimental approach

A novel technique has been developed to measure the number size distribution of WIA in near real-time. This technique involves capturing atmospheric aerosol particles in filtered ultrapure water and measuring the WIA size distribution with a liquid laser particle counter. Figure 3.1 shows a schematic diagram of the experimental setup. Air is drawn through an impinger (SKC Biosampler) which impacts aerosol particles into a

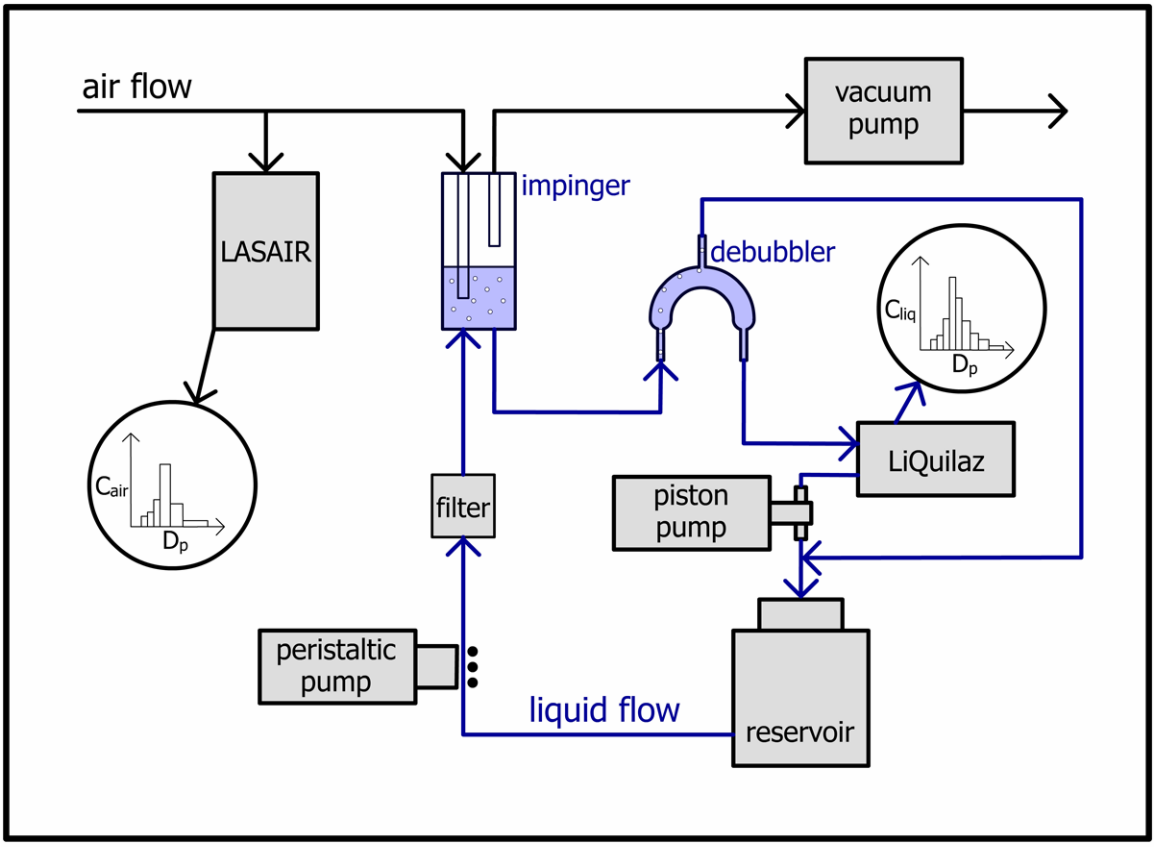

FIGURE 3.1. Schematic diagram of the WIA instrument setup

20 mL water reservoir. The impinger has been documented by the manufacturer to have a collection efficiency ranging from 80% for 0.3 μm particles to ~100% for particles greater than 1.0 μm. The SKC Biosampler is specifically designed to collect particles in a gentle manner without causing them to break apart upon impaction (the manufacturer's original objective is to collect bacteria without killing them). The air flow through the impinger jets is at sonic speed and is quite stable at a rate of approximately 12 $L \cdot min^{-1}$ (although sonic flow is a function of temperature and pressure).

The impinger's inlet liquid flow is filtered with a 0.1 μm pore-size Millipore filter and is then pushed into the impinger. For the experiments reported in this paper, the impinger liquid was ultrapure water. The same technique, however, could conceivably be used

with other solvents. The process of mixing the air and liquid streams in the impinger generates air bubbles in the liquid stream. These bubbles are removed by a passive glass debubbling device shaped like an inverted U. In the first half of the debubbler, the flow is in the same direction as the rise of the bubbles. At the top of the inverted U, bubble-laden water is removed and returned to the reservoir. In the second half of the debubbler, flow is in the opposite direction of the bubble rise and has a velocity of about 0.3 $cm \cdot s^{-1}$, approximately the same as the terminal rise velocity of a 3.0 μm bubble (i.e. bubbles larger than 3.0 μm will rise faster than the flow descends). Lab tests involving particle-free inlet air have indicated that large bubbles are effectively removed from the liquid stream. The flow is laminar throughout the debubbler, and the total residence time is less than 30 seconds. The liquid flow through both the impinger and debubbler is maintained by a peristaltic pump located upstream of the impinger and filter and is controlled by Omega Engineering FLV401 flow controllers. The liquid flow rate into the impinger is controlled at a rate which may be adjusted according to ambient particle concentration in order to produce a reasonable dilution factor. A typical flow rate for moderate water-insoluble particle concentration is 50 $mL \cdot min^{-1}$.

The liquid stream exiting the debubbler is sampled by a Particle Measuring Systems LiQuilaz-SO2 laser particle counter. The sample cell within the instrument is composed of a sapphire capillary tube with an inner diameter of approximately 1 mm. The LiQuilaz uses a 780 nm wavelength laser and measures the total integrated light scattered from 9 to 45° relative to the forward direction of the laser. It is capable of counting and sizing particles having diameters from 0.25->2.0 μm. The liquid flow rate through the instrument is 20 $mL \cdot min^{-1}$ and is driven by a Fluid Metering, Inc. Model QV ceramic piston pump located downstream of the particle counter. This flow is controlled by the positive displacement of the piston pump and the pump speed.

The relationship between the concentration of water-insoluble particles of a given size in the atmosphere to the concentration in the sample liquid is as follows:

$$C_{air,i} = C_{l,i} \frac{Q_l}{Q_{air}} \qquad (3.1)$$

where $C_{air,i}$ is the concentration of water-insoluble aerosol particles of size *i* in the atmosphere, $C_{l,i}$ the concentration of water-insoluble aerosol particles of corresponding size *i* in the impinger liquid, Q_l the liquid flow rate through the impinger, and Q_{air} the flow rate of air through the impinger.

Laboratory validation of this instrumentation was performed using Duke Scientific Corporation nanospheres. These polystyrene latex (PSL) particles are spherical, have a uniform and well-characterized index of refraction, are monodisperse, and are available in many sizes. PSL sizes used for this laboratory characterization ranged from 0.4-1.6 μm. Aerosol samples were created by atomizing the PSL spheres in ultrapure water and then passing the sample through a silica desiccant chamber to remove any residual water. This sample was supplemented with filtered air so that the combined flow rate of the PSL + clean air would equal the combined flow rates of the LASAIR and the air flow through the impinger. The concentration of PSL could be controlled by adjusting the flow rate through the atomizer. Any change in the atomizer flow rate would passively result in a corresponding change of opposite sign in the filtered air flow rate such that the total flow was constant. The size-resolved aerosol number concentration in the air stream was measured with a Particle Measuring Systems LASAIR 1002. The size distribution in the liquid stream was measured with a Particle Measuring Systems LiQuilaz-SO2 as mentioned previously. Given that PSL is completely insoluble in water, the concentrations measured by the LASAIR and the LiQuilaz were expected to agree with one another after adjustment according to equation (3.1). In addition, it should be noted

TABLE 3.1. Size-resolved detection limit of the WIA measurement apparatus in terms of both liquid concentration and equivalent air concentration based on a liquid flow rate of 50 $mL \cdot min^{-1}$.

channel	size range [μm]	detection limit [$\#\cdot mL^{-1}_{liquid}$]	detection limit [$\#\cdot cm^{-3}_{air}$]
1	0.25-0.3	177	0.71
2	0.3-0.35	97.5	0.39
3	0.35-0.4	57.1	0.23
4	0.4-0.45	33.5	0.13
5	0.45-0.5	20.6	0.08
6	0.5-0.6	23.7	0.09
7	0.6-0.7	12.7	0.05
8	0.7-0.8	9.2	0.04
9	0.8-0.9	9.5	0.04
10	0.9-1.0	9.8	0.04
11	1.0-1.1	10.5	0.04
12	1.1-1.25	15.6	0.06
13	1.25-1.5	13.6	0.05
14	1.5-2.0	5.8	0.02
15	> 2.0	164	0.66

that the LASAIR 1002 uses 8 channels to size particles between 0.1 and >2.0 μm while the LiQuilaz uses 15 channels between 0.25 and >2.0 μm.

3.3 Results and discussion

3.3.1 Laboratory characterization

The detection limit of the WIA measurement apparatus for each particle size is shown in Table 3.1. The average background concentration and standard deviation for the ultrapure water stream was determined for each channel when filtered air was

passed through the impinger. The detection limit is assumed to be twice the standard deviation of the background concentration.

An important objective of the development of this apparatus is to measure WIA with very fine time resolution. The time resolution of the instrumentation is determined by the amount of time required for the liquid particle counter to respond to changes in ambient concentration. This response time in turn is limited by the combined residence time of the impinger and debubbler. This residence time is less than two minutes. Figure 3.2 shows a time series plot of C_{air} measured by the LASAIR and estimated by the LiQuilaz according to equation (3.1) versus time. This plot shows a fifteen minute long pulse of 0.8 μm PSL introduced into the system at time = 0. The LASAIR responds to changes in PSL concentration in less than a minute (depending on the length of the inlet tube). The LiQuilaz responds one residence time after the LASAIR (approximately one to two

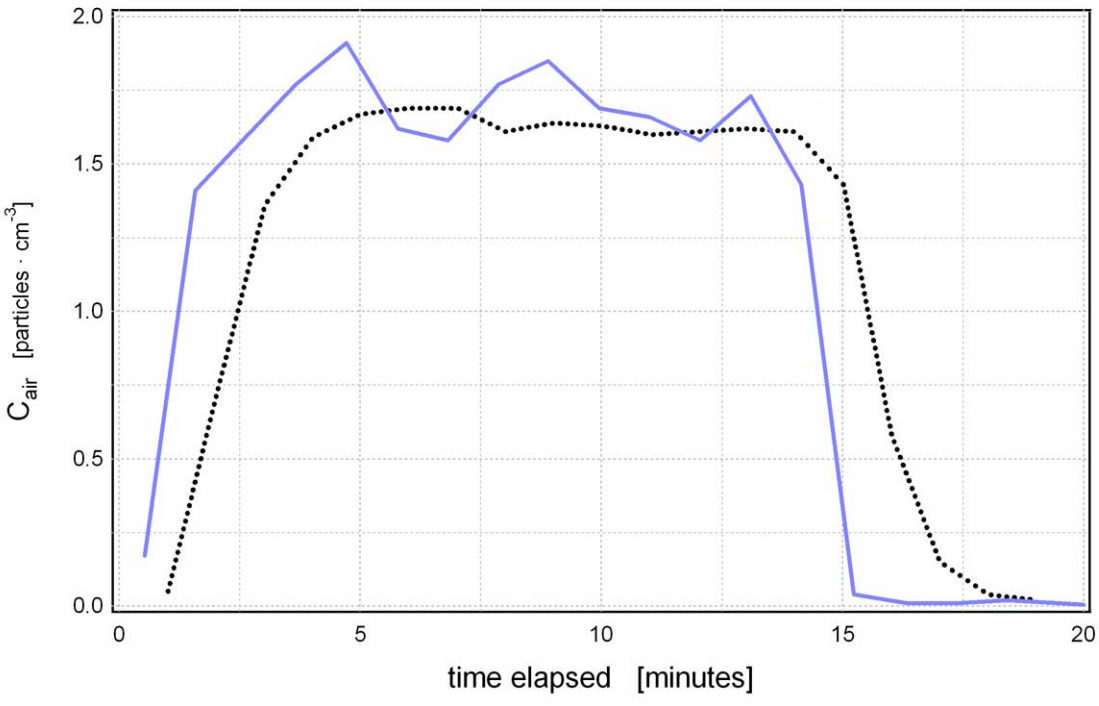

FIGURE 3.2. Time response of the WIA measurement apparatus. At time = 0, a 15 minute pulse of 0.8 μm PSL was introduced into the system. LASAIR LiQuilaz

minutes). The LASAIR clearly shows fluctuations in atomizer output during the time the pulse is turned on. As a consequence of mixing with particle-free water in the debubbler, these peaks are somewhat flattened by the LiQuilaz. At time = 15 minutes, the pulse is turned off. The LASAIR concentration returns to zero in less than a minute (the time between the collection of data points). At this time, the PSL concentration in the debubbler water begins an exponential decay, and in approximately four minutes, the LiQuilaz records a concentration equal to 1/*e* times the concentration of the pulse. It should be noted that a faster response is possible by increasing the liquid flow rate through the impinger, although doing so would also increase the dilution factor as calculated according to equation (3.1). This is acceptable for high ambient WIA concentrations, but when concentrations are low, it is necessary to make sure the liquid concentration is above the detection limit at all pertinent particle sizes.

The upper concentration limit of optical particle counters is limited by the coincidence of more than one particle passing through the laser beam simultaneously [*Jaenicke,*1972]. When this occurs, the photo-detectors measure the light scattered by both particles and infer that just one particle of a larger size had passed through the beam. Hence, when the coincidence limit of a particle counter has been reached, the measured particle concentration is lower than the actual concentration, and the measured size distribution shifts to larger particle diameters. The coincidence limit is typically defined as the point at which error is 5 or 10% and is a function of particle diameter. It is expected to be highest at small particle sizes (i.e. the concentration required for two large particles to be in the beam simultaneously is lower than for two small particles.)

The performance of the LiQuilaz was tested for six sizes of PSL spheres at concentrations ranging from below the detection limit to above the coincidence limit. Figure 3.3 shows the results of these laboratory tests. Each data point on these charts

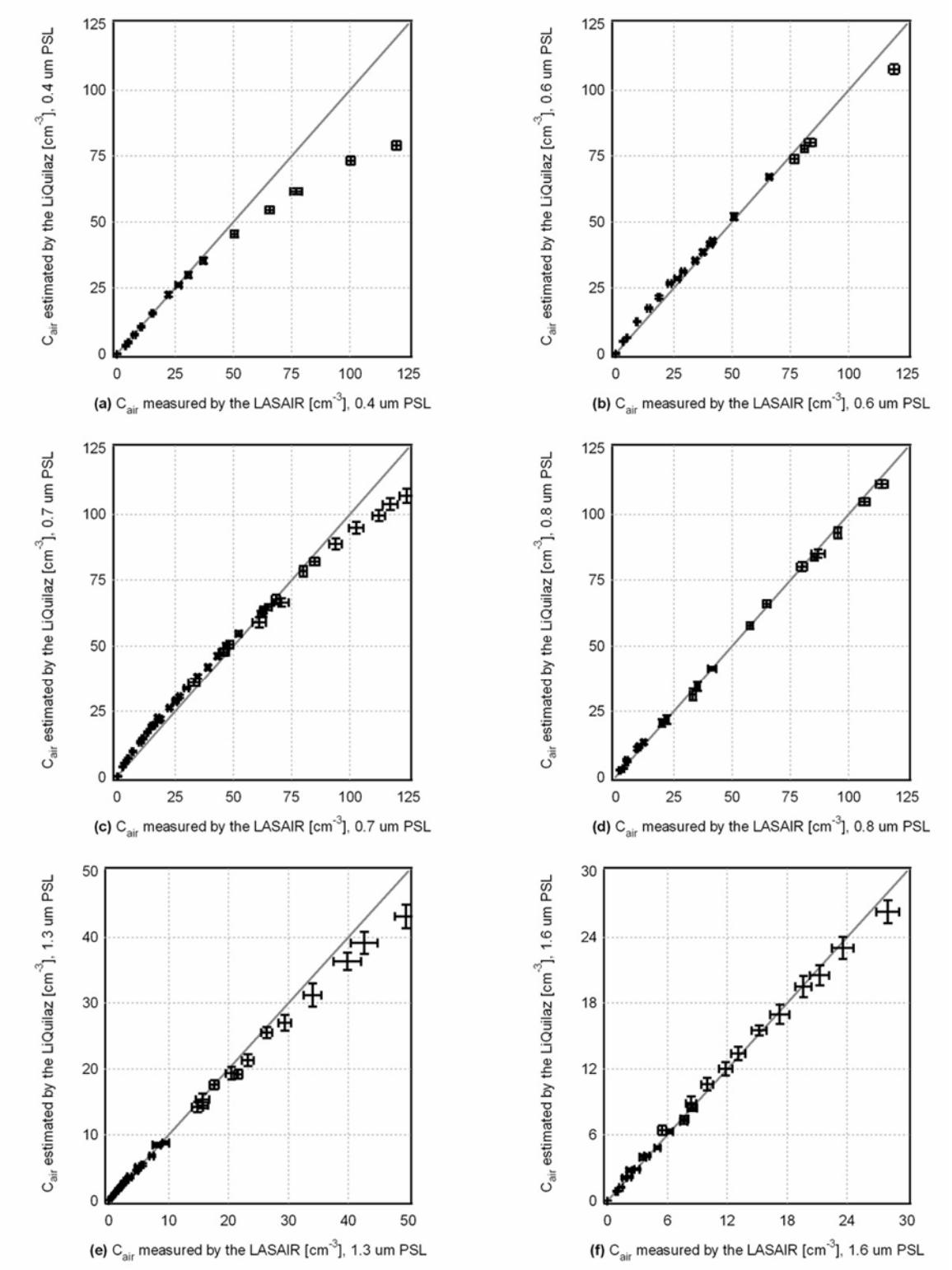

FIGURE 3.3. Comparison of PSL concentrations measured by a LASAIR 1002 (x-axis) with those estimated by a LiQuilaz SO2 (y-axis).

represents the average of approximately 20 minutes of sampling at a particular atomizer flow rate. The concentration of PSL produced by the atomizer at each flow rate is relatively constant over the time period sampled. Error bars on the charts represent the standard deviation of the PSL concentration produced by each atomizer flow rate. The diagonal line on each chart is a 1:1 line. Since PSL is completely insoluble in water, all data points were expected to fall on the 1:1 line until the coincidence limit was reached. Observations largely agree with this expectation, providing evidence against significant particle loss in the debubbler or sampling lines. The concentration at which the data points begin to deviate from the 1:1 line is interpreted as the coincidence limit for that particle size.

For 0.4 μm PSL, the coincidence limit was approximately $50 \cdot cm^{-3}_{air}$, for 0.6, 0.7, and 0.8 μm PSL, the coincidence limit was found to be between 75 and $100 \cdot cm^{-3}_{air}$. For 1.3 μm PSL, the coincidence limit was lower (as expected for a larger particle diameter) and was observed to be approximately $30 \cdot cm^{-3}_{air}$. For 1.6 μm PSL, the coincidence limit was not clearly apparent. This was due to the fact that high concentrations of large diameter PSL are difficult to achieve with this atomizer setup. Even though Figure 3.3f does not clearly illustrate the coincidence limit for 1.6 μm PSL, it does show very good agreement between the LiQuilaz and the LASAIR at concentrations up to $25 \cdot cm^{-3}_{air}$. The maximum ambient concentration of all insoluble particles larger than 1.3 μm yet recorded by our instrumentation is less than $1.0 \cdot cm^{-3}_{air}$. It should be pointed out that these calibration tests were performed with monodisperse aerosols, whereas ambient aerosol populations are typically polydisperse. According to the manufacturer's specifications, the total concentration of polydisperse insoluble particles should not exceed $10000 \cdot mL^{-1}$ liquid. This corresponds to approximately $50 \cdot cm^{-3}_{air}$, depending on the impinger liquid flow rate. Using the instrumental operating conditions described above, there is greater than 95%

agreement between the LiQuilaz and the LASAIR when sampling PSL spheres. The impinger's liquid flow rate may be adjusted in response to ambient insoluble particle concentrations so as to keep the liquid concentration below the coincidence limit of the LiQuilaz.

Another important concern during the development of this instrument was that the liquid particle counter only measure insoluble particles and not residual amounts of soluble particles still present in the solid phase. To confirm that the instrumentation was meeting this criterion, a test was performed using both soluble and insoluble particles. The soluble species chosen for this test was ammonium sulfate, $(NH_4)_2SO_4$, a common constituent of atmospheric aerosols. Figure 3.4 shows the resulting number size distributions from both the LASAIR and the LiQuilaz. For the distribution shown in Figure 3.4(a), only 0.4 μm PSL spheres are present. The size distributions of the two

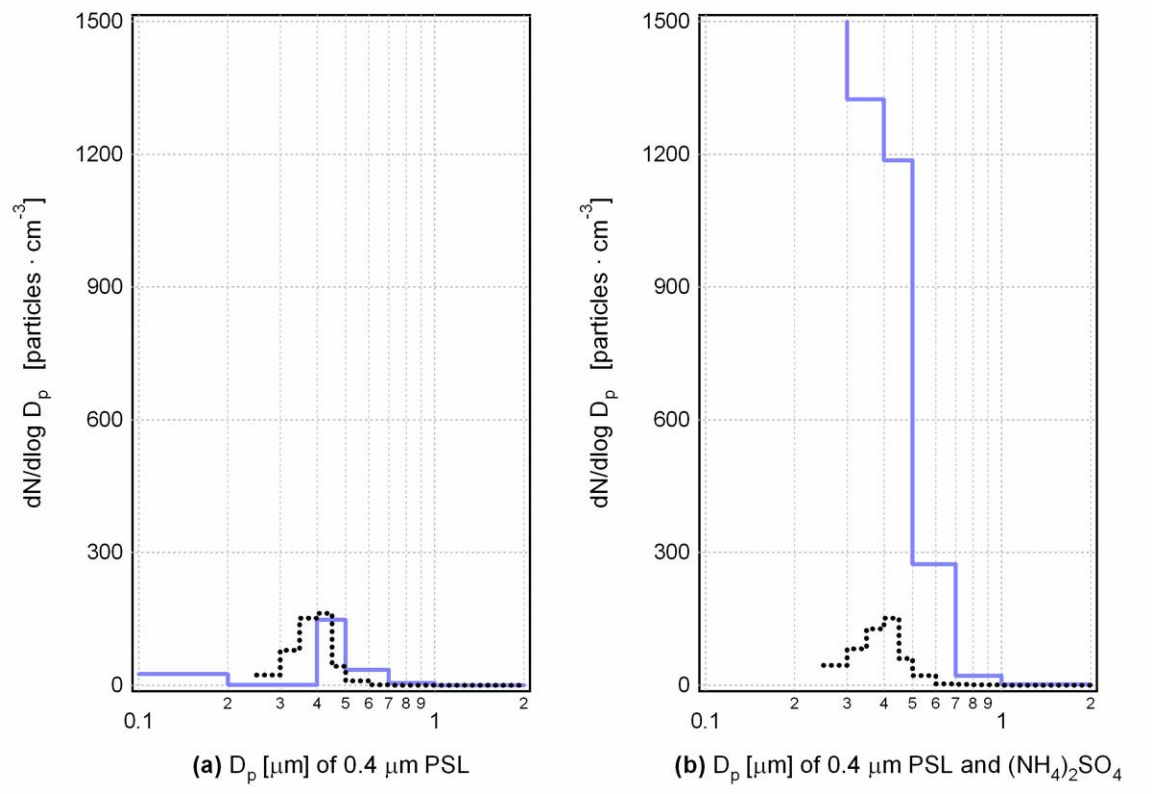

FIGURE 3.4. Particle size distributions recorded by the ——— LASAIR and ····· LiQuilaz when **(a)** 0.4 μm PSL and **(b)** both 0.4 μm PSL and $(NH_4)_2SO_4$ are introduced.

instruments agree well with another, given that their respective size channels do not exactly match one another. For the size distribution shown in Figure 3.4(b), a small amount of $(NH_4)_2SO_4$ was introduced into the atomizer. The LASAIR clearly detects the $(NH_4)_2SO_4$ particles, mainly at small diameters (< 0.5 μm). These particles are dissolved after contact with the water in the impinger and debubbler, and the LiQuilaz only detects the insoluble PSL particles. Ammonium sulfate is a very soluble ionic species, and as such, it is not surprising that it dissolves quickly in the impinger. Many organic species present in the atmosphere, however, have much lower solubility limits. Aqueous concentrations of these species in the impinger are likely to be orders of magnitude lower than found in cloud droplets, and consequently, this system may not detect slightly soluble substances which exist in the solid phase in the atmosphere.

3.3.2 Possible sources of measurement uncertainty

There are several important differences between the sampling conditions used in the laboratory characterization and those encountered when measuring ambient aerosols. These include differences in the refractive index, shape and size of ambient particles as compared with PSL. As has been reported many times in the literature [*Whitby and Vomela*, 1967; *Quenzel*, 1969; and others], the complex refractive index, $m = n + k \cdot i$, has a significant influence on the size measured by optical particle counters. For the PSL calibration standard, $m = 1.59 + 0.0\ i$ at 780 nm. The refractive index of ambient insoluble aerosol is highly variable depending on particle composition and is frequently substantially different from that of PSL. Ambient insoluble aerosols are typically composed of some combination of three classes of compounds: mineral aerosols, insoluble organic carbon, or elemental carbon (soot). For most mineral aerosols, $n = 1.5 - 1.6$ and $k \sim 0.0$ at visible and near-visible wavelengths [*Sokolik and Toon*, 1999]. The composition of organic aerosol is very complex and may involve any of thousands of

different compounds; however, classes of organic compounds which are water-insoluble tend to have n = 1.45 - 1.55 and k = 0.0 [*Lide*, 2004].

In comparison to either organic or mineral aerosols, the refractive index of ambient soot particles is highly variable. Single particle experiments to measure the optical properties of 1.5-8 μm diameter solid carbon spheres have found $m = 1.7 + 0.12\,i$ at λ = 488 nm [*Pluchino et al.*, 1980]. These experiments are not likely to be representative of ambient soot particles however, since transmission electron microscopy (TEM) analysis has repeatedly revealed that combustion-generated soot is composed of chain agglomerates of 20-60 nm diameter carbon spherules [*Medalia and Rivin*, 1982]. Early research to determine the refractive index of combustion soot found that both the real and imaginary portions of m depend on the amount of air contained within the particles and estimated that the refractive index of the bulk material is $m = 1.84 + 0.46\,i$ with little variation across the visible spectrum [*Medalia and Richards*, 1972]. Other measurements have determined m also depends on the hydrogen-carbon ratio of the soot particle with more non-carbon mass leading to higher values of n and lower values of k [*Batten*, 1985]. This same work found that m varies noticeably across the spectrum (about +10% for the real part between 500 and 740 nm) and in the case of compressed soot derived from a kerosene fuel, $m = 1.39 + 0.27\,i$ at λ = 740 nm. An oft-cited examination of the wavelength dependence of m experimentally determined an expression for both n and k as a function of wavelength and found that $m = 1.76 + 0.56\,i$ at λ = 710 nm for propane soot in the flame zone [*Chang and Charalampopoulos*, 1990]. It is important to note that the mean particle radius measured during these experiments was 30 nm, and as such, these results may be more representative of carbon spherules rather than chain agglomerates (indeed, this value agrees well with the earlier-cited value for the bulk material). Recent experimental and modeling work by *Hull et al* [2004]

used a coupled-dipole approach to describe the optical behavior of chain agglomerates and found a linear relationship between particle fill density and the apparent refractive index. Agglomerates with a fractal-like morphology and many open spaces have low *n* and *k* while dense agglomerates more closely represent a filled-sphere and have a refractive index close to that of bulk carbon. TEM analysis of diesel soot by *Park et al.* [2004] examined the relationship between the projected area diameter (closely related to the electrical mobility diameter) and the maximum length of the chain agglomerate and determined a power relationship of length = $0.44 \cdot D_p^{1.26}$. The ratio of the volume calculated from the projected area diameter to that calculated from the maximum length corresponds to particle fill density. The relationship determined by *Park et al*. suggests that soot particle fill density ranges from 40% for a 0.1 μm maximum length particle to 10% for a 1.0 μm particle. According to the relationship predicted by *Hull et al*., the refractive index of soot particles ranging from 10-40% filled would be $m = 1.1 + 0.1\,i$ to $m = 1.2 + 0.2\,i$ at $\lambda = 532$ nm.

Particle morphology influences light scattering in that a particle may be oriented in the sample volume such that a surface greater or less than its characteristic length is exposed to illumination. *Hull et al.* suggests that a population of randomly oriented diesel soot particles may optically behave in a very similar fashion as a spherical particle whose diameter is the same as the maximum distance between spherules in the agglomerate, provided that the particle's elongation and porosity falls within certain bounds. The experimental portion of this study indicated that diesel soot tended to meet these criteria.

A third important physical property of an aerosol which influences the amount of light it may scatter is particle size. Sampling studies using cascade impactors to examine the size-resolved concentration of various atmospheric aerosol species have found

significant amounts of mass with aerodynamic diameters smaller than the cutoff diameter for the LiQuilaz. *Venkataraman and Friedlander* [1994] found approximately 75% of the elemental carbon mass in the Los Angeles area in the summer season had aerodynamic diameters less than 0.25 μm while during the winter, this fraction was approximately 15%. Speciation analysis of particles collected in central Europe in 1997-1998 found that on average, 28% (by number) of soot particles had aerodynamic diameters less than 0.2 μm [*Ebert et al.,* 2004]. The detectable size range of the LiQuilaz is 0.25-2.0 μm, or put another way, this instrument is able to detect particles which scatter a greater or equal amount of light as a 0.25 μm PSL sphere. Although impactor studies suggest that a significant amount of insoluble particles are smaller than this minimum diameter, as is explained in the following paragraph, it is conceivable that some particles with a physical size less than 0.25 μm may scatter more light than a 0.25 μm PSL sphere. Nonetheless, it should be pointed out that this method of measuring the WIA size distribution is likely unable to detect a significant fraction of particles with diameters smaller than 0.25 μm.

Figure 3.5 shows our results of Mie theory analysis for hypothetical spherical particles of several different refractive indices using the specific operating parameters of the LiQuilaz. This analysis was performed using a modified version of the Mie theory algorithm put forth by *Wiscombe* [1980]. This plot shows scattered light normalized to incident light as a function of diameter. These results are for a wavelength of 780 nm with water as a medium and represent light scattered from 9-45°, the range of angles measured by the LiQuilaz. Since the instrument sizes particles based on a calibration using PSL nanospheres, curves to the left of the PSL curve represent particles which will be oversized by the instrument, and curves to the right represent undersized particles. Solid lines are for non-absorbing refractive indices as would be expected for insoluble

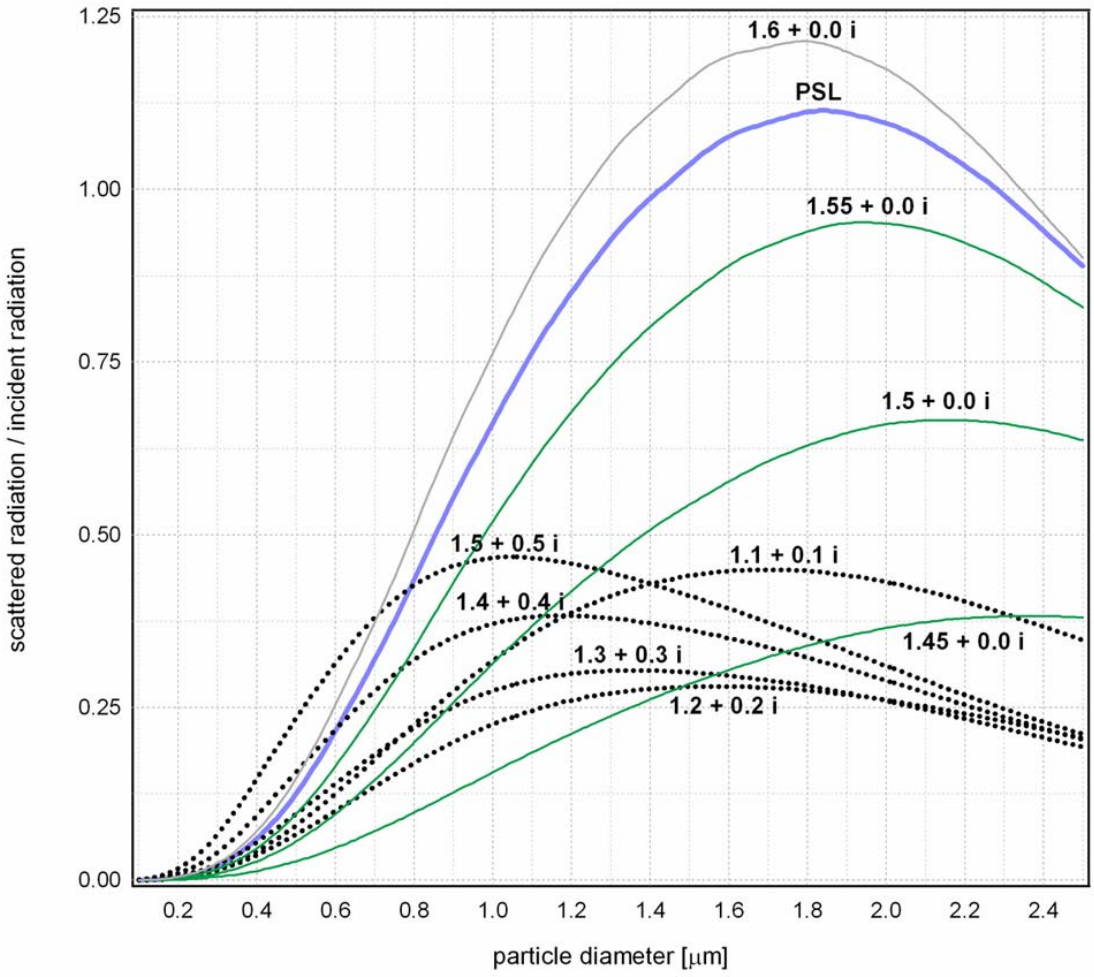

FIGURE 3.5. Predictions of relative light scattering as a function of particle size and refractive index based on a Mie theory algorithm. These model estimates are specific to the conditions of the LiQuilaz: $\lambda = 780$ nm, scattering is measured from 9º - 45°, and the scattering medium is water ($m = 1.33 + 0.0\ i$).

organic material, and dotted lines are for absorbing refractive indices. Since the refractive index of the medium is 1.33 + 0.0 *i*, the best scatterers under the conditions of the LiQuilaz are particles with a refractive index either significantly greater or less than 1.33 + 0.0 *i*. This theoretical analysis suggests that for most particles smaller than 0.6 μm, the LiQuilaz is able to provide a reasonable estimate of the optical diameter, though with a tendency to undersize particles by no more than 30%. Two exceptions to this statement are non-absorbing particles with a weak scattering component (*n* ~ 1.45)

which are undersized to a greater extent (approaching 50%) and strongly scattering absorbing particles (m = 1. 5 + 0.5 i) which are oversized by up to 30%. In the particle size range 0.6-1.0 μm, the difference in refractive indices of the particles becomes more pronounced such that a 1.0 μm absorbing particle may be undersized as much as 40% and a non-absorbing n = 1.45 may be undersized by 100%. It is important to notice that the maximum amount of scattering predicted for a soot particle is equivalent to that scattered by a 0.8 μm PSL sphere. In other words, it is impossible for a particle reported by the LiQuilaz to be larger than 0.8 μm to be composed of soot.

Finally, it is important to point out that this near real-time technique does not provide information on the mixing state (internal versus external) of the water insoluble atmospheric aerosols. For instance, a 0.5 μm water-insoluble aerosol particle measured by the LiQuilaz could have existed in the atmosphere as either an insoluble aerosol particle having a diameter of 0.5 μm, or a 0.5 μm insoluble particle coated with some amount of water soluble mass. Likewise, internally-mixed particles present in the atmosphere which contain insoluble cores with optical diameters less than 0.25 μm will not be detected at all by this instrumentation. In addition, it is possible that some particles may be broken by the impinging process or by the bursting action of bubbles and create fragments too small to be detected.

3.3.3 Ambient measurements

An initial field test of the WIA measurement apparatus was performed in conjunction with the Fall-Line Air Quality Study in August 2002. The sampling site for this study was a rural location near Griffin, Georgia on the southern edge of the metro-Atlanta region. Figure 3.6 shows a time series of the number concentration of particles between 0.25 and 2.0 μm recorded August 5-9, 2002. In this size range, the fraction (by number) of the

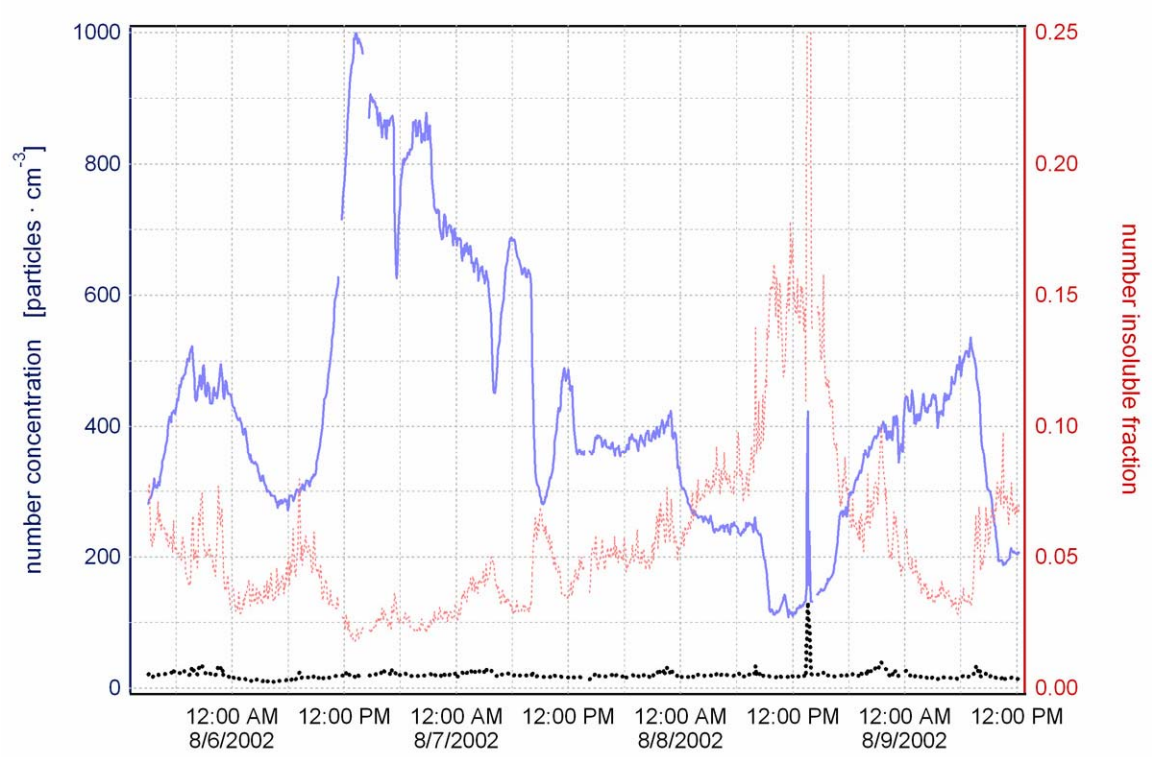

FIGURE 3.6. Field test of water-insoluble aerosol instrumentation near Griffin, Georgia. total particle concentration, ····· water-insoluble aerosol concentration, ····· insoluble fraction (by number). All data is of the size range 0.25 - 2.0 μm.

ambient aerosol which was water-insoluble averaged about 5% but fluctuated quickly and greatly and reached as high as 35%. Occasional spikes in both the total aerosol and the WIA concentration were observed with time resolution as fine as three minutes. During the largest of these spikes on the afternoon of August 8, the WIA concentration increased by two orders of magnitude within ten minutes, remained at that level for thirty minutes, and then returned to the previous level.

Figure 3.7 shows the number size distribution averaged over the four-day period shown in Figure 3.6. The number concentration was dominated by the smallest particles and spanned four orders of magnitude across the size distribution. In addition, the number concentration exceeded the detection limit by 2-3 orders of magnitude at all

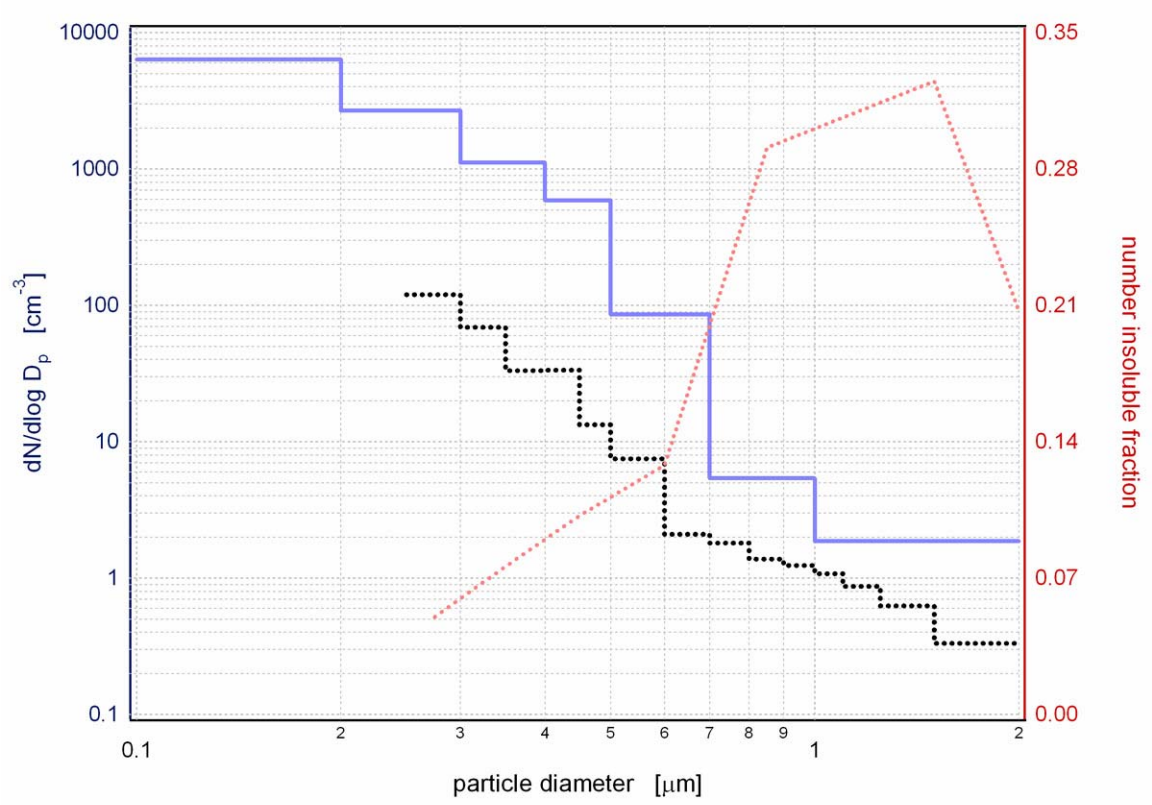

FIGURE 3.7. Number size distribution for the Griffin, Georgia field test averaged over the four days shown in Figure 3.6. ——— total particle concentration, ····· water-insoluble aerosol concentration, ····· number insoluble fraction.

sizes. For this week-long period, the insoluble fraction shows a peak of 30% between 1.0-1.2 μm.

A surprising finding of this sampling campaign was that the average insoluble fraction measured using this real-time technique was significantly lower than the fraction of organic carbon determined to be water-insoluble by previous investigators based on the analysis of filter samples. A possible explanation for this discrepancy is the undercounting of organic aerosols by the particle counter due to their refractive index being more similar to the refractive index of the water medium than that of other insoluble aerosols. In addition, given that organic aerosols frequently exist as a non-aqueous phase liquid, it is possible that organic aerosols are more likely than soot or

mineral aerosols to be broken apart during the impinging and debubbling process. The resulting remnants of a disintegrated organic aerosol would likely be too small to be detected by the particle counter. A final possibility is that the organic compounds determined to be insoluble by other techniques have a finite but small solubility in water. Since the continuously flowing impinger is well-mixed and essentially infinitely-dilute, it is possible that some organic aerosols determined to be insoluble by other techniques may dissolve before reaching the particle counter. Together, these properties of organic aerosols may explain the difference between the insoluble fraction measured using this technique and that determined by analysis of filter samples. As a consequence, this real-time technique may be more useful for measuring soot and mineral aerosols than insoluble organic aerosols.

This initial field test indicates that WIA is present in significant quantities in the atmosphere, that its concentration is variable on time scales too short to be detected by filter analysis, and that its size-distribution is not temporally uniform. Additional work is needed to compare the results of this real-time method with related size-resolved techniques such as cascade impactor filter analysis. Future studies will also focus on characterizing the WIA concentrations at a variety of urban and remote locations in order to determine the factors that influence water solubility of atmospheric aerosol as well as the impact these particles have on hygroscopic growth, cloud condensation nuclei formation and human health.

SIZE-RESOLVED, REAL-TIME MEASUREMENT OF WATER-INSOLUBLE AEROSOLS IN THE CHAMONIX AND MAURIENNE VALLEYS OF ALPINE FRANCE

Abstract

As part of the Pollution des Vallées Alpines (PoVA) program, the number concentration and size distribution of the total $PM_{2.5}$ population as well as the subset that is water-insoluble were measured in the Chamonix and Maurienne Valleys of the French Alps. This program included both summer and winter intensive campaigns in January and June-July 2003. The water-insoluble aerosol (WIA) measurements were performed using a new real-time technique developed at the Georgia Institute of Technology and described by *Greenwald et al*. [2005a]. The concentration of both the total aerosol population and WIA was found to be highly variable on time scales as brief as a few minutes and was generally much higher in winter than in summer. In addition, the fraction (by number) of aerosols which are not soluble in water was also found to be variable and slightly higher in winter. The average insoluble fraction in the size range of 0.25-2.0 μm was approximately 11% in Chamonix in both winter and summer. In the Maurienne Valley, the insoluble fraction was 10% in winter and 8% in summer. Although the number concentration of WIA is dominated by particles smaller than 0.35 μm, a peak is consistently observed between 0.4 and 0.5 μm. Size-resolved filter samples were also collected as part of the PoVA program and were analyzed for EC/OC mass. Comparison of these two data sets suggests that WIA in these valleys is dominated by elemental carbon emissions from motor vehicle traffic. Further analysis also indicates that water-soluble and -insoluble aerosols have sources which are independent of one another both temporally and spatially.

4.1 Introduction

Because of their influence on climate and health, it is important to characterize the size distribution and concentration of water-insoluble aerosols (WIA) at many different locations around the world at various times of year and under a range of meteorological conditions. Since the interaction of insoluble particles with atmospheric water vapor is quite different than that of soluble particles [*Saxena et al.*, 1995], it is important for climate modelers to possess information concerning the relative prevalence of WIA and their size distribution. WIAs exhibit less hygroscopic growth in the presence of water vapor than soluble particles and are also less likely to activate to form a cloud droplet [*Hanel,* 1976; *Laakonsen et al*., 1998]. Both of these properties imply that the influence of WIA on the radiation budget of the planet is different than that of soluble species. Inhalation of fine particulate matter is known to have a deleterious effect on human health [*Peel et al.*, 2005; *Brook et al*., 2002; *Peters et al*., 2001]. Elemental carbon in the form of soot has been observed to have specific properties harmful to lung tissue [*Sosnowski et al*., 2000] and to be highly correlated with cardiovascular problems [*Metzger et al*., 2004; *Le Tertre et al*., 2002]. Despite the relevance of these properties, very few ambient measurements of WIA concentration have been published in the literature, primarily due to a lack of appropriate instrumentation. A new technique to measure the size-resolved number concentration of WIA in near real-time has been developed at the Georgia Institute of Technology and is described in detail by *Greenwald et al*. [2005a]. This instrumentation for the first time provides a relatively easy method to measure in real-time the ambient concentration of WIA at remote locations around the world.

The first full-scale field use of this new technique was in conjunction with the Pollution des Vallées Alpines (PoVA) program in the French Alps in 2003. This program

was established to take advantage of a unique opportunity to determine the influence of transportation sources on the air quality of rugged mountain valleys: the temporary closing of the Mont Blanc tunnel. Most land traffic between the nations of France and Italy is routed on one of two highways between Lyon, France and Turin, Italy. The more heavily-traveled of these highways passes through the Chamonix Valley and crosses the Alps via the tunnel under Mont Blanc. The other highway runs through the Maurienne Valley and passes through the Fréjus tunnel. An accident in 1999 forced the closure of the Mont Blanc tunnel for several years while repairs were made. During this time period, all land traffic was rerouted through the Maurienne Valley. The PoVA program was begun in 2000 to make detailed measurements of all aspects of the air quality in these two valleys both before and after the reopening of the Mont Blanc tunnel. To meet this goal, intensive sampling campaigns were conducted in each valley in both summer and winter 2000 and again in the winter and summer of 2003. The WIA sampling system was only used during the last two campaigns in January and June-July 2003 after the tunnel had been reopened.

In addition to demonstrating the field performance of the insoluble aerosol measurement system, this paper is intended to provide detailed information concerning the size distribution and concentration of WIA in these valleys and to describe the temporal variability of these values on both a long and short term scale. By comparing the data retrieved from the WIA sampling apparatus with that gathered by other components of the PoVA program, it is also possible to examine possible sources for WIA, to infer some information concerning the chemical speciation of WIA, and to observe the behavior of WIA under the influence of various atmospheric processes such as precipitation events and changes in solar insolation and atmospheric humidity.

4.2 Experimental approach

4.2.1 Instrumentation

The number size distribution and concentration of WIA were measured using a newly developed real-time technique. This system uses an SKC Biosampler impinger to entrain particles into a circulating water stream. Filtered, ultrapure water is pumped into the impinger chamber where it is mixed with ambient air. The impinger has a very high collection efficiency (>90%) at all measured particle sizes. The liquid outflow from the impinger is sent through a passive debubbling device and then through a Particle Measuring Systems LiQuilaz SO2 optical particle counter. The concentration of WIA in the air may be calculated from the measured concentration in the liquid by the following equation:

$$C_{air,i} = C_{l,i} \frac{Q_l}{Q_{air}} \qquad (4.1)$$

where $C_{air,i}$ is the concentration of particles of size *i* in the air, $C_{l,i}$ is the concentration of particles of size *i* in the liquid, Q_{air} is the flow rate of ambient air, and Q_l is the liquid flow rate.

The LiQuilaz SO2 uses a 780 nm wavelength laser and detects light scattering from 9-45° relative to the forward direction of the light source. This instrument uses a liquid medium for light scattering which in the case of this study was water. The refractive index of water is 1.33 + 0.0 *i* , so consequently, only particles with a refractive index significantly different from this value are detectable by the LiQuilaz . This instrument measures the particle size distribution in fifteen size channels ranging from 0.25-2.0 μm based on a calibration using polystyrene latex (PSL) spheres of various known diameters.

The size-resolved total concentration of particles in the air was measured simultaneously using a GRIMM dust monitor model 1.100. This model of optical particle counter sizes aerosols in seven channels between 0.3-2.0 μm and eight channels between 2.0-20 μm. By comparing the concentration of WIA in the air derived from equation (4.1) to the total concentration measured by the GRIMM dust monitor, the real-time fraction of particles which are water-insoluble may be calculated on a size-resolved basis. For this study, the time resolution used was five minutes. The water-insoluble instrumentation was installed inside a portable wooden shelter about 2 m^3 in volume. The ambient air inlet was located approximately 2 m above the ground. The GRIMM dust monitor was installed on the top of this shelter.

Filter samples were also collected and analyzed for elemental and organic carbon (EC/OC) mass using the thermal/optical transmittance (TOT) method developed by Sunset Laboratory [*Birch and Cary*, 1996]. This technique is subject to two sources of uncertainty: error in determining the distinction between EC and OC as well as positive OC artifacts due to adsorption of gas-phase organics [*Turpin et al*., 2000]. The uncertainty in the EC/OC split point does not influence the total amount of carbon detected such that shifting the split toward higher OC mass results in correspondingly less EC mass and vice versa. The uncertainty due to positive OC artifacts from adsorbed gas-phase species may be significant and as high as 20-30%. The reported mass inferred from TOT analysis is the mass of carbon alone and does not include the mass of other elements present in the particle. In the case of EC, carbon mass and particle mass are very close, but in the case of OC, particle mass may be 1.4-2.1 times higher than carbon mass [*ibid*.]. Two different filtering systems were used for TOT analysis: total $PM_{2.5}$ mass was collected on quartz filters over a period of four hours and size resolved EC/OC mass was collected over a period of 24 hours using a Dekati low

pressure cascade impactor. These results are discussed in more detail by *Jaffrezo et al*. [2005b]. Another set of sized-resolved filter measurements were made on Teflon filters over a period of 48 hours using a MOUDI cascade impactor in order to gravimetrically determine total particle mass.

4.2.2 Discussion of measurement uncertainty

As has been observed since the earliest uses of optical particle counters, instruments which rely on aerosol light scattering to measure particle size and concentration inherently depend on assumptions of particle shape and refractive index [*Quenzel*,1969; *Whitby*, 1967]. Uncertainty in the size of detected particles arises from the fact that many ambient insoluble particles are non-spherical and have a refractive index significantly different from that of the most common calibration standard, polystyrene latex (PSL). The refractive index of this material is 1.59 + 0.0 *i* at λ = 780 nm. Estimates of the refractive index of black carbon chain agglomerates range from 1.1 + 0.1 *i* for agglomerates with an open structure and many air spaces to 1.5 + 0.5 *i* for more densely packed agglomerates [*Hull et al*., 2004; see *Greenwald et al*., 2005a for more thorough analysis]. Mineral aerosols generally have a real refractive index of 1.5-1.6 with a minimal absorptive component in the visible and near-visible range [*Sokolik and Toon*, 1999]. The composition of organic aerosols is quite complex and largely unknown, although the refractive indices of individual organic compounds known to be water-insoluble are generally 1.4-1.5 [*Lide*, 2004].

Mie theory analysis of this instrument to estimate the influence of particle refractive index has suggested that the LiQuilaz is accurate within ±20-30% for particles smaller than 0.6 μm. For particles greater than 0.6 μm, the resulting uncertainty in inferred particle size is nearly always negative (i.e. particles are undersized) and of somewhat

greater magnitude (as much as 50%). As discussed in *Greenwald et al.* [2005a], it is highly unlikely that particles reported by the LiQuilaz to be larger than 0.8 μm may be composed of black carbon (BC). This does not imply that such large BC particles are not detected, but rather that they are undersized by the LiQuilaz on the order of 40-80%. Particles which are indicated to be greater than 0.8 μm must therefore be composed of some different insoluble material. Since the size distribution of mineral aerosols tends to be shifted toward larger sizes relative to that of organic aerosols [Ebert et al., 2004], these particles are more likely to be of crustal origin.

In the case of internally-mixed aerosols, particle refractive index is also influenced by the presence of extraneous material. Agglomerates of black carbon typically contain some quantity of organic compounds, and well-aged soot particles are often coated by a substantial amount of organic and inorganic matter [*Pósfai et al*., 1999]. Inorganic matter such as sulfate and a substantial portion of the organic matter is likely to be water-soluble and therefore dissolve before reaching the LiQuilaz used in this study. The real-time technique to measure WIA number concentration used for this study is not able to provide information on the mixing state of particles or quantify the amount of soluble material present on a particle in its atmospheric state. Insoluble particles reported to be a specific size by this technique may have existed in the atmosphere as a larger internally-mixed particle containing both soluble and insoluble mass. Similarly, mostly-soluble particles with only a small insoluble core may not be detected at all if that core is smaller than approximately 0.25 μm. On the other hand, provided that the illuminated surface of a particle is of sufficient size and refractive index to scatter a quantity of light greater than the sensitivity of the photodetectors, the measured number concentration is generally considered to be accurate at concentrations up to the coincidence limit.

Ambient particle concentration was below this instrument's coincidence limit at all times during this study.

Measurements of the fraction of organic aerosol mass which is water-soluble at the same alpine sites as examined in this study have found a seasonal pattern with 55±8% of the organic mass being water-soluble in the winter and 76±6% in the summer [*Jaffrezo et al*., 2005a]. The real-time technique is less efficient at measuring water-insoluble organic carbon than other types of insoluble aerosols. This is likely due to the combined effect of three properties of organic aerosols. First, the refractive index of insoluble organic compounds is frequently similar to that of the scattering medium of the particle counter. Many insoluble organic compounds therefore do not scatter enough light to be detected by the LiQuilaz. Organics which are detected by the particle counter are likely to be undersized to a greater extent than other types of insoluble particles. The net result is an undercounting of insoluble organic aerosols. Second, it is possible that organic particles are more susceptible to disintegration in the impinging process due to their low surface cohesion compared to soot or mineral aerosols. Finally, since the environment inside of the impinging chamber is nearly infinitely dilute, particles determined to be insoluble by filter-based analysis techniques may in fact be partially soluble in our system.

4.2.3 Comparison of data sets

The process of sizing of elemental carbon particles with a cascade impactor and TOT filter analysis results in a particle diameter which is not perfectly analogous to the size reported by the LiQuilaz even in the absence of the previously-mentioned uncertainty. Cascade impactors segregate particles based on inertia. Particle inertia is a function of mass, shape and velocity. Internally-mixed particles are sized based on the combined mass of all species; however, it is known that well-aged soot particles tend to

contain a significant coating of water-soluble organic or ionic compounds [*Pósfai et al*., 1999]. This coating material will dissolve in the water stream sampled by the LiQuilaz, resulting in a diameter smaller than that suggested by impactor filter analysis for EC particles. In addition, filter samples provide a measurement of mass concentration, whereas particle counters report a number concentration. Data conversion between the two concentrations is not a straight-forward process since particle density and shape is unknown and particularly in the case of soot particles, highly variable. For purposes of comparison of the data sets, an approximation of WIA mass was calculated from the number concentrations by assuming that particles are spherical with a diameter equal to the log-average of the corresponding instrument channel and have a density of 1.7 g · cm^{-3} (typical for ionic aerosols) for the total population and 1.8 g · cm^{-3} (representative of elemental carbon) for WIA [*Janzen*, 1980]. Since volume is a function of diameter cubed, small inaccuracies in the measurement of diameter can result in large inaccuracies in the estimate of mass. In addition, the density of soot is also uncertain and likely varies as a function of size. The bulk density of carbon black has been estimated to be approximately 2 g · cm^{-3} [*Hess and Herd*, 1993]. This value represents the maximum possible density of an individual soot particle; as porosity increases, particle density decreases correspondingly. Although these filter measurements have poor time resolution (4-48 hours vs. 5 minutes), use a different method to size particles (inertia vs. light scattering), and measure mass instead of number, comparison of the resulting data with the real-time WIA measurements is still able to reveal a great deal of information concerning the composition and possible sources of WIA.

4.2.4 Sampling sites

Sampling sites for the intensive field campaigns were chosen at representative locations in both the Chamonix and Maurienne Valleys. The Chamonix Valley is a 23 km

long valley on the borders of France, Italy, and Switzerland. The mean elevation of the valley floor is 1000 m above sea level. It is 1-2 km wide on average and is bounded by very steep mountain slopes, the tallest of which is Mont Blanc at 4807 m. There are 12000 permanent residents in the valley, but this number is exceeded by the tourist population of roughly 5 million overnight visits per year. There are no major industrial installations in this valley, although it does contain a major highway which passes through the Mont Blanc tunnel to Italy. During the winter campaign, the traffic on this highway was comprised of approximately 1800 personal vehicles and 600 heavy trucks per day. During the summer campaign, these numbers had increased to 4200 personal vehicles and 900 trucks per day. Approximately half of the personal vehicles are diesel powered. The valley also contains a much smaller road traversing the length of the valley through the high mountain pass leading to Switzerland (the Col des Montets). This road carries much less traffic, largely personal vehicles driven by tourists. There are also many secondary roads leading only to small villages and neighborhoods near the floor of the valley. In Chamonix, the instrumentation was set up in the backyard of a chalet owned by LGGE in a residential area known as Le Clos de l'Ours, about 1 km from the center of the town of Chamonix. This site is located 2 km up the valley from the entrance to the Mont Blanc tunnel. The sampling period in Chamonix was January 18-22, 2003 and July 4-11, 2003.

The Maurienne Valley is much longer than Chamonix (about 80 km long) and is generally wider (about 3-5 km wide), although there are several points where the valley floor is only a few hundred meters wide. The elevation of the valley floor ranges from 400 m at the mouth to 2000 m at the pass at the upper end, and the surrounding mountains are not as high as in Chamonix (the highest is 3852 m tall). The permanent population is much higher (about 45000), but most is concentrated in a few small cities at the lower end of the valley. There are also several industrial sites in the lower part of

the valley including plants for steel and aluminum production. As in Chamonix, this valley contains both a major highway which utilizes a tunnel to cross the Alps into Italy (the Fréjus tunnel in this case) and a smaller roadway which winds over the pass at the top end of the valley. The intensive sample site in the Maurienne Valley was located at an unoccupied public camping ground in the small town of Orelle. This site is 20 km up the valley from St. Jean de Maurienne (the major population and industrial center of the valley) and 13 km down the valley from Modane (where the entrance to the Fréjus tunnel is located). The valley floor is only a few hundred meters wide in Orelle, so the highway at this point is constructed through a tunnel in the side of the mountain for a distance of a few kilometers. Although vehicle traffic is underground as it passes the sample site, a ventilation outlet for this tunnel is located approximately 500 m up the valley and 20 m lower in elevation. The sampling period in Orelle was January 24-30, 2003 and June 25-July 2, 2003.

The topography of steep alpine valleys such as Chamonix and Maurienne lead to several unique meteorological phenomena. In terms of influence on particle concentration, the two most important of these are related to the diurnal variation of the mixing height and the cycle between up-valley and down-valley winds [*Anquetin et al.*, 1998]. The diurnal variation in the thickness of the well-mixed boundary layer in alpine valleys is exaggerated when compared to more open terrain. As is typical for many types of topography, ground-level inversion layers tend to develop overnight and then are broken up in the morning as a result of solar heating of the surface. In steep valleys, two special factors serve to make this cycle more pronounced. First, the height of the valley walls prevents penetration of sunlight to the valley floor until later in the morning. This serves to preserve the inversion layer for a longer portion of the day as well as to reduce the ultimate height the mixing layer can achieve before nightfall. This effect is more pronounced during the winter season at mid- to high-latitudes. Second, the close

horizontal spacing of the valley walls confine emissions to a much smaller mixing volume compared to open terrain resulting in much higher concentrations for otherwise identical sources. In addition, the valley walls also act as a profound constraint on wind direction. For this reason, it is more useful to refer to wind direction in terms of up-valley (from low elevation to high-elevation) or down-valley rather than cardinal direction. During daylight hours, solar insolation heats the surface-level air parcels and induces them to rise which leads to up-valley air flow. This results in mixing of the valley air with regional-scale air parcels. At night, radiative cooling of surface-level air leads to subsidence and a down-valley air flow. This nighttime wind is typically weaker than the daytime up-valley wind. This pattern is more pronounced during the summer season when there is more intense surface insolation [*ibid*.]. At all times of year, this cycle is influenced by synoptic-scale circulation.

4.3 Results and discussion

Recognizing that the underlying meteorology has significant differences between winter and summer, the results of the intensive campaigns have been organized to allow more logical analysis of the data. Results are presented first by season and then by location, resulting in four different sets of results. Each set is organized in a similar manner, therefore a detailed explanation is only provided for the first case. For the remaining three cases, only interesting observations or implications are discussed.

4.3.1 Winter results

4.3.1.1 the Chamonix Valley

Figure 4.1 shows a time series of the total aerosol and WIA number concentration in the Chamonix Valley during the winter 2003 campaign. These number concentrations

are shown on the left axis while the fraction (by number) of particles which are water-insoluble is shown on the right axis. This data is the sum of all particles in the size range 0.3-2.0 μm. Simultaneous measurements of mass concentration using a MOUDI cascade impactor indicate that 75-85% of the particle mass is within this size range. The number concentration varies by as much as an order of magnitude on time scales as short as a matter of minutes. The number insoluble fraction averaged 11% over this time period but reached as high as 60% and was occasionally at levels over 30% for several hours at a time. It is apparent from this graph that the WIA and total aerosol concentrations fluctuate independently. The inset enlarges a four hour time period to further illustrate this point. It may be seen from the inset that there are time periods when the water-soluble and -insoluble concentrations are anti-correlated.

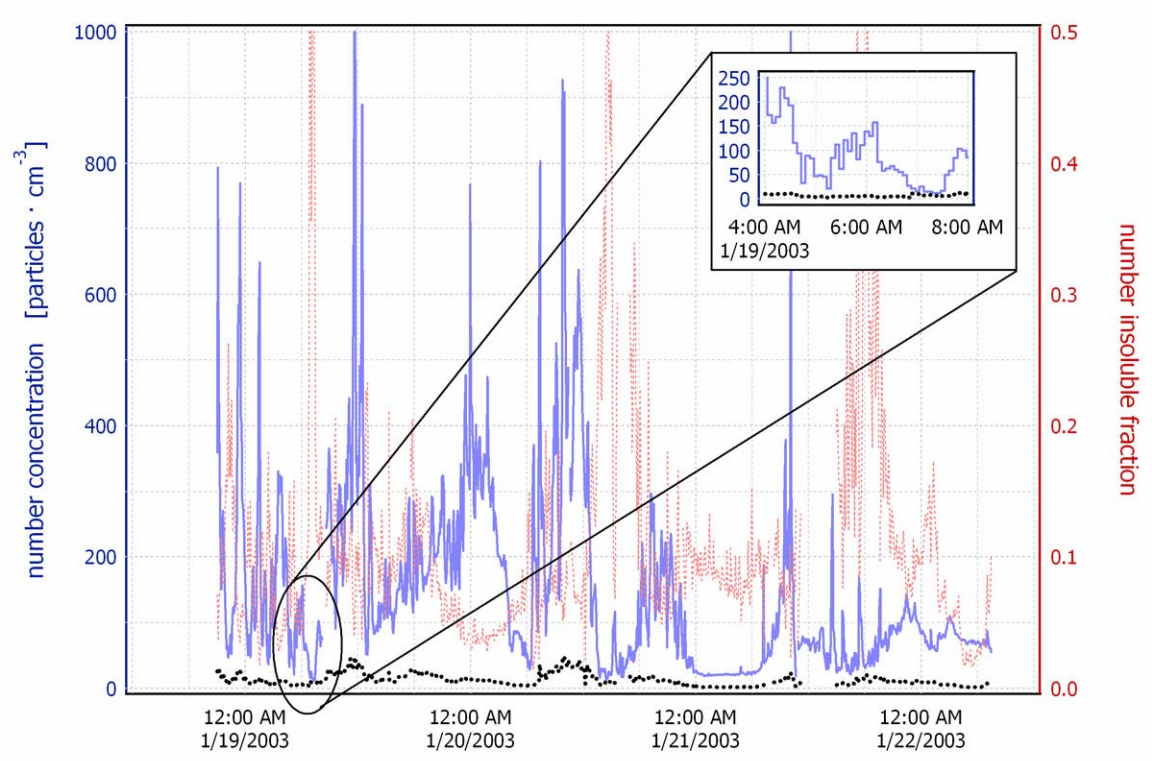

FIGURE 4.1. Time series of the total aerosol and WIA number concentration in the Chamonix Valley during the winter 2003 campaign. Displayed data is the sum of all particles in the size range 0.3 - 2.0 μm. total aerosol WIA number insoluble fraction

Figure 4.2 illustrates the size distribution over several time intervals during the week of sampling. Figure 4.2(a) shows the size distribution averaged over the entire week, Figure 4.2(b) shows the time around midnight on Jan. 20, 2003 when the total particle concentration was elevated for a period of several hours, and Figure 4.2(c) shows the period in the morning of Jan. 21, 2003 when the concentration was quite low for several hours. Note that the scales are different on these charts. These charts show little difference in size distribution with concentration, and all exhibit peaks in the insoluble fraction at 0.45 and 1.1 μm. The insoluble fraction tends to be higher at all sizes when

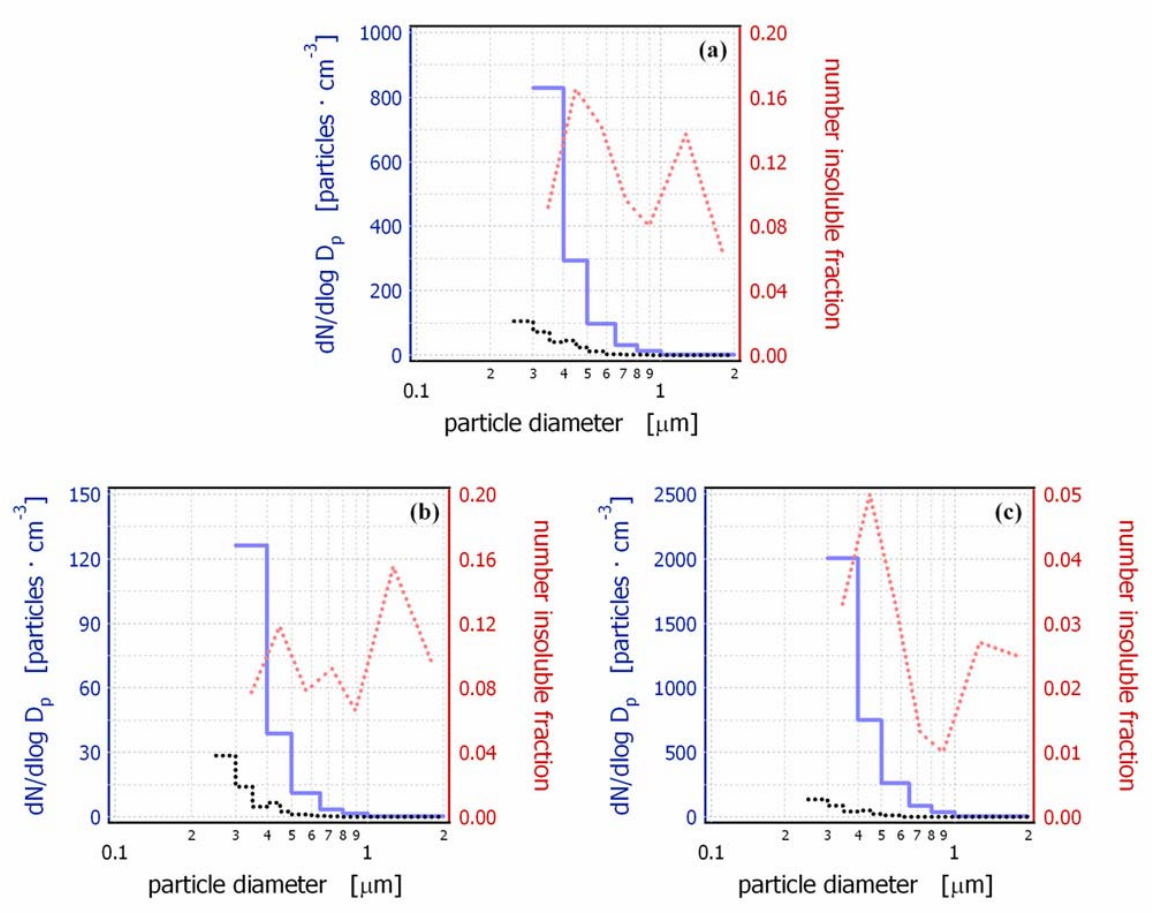

FIGURE 4.2. Number size distribution of the total aerosol and WIA number concentration in the Chamonix Valley during the winter 2003 campaign. Figure 4.2(a) is averaged over the entire sampling period, Figure 4.2(b) shows the period around midnight on January 20 when concentrations were elevated for several hours, and Figure 4.2(c) is the period during the morning of January 21 when the concentration was low for several hours.
total aerosol ····· WIA ····· number insoluble fraction

the total particle concentration is lower.

Figure 4.3 shows size-resolved mass concentration (dm/dlog D_p) for five different data sets averaged over the time periods of the MOUDI runs. The first three data sets are the EC, OC and EC+OC concentrations determined from the Dekati impactor samples, the next data set is the total particle mass measured gravimetrically using the MOUDI impactor filters, and the final set is an estimate of the WIA mass concentration derived from the average number concentrations over the same time period. Figure 4.3(a) shows dm/dlog Dp for the MOUDI run of Jan. 18-20, 2003, and Figure 4.3(b) is the run of Jan. 20-22, 2003. The concentration of non-carbonaceous mass (sulfate, nitrate, metals, etc.) is not shown. Therefore, it is expected that the MOUDI total mass should exceed EC+OC mass at all sizes. This largely holds true except for two impactor stages in Figure 4.3(b). This discrepancy may be the result of positive artifacts in OC mass due to adsorption onto the filters of gas-phase organic material. Since EC is insoluble in water, it was expected that the mass estimated by the LiQuilaz would be equal to or greater than the measured EC mass at all sizes; however, the opposite is more often observed. This is likely due to a combination of the sizing errors explained in

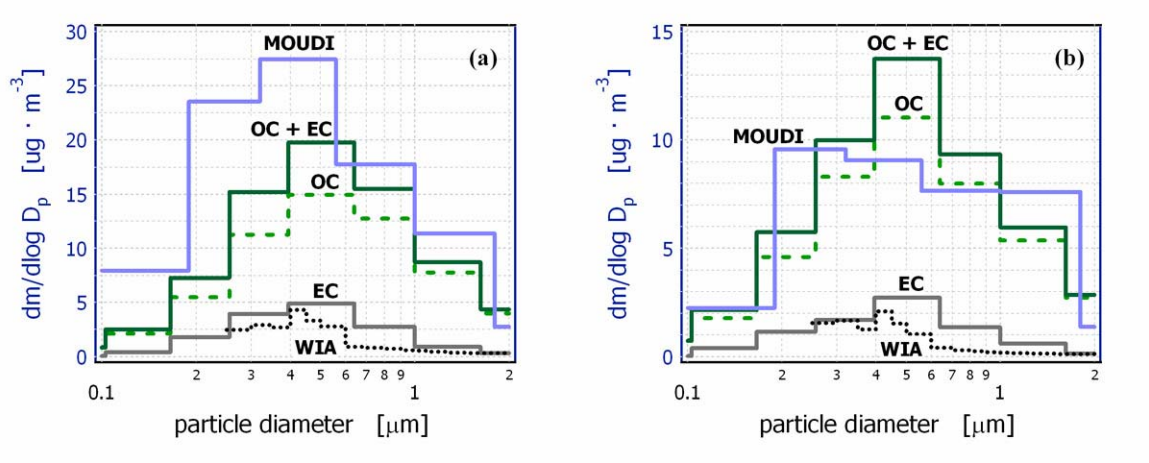

FIGURE 4.3. Mass size distributions in the Chamonix Valley during the winter 2003 campaign. Total mass was measured gravimetrically using a MOUDI cascade impactor, and carbonaceous mass was measured by TOT analysis of Dekati cascade impactor samples. Figure 4.3(a) is for the time period of January 18 - 20 and Figure 4.3(b) is for January 20 - 22, 2003.

the previous section, namely that the impactor tends to oversize EC relative to the LiQuilaz (depending on the mixing state of atmospheric aerosols) and that the LiQuilaz likely undersizes particles due to a difference between the refractive index of the ambient particles and the calibration standard. The latter of these errors is compounded by the fact that WIA mass is an estimated value calculated as a function of particle diameter cubed. Even a slight increase in the size of particles measured by the LiQuilaz would result in much larger WIA mass. In addition, for the purposes of estimating insoluble mass, particles were assumed to be spherical, even though soot particles are known to be fractal agglomerates. The mass estimated by this procedure may conceivably be greater or less than actual insoluble mass. Since these mass calculations are subject to an unquantified uncertainty, these estimates should be

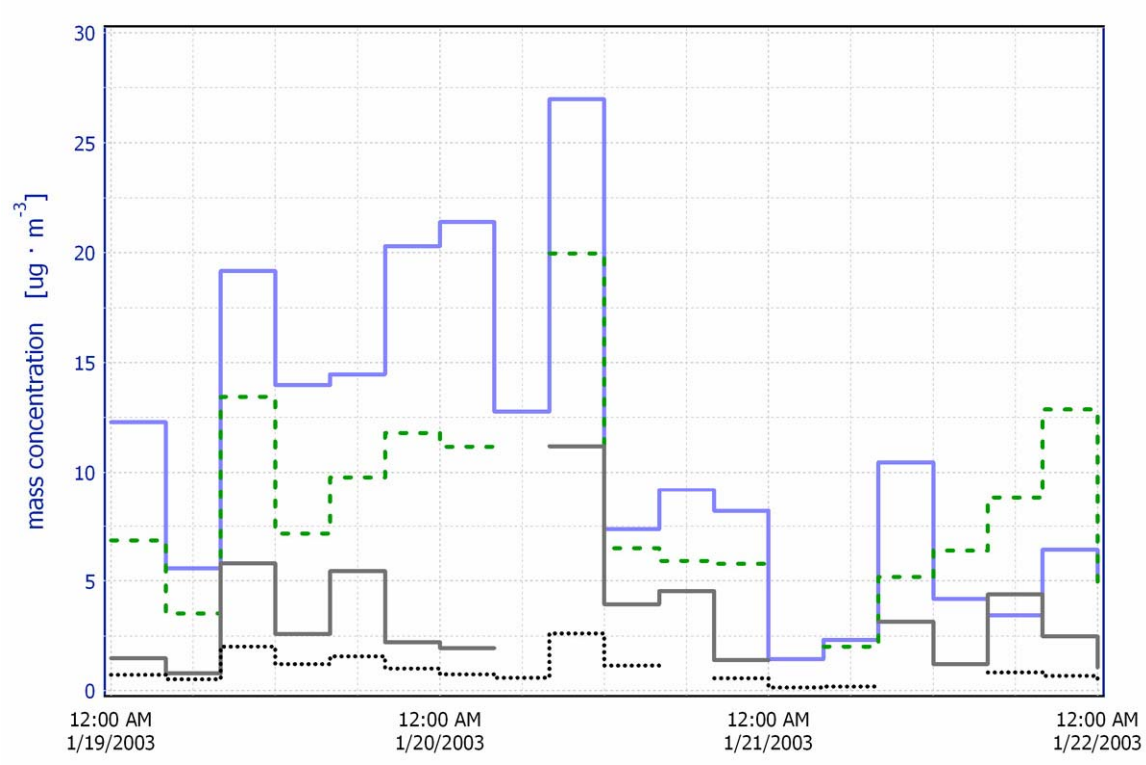

FIGURE 4.4. Time series of the elemental and organic carbon mass concentration in the Chamonix Valley during the winter 2003 campaign. This data was obtained from TOT analysis of PM2.5 filters sampled on four-hour intervals. Estimates of the total aerosol and WIA mass concentration calculated from the measured number concentration in the size range 0.3 - 2.0 μm are also shown.

interpreted qualitatively. Therefore, the most important observation which can be made from the comparison of the WIA calculated mass to the mass measured by the filter samples is that the structure of the particle size distributions are consistent with one another, with peaks between 0.4-0.6 μm.

Figure 4.4 shows a time series of the $PM_{2.5}$ EC and OC mass in the Chamonix Valley measured using TOT analysis of the four-hour filters. For comparison, estimates of the total and WIA mass averaged over the same time periods are also shown. These mass estimates were calculated from the real-time number concentrations as described in the previous section. The filters collect particles of all sizes smaller than 2.5 μm, whereas the real-time instrument only measures the size range of 0.25-2.0 μm. Examination of the impactor data reveals that in winter, 18% of the $PM_{2.5}$ EC mass and 15% of the $PM_{2.5}$ OC mass is smaller than 0.2 μm while in summer, 25% of the $PM_{2.5}$ EC mass and 32% of the $PM_{2.5}$ OC mass is smaller than 0.2 μm. Since the size ranges measured by these two methods do not perfectly correspond to one another, the data is expected to contain noticeable discrepancies even in the absence of other uncertainty. However, a comparison is still useful in that it allows observation of the relative changes in EC and WIA concentration. The structure of each of these time series is for the most part parallel. EC mass consistently exceeds WIA mass by a factor of approximately three. This is likely due to the size range issues described above as well as the uncertainty in the sizing of soot particles by the LiQuilaz which is compounded during the conversion from number to mass concentration.

Figure 4.5 shows EC and OC four-hour average mass plotted against the estimated mass of WIA averaged over the same time periods. Linear regressions are shown as solid lines. Figure 4.5(a) shows the winter results from the Chamonix Valley. The WIA mass is more closely correlated with EC mass than with OC mass. Given that EC is

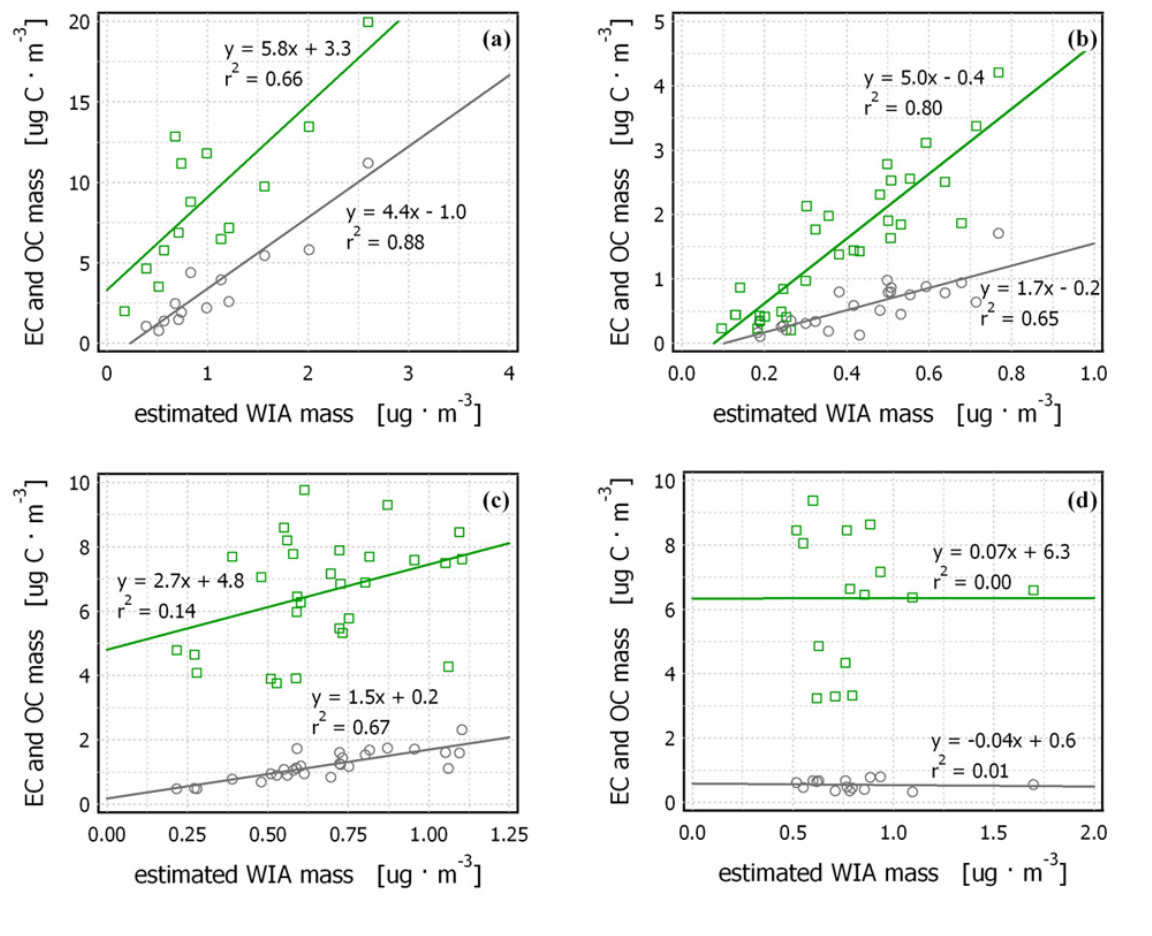

FIGURE 4.5. Linear regressions of measured EC and OC mass with the estimated WIA mass concentration. Figure 4.5(a) is for Chamonix winter, Figure 4.5(b) is for Maurienne winter, Figure 4.5(c) is for Chamonix summer, and Figure 4.5(d) is for Maurienne summer. ○ EC ▫ OC

completely water-insoluble, the slope of the WIA-EC regression should theoretically be less than or equal to unity. The fact that it is significantly greater than one during three of the four campaigns is most likely a result of uncertainty in calculating WIA mass from the number concentration and the difference in size ranges measured by the two methods. The slope of the WIA-EC regression is approximately three times higher in the Chamonix Valley during the winter campaign than in any of the other campaign phases. By comparing the EC size distributions of Figure 4.4 to those for the other sites, it may be seen that the EC size distribution in the Chamonix Valley during the winter campaign

was slightly shifted toward larger sizes relative to other sites. As previously mentioned, EC particles larger than 0.8 μm are undersized by the LiQuilaz SO2, and this uncertainty in sizing may have lead to an underestimation of WIA mass and consequently a higher WIA-EC regression slope. This site was more significantly influenced by smoke from wood-burning stoves than other sites, and it may be possible that this difference in EC sources may have lead to the observed differences in the size distributions [*Marchand*, 2003].

4.3.1.2 the Maurienne Valley

A time series of the number concentration in the Maurienne Valley during the winter campaign is shown in Figure 4.6. The concentration was generally about a factor of two

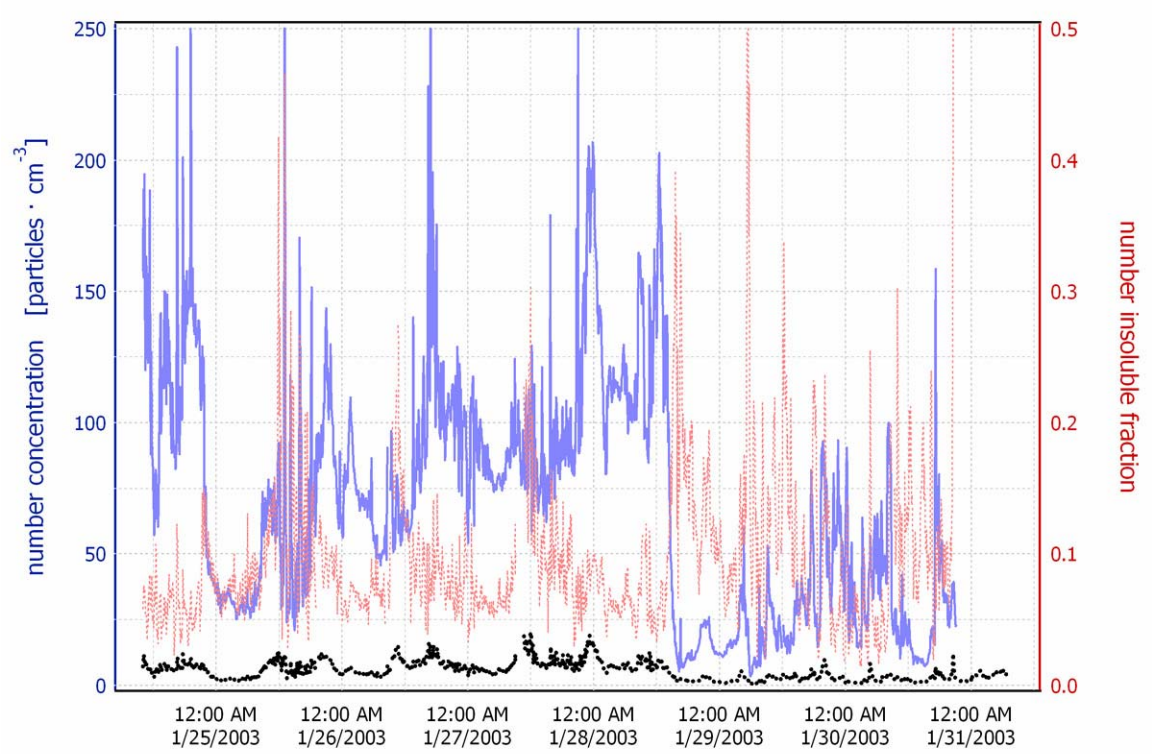

FIGURE 4.6. Time series of the total aerosol and WIA number concentration in the Maurienne Valley during the winter 2003 campaign. Displayed data is the sum of all particles in the size range 0.3 - 2.0 μm. ——— total aerosol ····· WIA ····· number insoluble fraction

lower in Maurienne than in Chamonix and again varied dramatically on short time scales. Despite this abrupt variation in total concentration, the number insoluble fraction did not vary much (especially during the first half of the week) and averaged 9.5% over the entire sample period. Examination of the time series suggests that a likely reason for this lack of variability in the insoluble fraction is simply that both the total and WIA concentration frequently vary concurrently. This seems to imply these particles have remote sources and that concentration variability is due to meteorological conditions (such as mixing height and wind speed and direction) acting on both classes of particle.

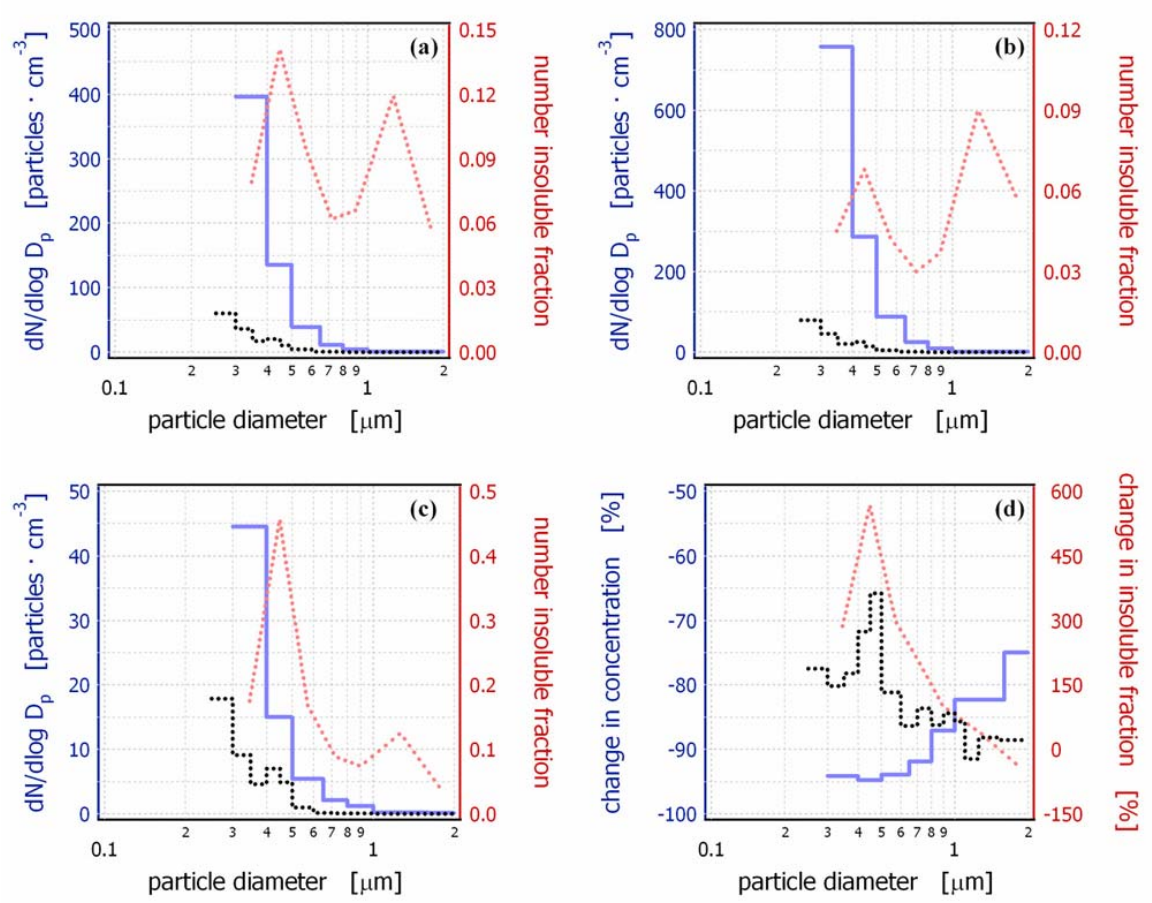

FIGURE 4.7. Number size distribution of the total aerosol and WIA number concentration in the Maurienne Valley during the winter 2003 campaign. Figure 4.7(a) is averaged over the entire sampling period, Figure 4.7(b) shows the thirty minute period before the snowfall event of January 28, and Figure 4.7(c) is the thirty minutes following the commencement of snowfall. Figure 4.7(d) shows the percent change in concentration between before and after snowfall.
total aerosol ····· WIA ····· number insoluble fraction

Indeed, the sample site in the Maurienne Valley is not near major sources of particles considering that it is located in a very small town and that the highway is underground as it passes the sample site.

A heavy snowfall event began on the afternoon of January 28 and continued into the following day. Following the onset of snowfall, the total particle concentration quickly dropped by an order of magnitude. The WIA concentration on the other hand did not diminish to a similar degree and the insoluble fraction consequently increased by a factor of eight (from 5% to 40%) over the course of two hours. Figure 4.7 shows the number size distributions for the Maurienne Valley. Figure 4.7(a) shows the average size distribution for the entire week, but more interestingly, Figures 4.7(b) and (c) shows the size distribution for the thirty minute periods preceding and following the commencement of the snowfall event. The insoluble fraction increased for all but the largest particles following the snow, but this increase was much more pronounced at 0.45 μm (increase from 6.8% to 45.6% in a matter of minutes). An air mass change was associated with this snowfall event and the wind direction shifted from up-valley to down-valley. Figure 4.7(d) shows as a function of size the percent change in number concentration (left axis) and insoluble fraction (right axis) between the thirty minutes before the snow began and the thirty minutes after. This graph shows that the change in concentration is negative for all particles, but more negative for the smallest ones. This is contrary to the expected result given that the principal physical mechanisms for the removal of particles by precipitation are impaction and diffusion, which preferentially remove particles larger than 1.0 μm and smaller than 0.1 μm respectively [*Greenfield*, 1957]. In other words, the change in concentration was expected to be least negative for particles 0.1-1.0 μm, whereas the opposite is observed. For insoluble particles, the structure of this graph is more complex and difficult to interpret. The concentration of insoluble particles larger

than 0.5 μm is diminished by roughly 80-90% from what it had been before the snowfall, but for particles between 0.4-0.5 μm, the concentration is reduced by just over half. This results in the number insoluble fraction at this size to be extremely high during the period following the onset of snow, reaching as high as 40%. This unusual structure gradually diminishes over a period beginning approximately thirty minutes after the snowfall began until six hours later, at which time the structure of the size distribution once again closely resembled the average for the week. Snow was falling heavily this entire time. It is possible that the advance of the cold front introduced a new particle population which simply contained a higher percentage of insoluble particles in the size range of 0.4-0.6 μm. However, another intriguing possibility is that the instrumentation was detecting the nuclei at the core of the snowflakes. When precipitation forms in the solid phase rather than the liquid phase, the hydrophobicity of the nuclei is not as great of a deterrent to activation. It has been shown that atmospheric soot particles serve as effective ice nuclei (IN) in the lower atmosphere [*Gorbunov et al*., 2001]. This process has been observed to be more efficient if the soot particles are large and exhibit surface oxidation typical of well-aged aerosols, and if the precipitating clouds are low-lying. All of these conditions appear to have been met in the case of the snowfall event of January 28. The clouds were observed to be quite low, and the down-valley wind direction suggests that the air parcels were arriving from the direction of the industrial region on the Italian side of the Alps (i.e. were well-aged). If soot particles were in fact serving as IN for this snowfall event, then the WIA instrumentation would have been sampling both insoluble particles in the surface layer as well as the soot IN of the snowflakes being transported from aloft. This would have led to an increase in the concentration of WIA in the size range of the IN relative to the concentration at the surface. If the optical diameter of IN for this event were 0.4-0.6 μm, then our observations were consistent with this hypothesis.

Figure 4.8 shows a time series of EC and OC four-hour average mass as well as estimates of total aerosol and WIA mass. As in Chamonix, the structure of these curves closely match one another. Figure 4.5(b) shows EC and OC mass plotted against the estimated mass of WIA for the Maurienne Valley in winter. This graph shows a close correlation of EC and WIA mass, although unlike in Chamonix, the correlation of OC and WIA is higher than that of EC and WIA mass. This high correlation could conceivably be the result of either the presence of insoluble organic aerosols or simply the fact that OC mass is highly correlated with EC mass.

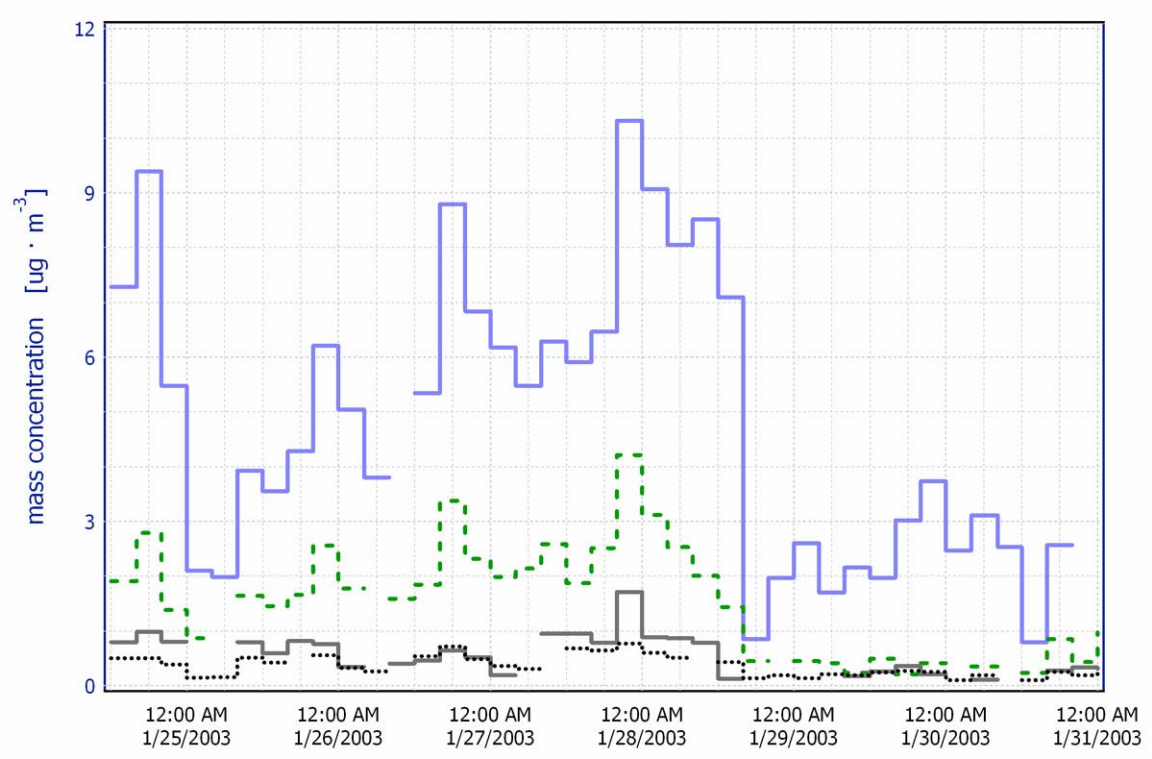

FIGURE 4.8. Time series of the elemental and organic carbon mass concentration in the Maurienne Valley during the winter 2003 campaign. This data was obtained from TOT analysis of PM2.5 filters sampled on four-hour intervals. Estimates of the total aerosol and WIA mass concentration calculated from the measured number concentration in the size range 0.3 - 2.0 μm are also shown.

4.3.2 Summer results

4.3.2.1 the Chamonix Valley

Figure 4.9 shows a time series of the total aerosol and WIA number concentrations in the Chamonix Valley during the summer campaign. The concentration in the summer averaged about a factor of two lower than during the winter campaign, most likely due to the fact that the afternoon mixing height is typically much higher in the summer and that there was less biomass burning for residential heating. The average insoluble fraction was 11.2%, essentially the same as was observed in January. The first day of the Chamonix summer campaign was cool with steady rainfall. The rest of the campaign was characterized by exceptionally hot and sunny stagnant conditions. Following the initial rainfall, the atmosphere was relatively clean, and the total particle concentration

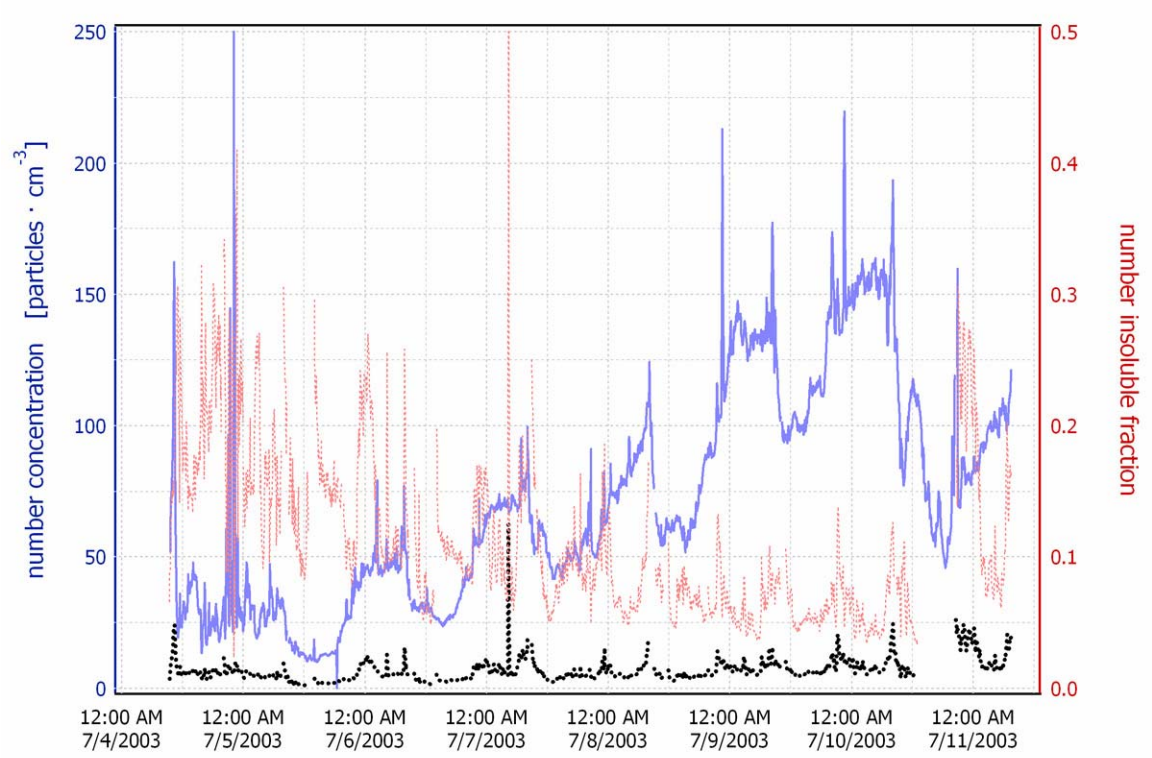

FIGURE 4.9. Time series of the total aerosol and WIA number concentration in the Chamonix Valley during the summer 2003 campaign. Displayed data is the sum of all particles in the size range 0.3 - 2.0 µm. —— total aerosol ····· WIA ····· number insoluble fraction

steadily increased throughout the week as a result of stagnant meteorological conditions favoring secondary organic aerosol formation. Unlike during the winter campaign, there was a clear diurnal pattern in particle number concentration, with higher concentrations being observed at night and during the early morning hours when the mixing height is at a minimum. Contrary to the total particle concentration, the WIA concentration did not display an upward or downward trend throughout the week. Thus there was a clear downward trend in the insoluble fraction as the week progressed. This can be explained by noting that during summertime mornings, as the mixing height increases, well-mixed air from outside the valley is introduced by the up-valley wind. Each day, this outside-the-valley background concentration increased due to continental-scale meteorology resulting in higher total number concentrations. The WIA concentration on the other hand is more a function of vehicular sources within the valley. These sources remained generally the same throughout the week, resulting in little change in WIA concentration aside from the diurnal variation.

Figure 4.10 shows a series of size distributions averaged over several time periods during the Chamonix summer campaign. Figure 4.10(a) shows the average time period for the entire week. Figure 4.10(b) shows a typical daytime period (July 8), and Figure 4.10(c) shows a nighttime period (July 8-9). The structure of these size distributions is similar during each time period, although there is a slightly higher fraction of large insoluble aerosols observed during the day than during the night.

Figure 4.11 shows the size distributions associated with the time periods of the MOUDI runs. Figure 4.11(a) is averaged over the time period July 4-6, Figure 4.11(b) is averaged over July 6-8, Figure 4.11(c) is averaged over July 8-10, and Figure 4.11(d) is averaged over July 10-11. These charts show excellent agreement between the different measurement methods. The total MOUDI mass is equal to or exceeds EC+OC at most sizes for all four runs as expected. In addition, the estimated WIA mass equals or

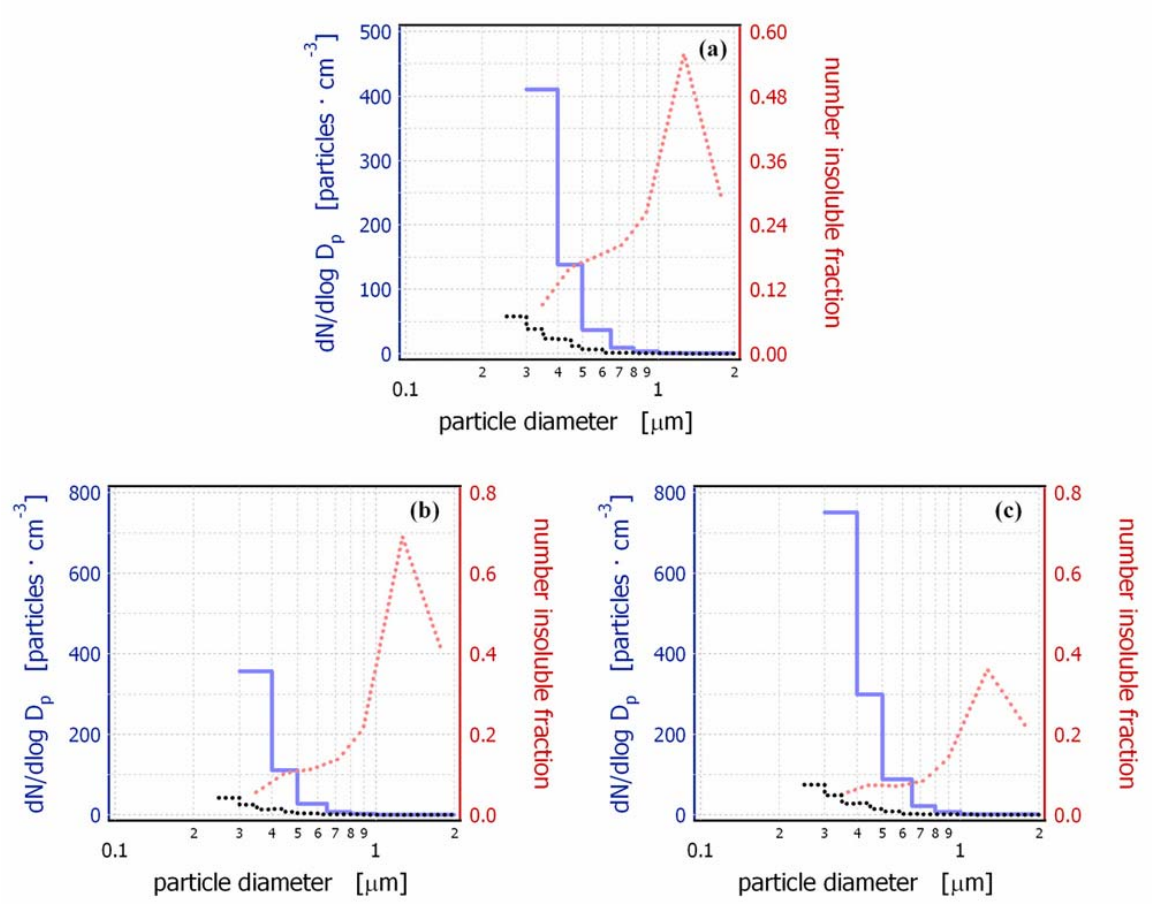

FIGURE 4.10. Number size distribution of the total aerosol and WIA number concentration in the Chamonix Valley during the summer 2003 campaign. Figure 4.10(a) is averaged over the entire sampling period, Figure 4.10(b) shows a typical daytime period (July 8) while Figure 4.10(c) shows a typical nighttime period (July 8 -9).
total aerosol ····· WIA ····· number insoluble fraction

exceeds the EC mass at all sizes on all runs; however, since there is significant uncertainty associated with estimating WIA mass from number concentration, this does not necessarily suggest that WIA is entirely composed of EC. A substantial portion of WIA mass could conceivably be composed of OC or crustal elements. During all four periods, there is a slight trend toward increasing WIA mass at sizes larger than 1.0 μm. This same trend is not observed in either the EC or OC mass size distributions, suggesting wind-blown dust as a possible source of these particles. As particle

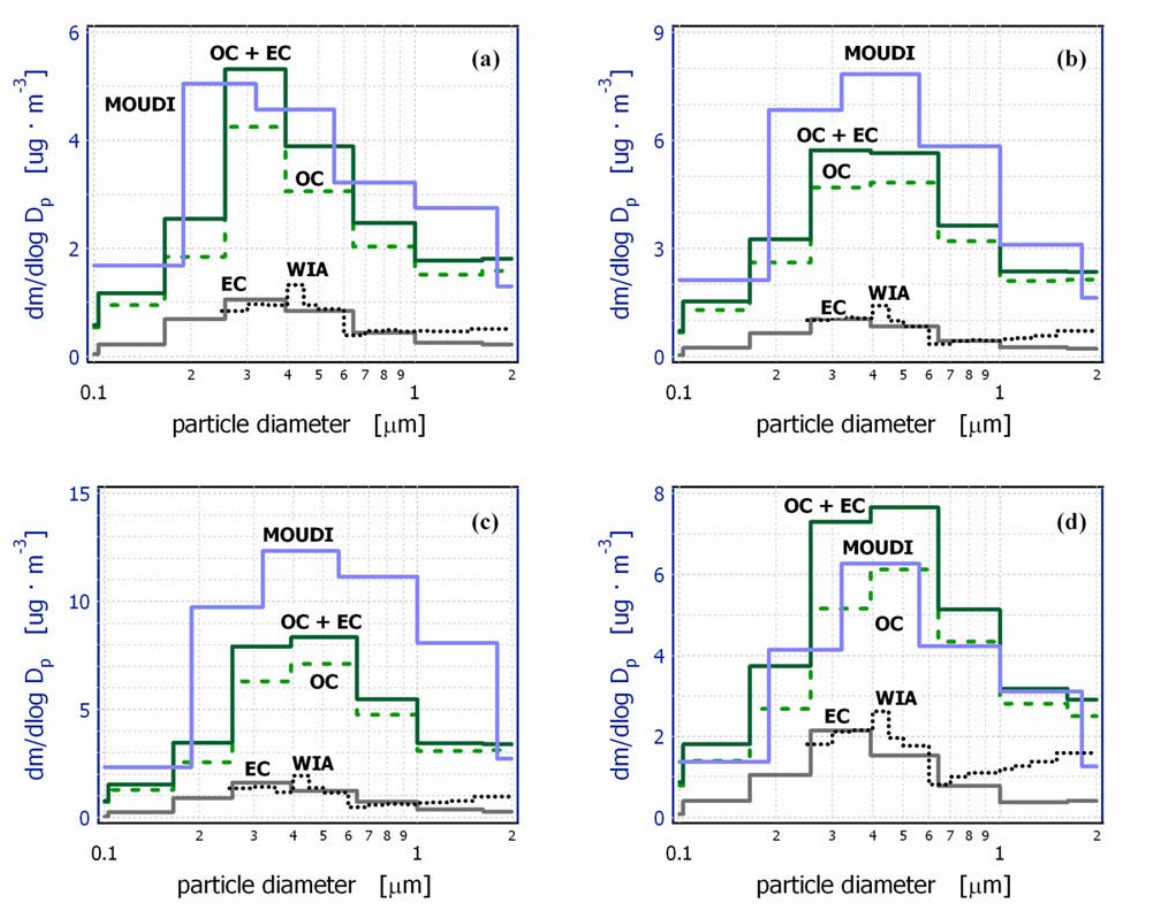

FIGURE 4.11. Mass size distributions in the Chamonix Valley during the summer 2003 campaign. Figure 4.11(a) is for the time period of July 4 - 6, Figure 4.11(b) is for July 6 - 8, Figure 4.11(c) is for July 8 - 10, and Figure 4.11(d) is for July 10 - 11, 2003.

concentrations increased throughout the week, the size distributions exhibited a slight shift toward larger diameters.

Figure 4.12 shows a time series the EC and OC mass measured by the four-hour filters plotted alongside estimates of the total and WIA mass averaged over the same time periods. Although EC mass exceeds the estimate of WIA mass at all time intervals, the two values fluctuate concurrently. This may not be said of WIA estimated mass and OC mass. OC mass is frequently observed to increase while WIA mass decreases and vice versa. Figure 4.5(c) shows a regression of EC and OC mass measured by the four-

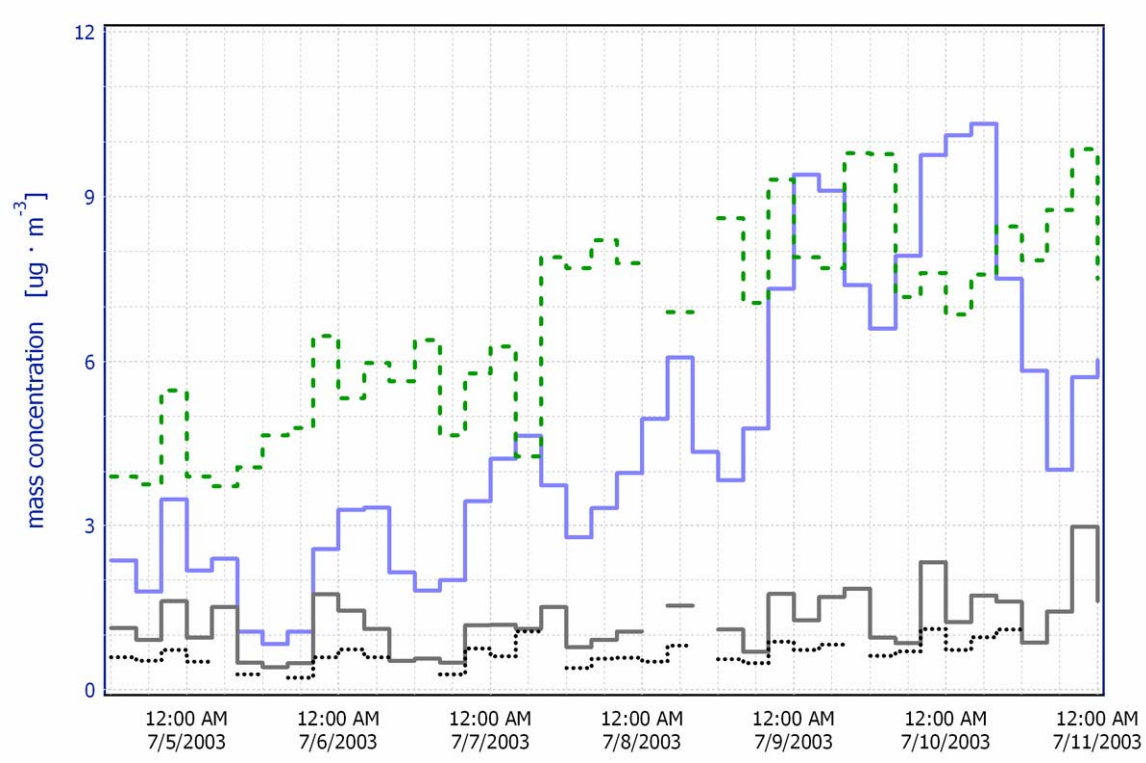

FIGURE 4.12. Time series of the elemental and organic carbon mass concentration in the Chamonix Valley during the summer 2003 campaign. This data was obtained from TOT analysis of PM2.5 filters sampled on four-hour intervals. Estimates of the total aerosol and WIA mass concentration calculated from the measured number concentration in the size range 0.3 - 2.0 μm are also shown.

hour filter samples with estimated WIA mass averaged over the same time period. WIA mass is highly correlated with EC, but essentially uncorrelated with OC. The slope of the EC-WIA regression is again greater than one for the same reasons discussed above.

4.3.2.2 the Maurienne Valley

Due to transportation and shipping delays, the WIA instrumentation was only able to run for the final three days of the summer campaign in the Maurienne Valley. The total aerosol particle counter was taken off-line for transport to Chamonix a day in advance of the WIA instrumentation, resulting in just two days of concurrent measurements. A time series of the number concentration observations is shown in Figure 4.13. The total

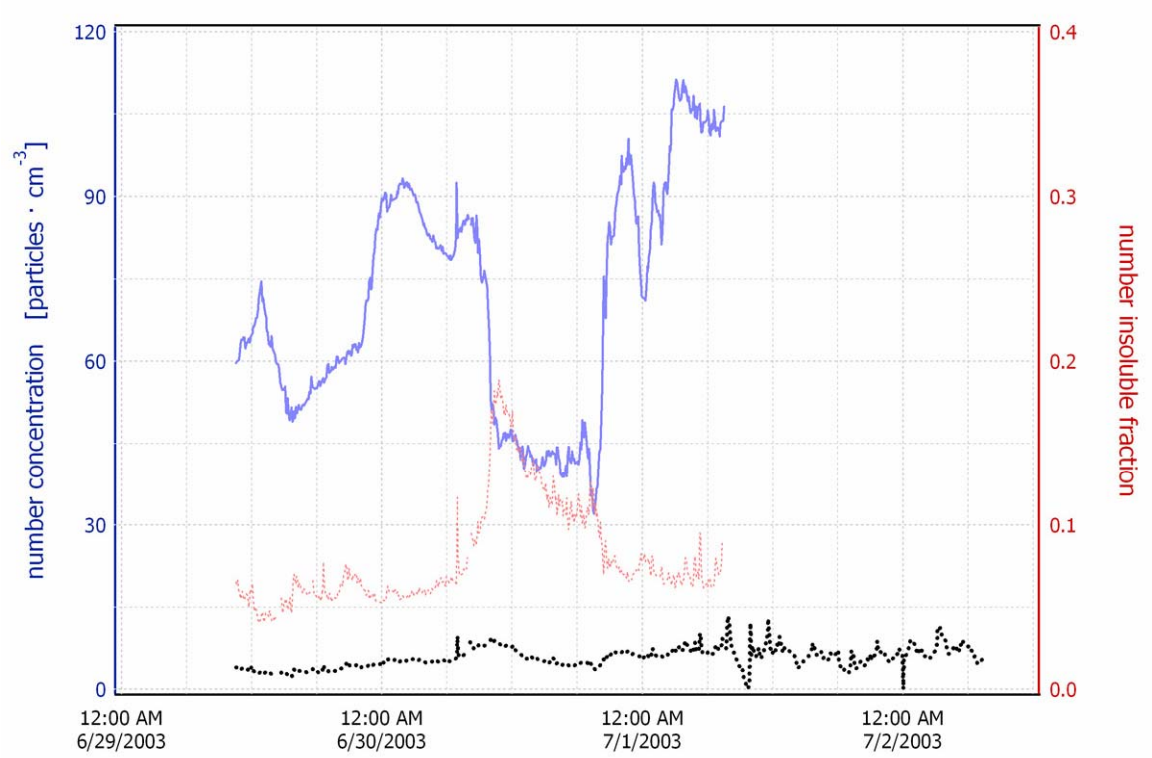

FIGURE 4.13. Time series of the total aerosol and WIA number concentration in the Maurienne Valley during the summer 2003 campaign. Displayed data is the sum of all particles in the size range 0.3 - 2.0 μm. ——— total aerosol ····· WIA ····· number insoluble fraction

concentration in Maurienne was about a third lower than in Chamonix. The insoluble fraction over this time period ranged from 5-19% with an average of 8.2%. Although only one complete diurnal cycle is observed, the pattern is consistent with that observed in the Chamonix Valley: the total particle concentration is highest at night when the mixing height is lowest and decreases during the day as the mixing height is elevated and outside air is advected into the valley. The water-insoluble aerosol concentration is not significantly influenced by the air from outside the valley and appears to fluctuate mainly in response to the patterns of traffic sources within the valley.

Figure 4.14 shows a size distribution obtained during a MOUDI run. The total particle mass exceeds the sum of EC and OC mass for all particles smaller than 2.0 μm. There

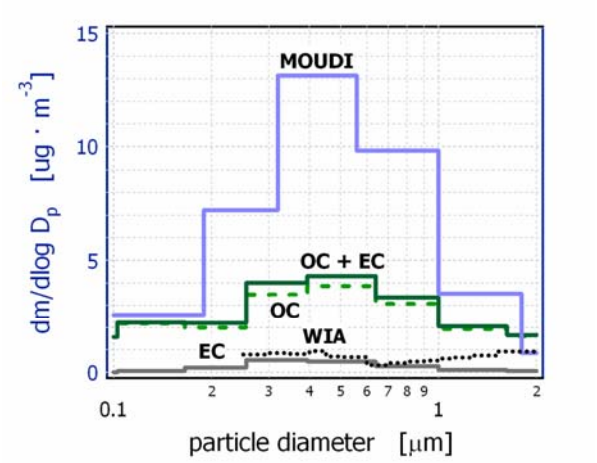

FIGURE 4.14. Mass size distribution in the Maurienne Valley during the summer 2003 campaign. The time period for these impactor samples was June 29 - 30, 2003.

is a peak in both the total and the OC mass between 0.3-0.6 μm. EC mass has a very broad peak between 0.25-1.0 μm. Estimated WIA mass exceeds EC mass at all sizes. Figure 4.15 shows a time series of the four-hour averages of EC and OC mass. Estimated WIA mass is equal to or greater than EC mass at all times. Beginning in the early morning of June 30, the estimated WIA mass seems to be decoupled from EC or OC concentration. The magnitude of this decoupling reaches a maximum on the afternoon of June 30, though the WIA concentration continues to fluctuate independently of EC mass for the remainder of the sampling period. Figure 4.16 shows the number size distributions averaged over eight hour periods both during and before this occurred. It may be seen from these charts that the size distribution of both the total aerosol population and WIA shifted toward larger sizes during this time period. Possible explanations for these larger insoluble particles include pollen and dust. The OC concentration of the same size particles actually decreases at this time, but this does not necessarily exclude pollen as a possibility since other sources of OC could have decreased by an even greater amount. Another possibility is wind-blown dust.

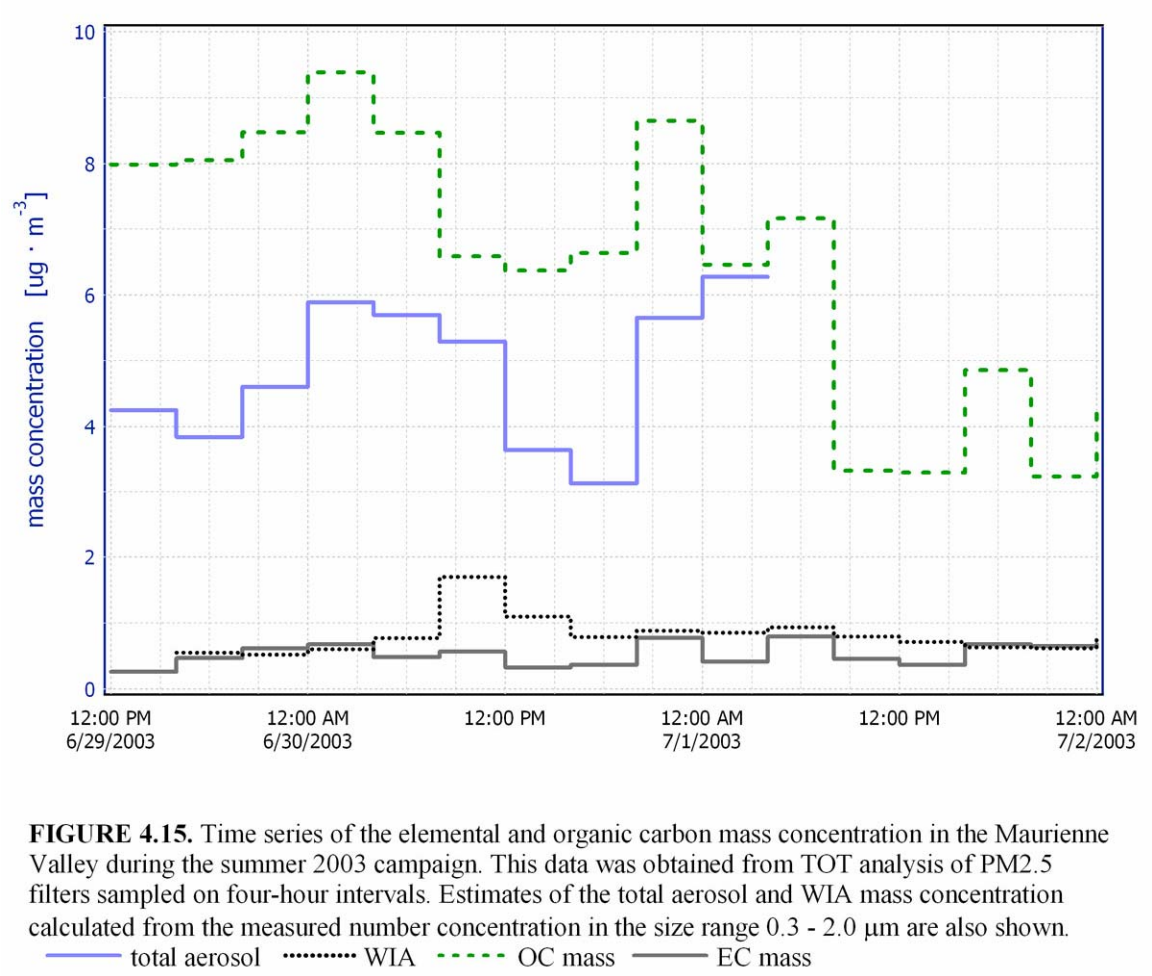

FIGURE 4.15. Time series of the elemental and organic carbon mass concentration in the Maurienne Valley during the summer 2003 campaign. This data was obtained from TOT analysis of PM2.5 filters sampled on four-hour intervals. Estimates of the total aerosol and WIA mass concentration calculated from the measured number concentration in the size range 0.3 - 2.0 μm are also shown.

Examination of the total aerosol concentration measured by the GRIMM dust monitor reveals that the percentage of particles larger than 2.0 μm increased by a factor of four during this time period (from 0.03% to 0.12%). Particles of that diameter are too large to be sized by the LiQuilaz, so it is not known whether or not they are insoluble, but an increase in the concentration of extremely large particles is consistent with an influx of wind-blown dust.

Figure 4.5(d) shows a regression of EC and OC mass against estimated WIA mass. There are far fewer data points for this campaign than for the three others. In addition, as discussed in the previous paragraph, the time series of WIA concentration shows

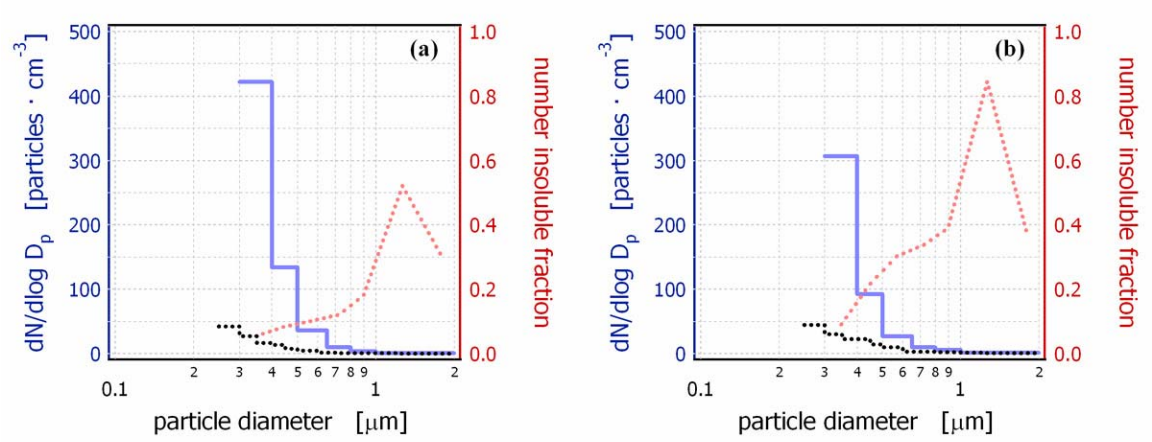

FIGURE 4.16. Number size distribution of the total aerosol and WIA number concentration in the Maurienne Valley during the summer 2003 campaign. Figure 4.16(a) is for the night of June 29 - 30 when WIA and EC concentrations tracked together and Figure 4.16(b) is for the daylight period of June 30 when the two concentrations diverged.
total aerosol ····· WIA ····· number insoluble fraction

evidence of being influenced by a non-carbonaceous particle source, possibly mineral aerosols. For this reason, the estimated WIA mass shows no correlation with either EC or OC mass.

4.4 Conclusions

A method to measure the size-resolved concentration of water-insoluble aerosol in real-time has been developed and successfully implemented in a field study in the Chamonix and Maurienne Valleys of the French Alps. This technique has shown that the concentration of insoluble particles is significant and that it fluctuates on time scales much too brief to be captured by filter samples, as short as a few minutes. In the alpine valleys examined in this study, the fraction (by number) of particles which are water-insoluble averages around 10% in both summer and winter. This is a factor of two higher than the insoluble fraction observed during a field test of this instrumentation in a rural

area near Atlanta, Georgia in August 2002 even though the total number concentrations at the two sites were comparable [*Greenwald et al*., 2005a]. Examination of the time evolution of particle concentrations shows a pattern of WIA being independently superimposed upon a larger background concentration of all types of aerosol. This pattern is especially pronounced during the summer when the daily evolution of mixing height draws in well-mixed air from outside the valley. In addition, the very rapid response of WIA concentration to local traffic patterns suggests that vehicular traffic is the primary source for insoluble aerosol in these valleys. Comparison of the time-series of WIA concentration with filter-based EC and OC measurements shows closer correlation with elemental carbon than organic carbon. Likewise, comparison of estimated size-resolved WIA mass concentration derived from optically-measured number concentration shows reasonable agreement with size-resolved elemental carbon measurements. The size-resolved insoluble fraction consistently exhibits a bi-modal distribution with peaks observed at 0.45 μm and 1.1 μm during all four campaigns.

The size distribution of WIA appears to be relatively consistent with only a few exceptions. During the winter-phase of sampling in the Maurienne Valley, a snowfall event was observed to substantially increase the insoluble peak at 0.45 μm. It is possible that the increase in the fraction of insoluble particles of this size is the result of measurement of the insoluble nuclei of snowflakes being added to the concentration of ground-level WIA. It is also possible that this increase in insoluble fraction was also influenced by an air mass change associated with the advance of a cold front through the valley. During the summer campaign in the Maurienne Valley, there was an extended time period during which the WIA concentration increased significantly with no corresponding increase in elemental carbon. At this time, the size distribution of the insoluble fraction was observed to shift larger sizes. Simultaneously, the fraction of

particles larger than 2.0 μm increased by a factor of four. Although it is not known if these large particles were insoluble, these observations are consistent with an increase in the concentration of wind-blown dust.

This field implementation of the WIA measurement technique has demonstrated the utility of this system and suggested the importance of its continued use. The results of this study imply that the dominate source of WIA in the regions examined is anthropogenic soot from motor vehicle emissions. An important secondary source is mineral dust. Furthermore, by examining the location of the peak of the WIA size distribution, it is possible to distinguish between the two. Given the significance of the climatic and health implications of soot and mineral dust, the information gleaned from this and similar future studies is of relevance to climate modelers and policy makers and merits pursuance.

SIZE-RESOLVED, REAL-TIME MEASUREMENT OF WATER-INSOLUBLE AEROSOLS IN METROPOLITAN ATLANTA DURING THE SUMMER OF 2004

Abstract

During the month of August 2004, the size-resolved number concentration of water-insoluble aerosols (WIA) from 0.25 to 2.0 μm was measured in real-time in the urban center of Atlanta, Georgia. Simultaneous measurements were performed for the total aerosol size distribution from 0.1 to 2.0 μm, absorption coefficient, dry (RH = 30%) and wet (RH = 80%) scattering coefficients and elemental and organic carbon mass concentration. While the concentrations of both the total aerosol and WIA population were found to fluctuate significantly on time scales of less than one hour, these fluctuations were frequently observed to occur independently of one another. The WIA population was found to follow a consistent diurnal pattern throughout the month with concentration maxima concurring with peaks in vehicular traffic flow. WIA concentration also responded to changes in meteorological conditions such as boundary layer depth and precipitation events. The temporal variability of the absorption coefficient followed an identical pattern to that of WIA. The WIA concentration was highly correlated with both the absorption coefficient and elemental carbon mass concentration. The total aerosol concentration and the scattering coefficient likewise followed an identical temporal pattern and were highly correlated with one another. These results suggest that WIA measurements are dominated by fresh emissions of particulate soot whereas the total aerosol population is dominated by highly-scattering aerosols from separate sources. For both the total aerosol and the WIA size distributions, the maximum number

concentration was observed at the smallest sizes; however the WIA size distribution also exhibited a peak at 0.45 μm which was not observed in the total population. Over 60% of the particles greater than 1.0 μm were observed to be water-insoluble according to our operational definition. As will be discussed in this paper, it is highly unlikely that these particles could be carbonaceous in origin, suggesting a crustal source for super-micron WIA.

5.1 Introduction

Atmospheric particulate matter influences the global climate both directly and indirectly [*Charlson et al*., 1992]. Aerosols directly influence climate by scattering [*Ångström*, 1929] and absorbing [*Lindberg*, 1975] solar radiation. Aerosol light scattering is a function of particle size [*Mie*, 1908] which is in turn a function of the amount of hygroscopic growth a particle experiences under high humidity [*Hobbs et al*., 1974] which is itself influenced by particle aqueous solubility [*Saxena et al*., 1995]. Light absorption (of visible wavelengths) is a size-dependent process dominated by particulate soot [*Lindberg*, 1975; *Rosen et al*., 1979], an insoluble aerosol. Aerosols indirectly influence climate by increasing the albedo [*Twomey*, 1974] and lifetime [*Albrecht*, 1989] of clouds. The ability of an aerosol to serve as a cloud condensation nucleus (CCN) and contribute to these indirect effects is also a function of a particle's affinity for water [*Saxena et al*., 1995], and hence is related to solubility. The negative influence of fine particulate matter on human health has been repeatedly documented [*Peel et al*., 2005; *Metzger et al*., 2004; *Brook et al.*, 2002; *Peters et al*., 2001]. Particulate soot has been identified as having unique properties which may pose a specific threat to human

respiratory health [*Sosnowski et al*., 2000] and has been observed to be highly correlated with cardiovascular disease [*Metzger et al*., 2004; *Le Tertre et al*., 2002].

Despite the significance of the influence of water-insoluble aerosol (WIA) on both climate and health, very few ambient measurements focusing specifically on the concentration of WIA have been conducted to date. Some studies have used cascade impactors to examine the size distribution of specific water-insoluble components of atmospheric aerosols such as elemental carbon [*Venkataraman and Friedlander*, 1994; *Jaffrezo et al*., 2005b]. Other studies have focused on the fraction of organic particulate matter which is water soluble and inferred by subtraction the amount of insoluble organic mass. *Zappoli et al*. [1999] found that 25-35% of the fine aerosol mass at several sites in Europe was water-insoluble and that approximately 10% of this mass was composed of organic compounds. Similar measurements performed by *Xu et al*. [2002] in the Yangtze delta region of China in November 1999 found that ~40% of the fine mode mass was water-insoluble organic carbon. All of the studies cited above are based on the analysis of filter samples which are generally run for a minimum of four hours for non-size-resolved mass or 24 hours for size-resolved mass. In order to observe the fluctuation of WIA on shorter time-scales, a technique to measure the size-resolved number concentration of WIA in near real-time has been developed [*Greenwald et al*., 2005a]. This system was implemented in a large field study in 2003 in a region of the French Alps that is heavily influenced by diesel truck emissions [*Greenwald et al.*, 2005b], and WIA was found to be highly correlated with elemental carbon mass. The size distribution of WIA was found to be consistent with the elemental carbon size distribution as measured using a cascade impactor. It was also observed that WIA concentration and size distribution varied on time scales far too short to be detected by filter-based measurements, illustrating the advantages of a real-time system.

In order to examine the concentration and temporal patterns of WIA in an urban environment, the WIA measurement system was installed in the ambient monitoring laboratory on the roof of the ES&T building on the campus of the Georgia Institute of Technology in August 2004. This paper examines the results of these measurements and discusses comparisons of this data with concurrent observations of the absorption and scattering coefficients as well as elemental and organic carbon mass.

5.2. Experimental approach

5.2.1 Instrumentation

The WIA instrumentation employed for this study is described in detail by *Greenwald et al*. [2005a]. This systems uses an impinger to entrain atmospheric particles into a liquid stream and then optically counts and sizes the particles which remain in the particle phase using a LiQuilaz SO2 manufactured by Particle Measuring Systems of Boulder, Colorado. Laboratory characterization experiments have demonstrated that this system correctly measures the concentration and size distribution of polystyrene latex spheres [*ibid*.]. For the ambient measurements discussed in this paper, the liquid solvent used in the impinger was ultrapure water. Since water was the medium in which particle light scattering was measured, only WIA with a refractive index significantly different from water (1.33 + 0.0 *i*) are capable of being detected. To elucidate the influence of particle refractive index on reported particle diameter, theoretical evaluation of this system was performed based on a Mie theory algorithm [*ibid*.]. This analysis has shown that for the range of refractive indices likely to be exhibited by WIA, reported size information is reasonably accurate for particles 0.25-0.6 μm with a slight tendency to undersize the particles by no more than 30%. For low refractive index particles (such as some soot and organic particles), as diameter increases, the tendency to undersize

becomes more pronounced, approaching 50%. For higher refractive index particles (such as mineral aerosols), reported particle size is nearly accurate at most diameters. This analysis also suggests that it is highly unlikely that particles reported by the LiQuilaz to be larger than 0.8 μm are composed of particulate soot. Such large insoluble particles are possibly organic or more likely crustal in origin. Despite uncertainty in sizing, concentration measurements are expected to be accurate in the size range of 0.25-2.0 μm. Measurement of the total (soluble + insoluble) aerosol number concentration was performed using a LASAIR 1002 also manufactured by Particle Measuring Systems. This instrument counts and sizes airborne particles in eight channels between 0.1 and >2.0 μm. For this study, the time resolution for both of these instruments was one minute.

In addition to number concentration data, the mass concentration of elemental and organic carbon (EC, OC) was monitored using a Sunset Laboratory carbon aerosol analysis field instrument Model 3F. This is a semi-continuous monitor which measures EC/OC mass using the thermal/optical transmittance (TOT) method described by *Birch and Cary* [1996]. During this study, the instrument was configured to collect particles on a quartz filter substrate for 45 minutes (starting at the top of each hour) and then perform sample analysis for the remaining 15 minutes of the hour. A $PM_{2.5}$ cyclone was installed at the inlet. It is important to note that this instrument measures the cumulative mass of all carbonaceous particles with an aerodynamic diameter less than 2.5 μm, including particles smaller than the 0.25 μm optical diameter cutoff for the LiQuilaz.

The particle absorption (σ_{ap}) and scattering (σ_{sp}) coefficients were also continuously monitored. σ_{ap} was measured using a Particle Soot Absorption Photometer (PSAP) manufactured by Radiance Research of Seattle, Washington and described in the literature by *Bond et al*. [1999]. σ_{ap} was adjusted according to the procedure described

by *Bond et al.* [1999] in order to account for the actual flow rate of the instrument and for the effect of extinction by scattering particles. In order to gauge the amount of hygroscopic growth particles experienced as a function of humidity, the scattering coefficient at both low and high relative humidity was measured using two Radiance Research nephelometers operating in parallel. A factor to parameterize particle hygroscopic growth, referred to here as f(RH), was calculated by dividing σ_{sp} (RH = 80%) by σ_{sp} (RH = 30%). The relative humidity of the ambient sample was lowered to 29.0±2.1% using a Nafion PD-Series gas dryer manufactured by Perma Pure LLC of Toms River, New Jersey. The sample line was then split with one part of the sample being sent to the first nephelometer to measure dry σ_{sp} and the other part being sent through a humidifier which raised the relative humidity to 78.7±1.7% and subsequently to the second nephelometer to measure wet σ_{sp}. The humidifier used for this study was a device of our own design which utilizes a Perma Pure MH-Series permeable membrane moisture exchanger. The relative humidity of the sample was maintained by using a PID controller to regulate the temperature of the moisture exchanger's continuously flowing water supply. Since f(RH) is highly sensitive to RH, only scattering measurements for which the RH was 80±2% were included in the f(RH) calculations.

5.2.2 Sampling site

The sampling instrumentation was installed in a laboratory on the roof of the ES&T building on the campus of Georgia Tech. This laboratory was specifically designed to permit measurements of the ambient atmosphere. Sample inlets are located approximately 15 m above the ground and 1.5 m above the surface of the roof. As shown in Figure 5.1, this building is located in the heart of the Atlanta metro region, approximately 1 km north of downtown Atlanta. A large freeway (Interstate 75/85) is

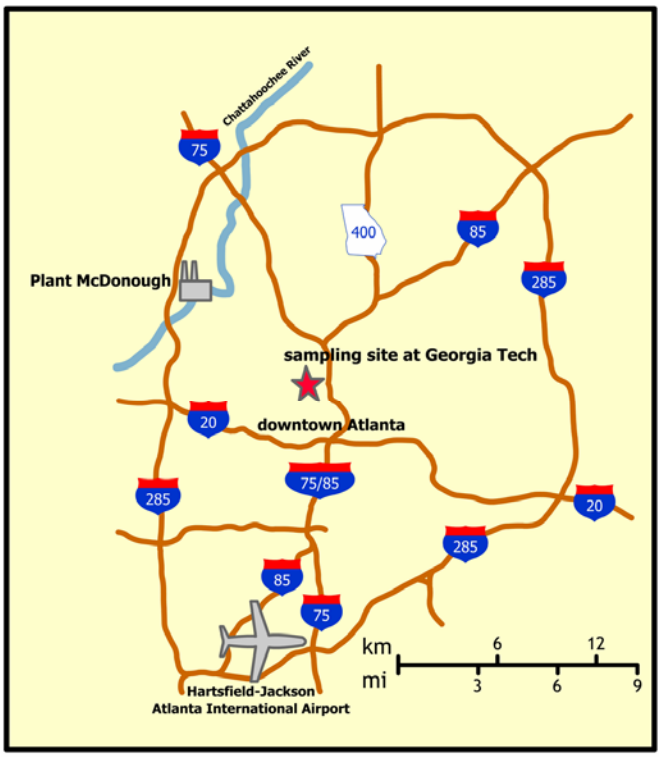

FIGURE 5.1. Location of sampling site in Atlanta, Georgia

located 500 m to the east, and a freeway loop encircling Atlanta (Interstate 285) forms an ellipse around the sampling site situated approximately 10 km to the east, west and south and 15 km to the north. A very large airport is located 10 km to the south, and there are nine major coal-fired power plants within 150 km, mostly to the west and northwest. Although wind direction and speed were not recorded at the sample site, the climatological wind field maintained by the National Climatic Data Center shows that in the month of August in Atlanta, the average wind direction is from the west or northwest 25% of the time, from the east 25% of the time, and all other directions 50% of the time. Wind speed is highest when blowing from the east. The typical late-summer weather pattern for Atlanta consists of warm and sunny conditions with temperatures ranging from 21-33°C punctuated by intense convective thunderstorms of varying frequency though most often in the late afternoon.

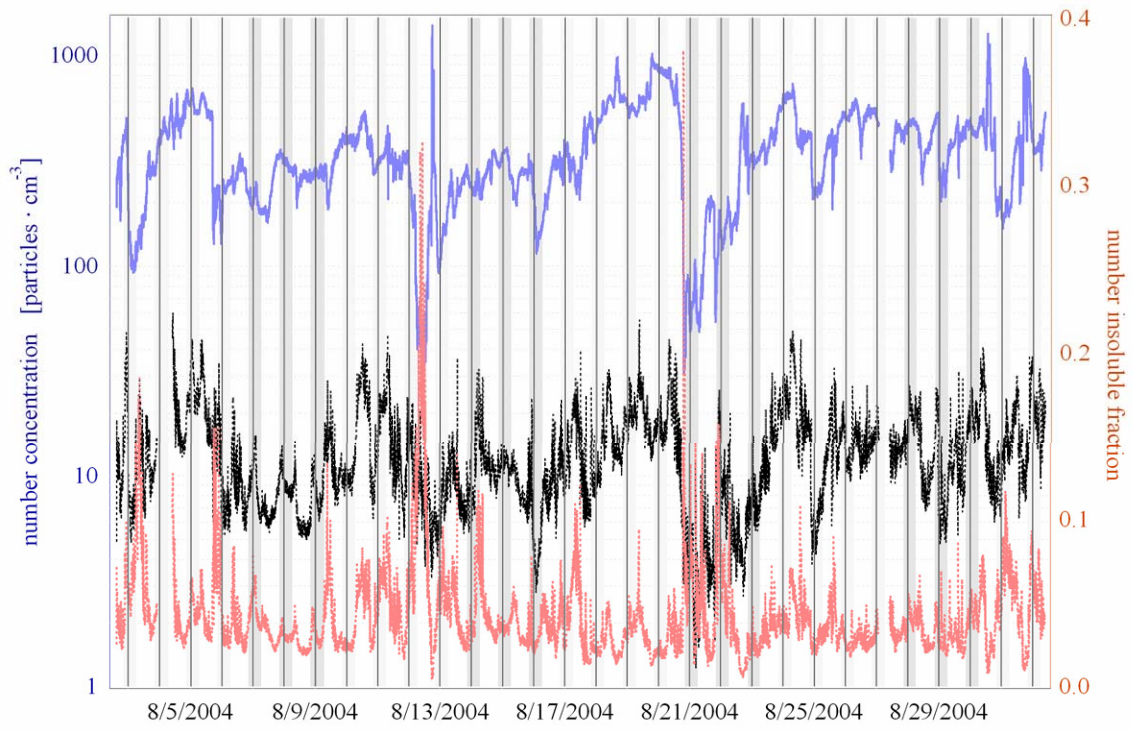

FIGURE 5.2. Time series of the total aerosol (blue) and WIA (black) number concentration for the month of August 2004 in Atlanta, Georgia. The number insoluble fraction (red) is shown on a linear scale on the right axis. Displayed data is the sum of all particles in the size range of 0.25-2.0 μm. Weekday nighttime periods are shaded light gray and weekend nighttimes are shaded a darker gray.

5.3 Results and discussion

5.3.1 Temporal trends

Figure 5.2 shows a time series of the number concentrations of both the total and water-insoluble aerosol populations for the entire month. These concentrations are the sum of all particles in the size range of 0.25-2.0 μm. Weekday nighttime periods are shaded light gray and weekend nighttimes are shaded a darker gray. Note that the total aerosol and WIA concentrations are shown on a log-scale on the left axis while the number insoluble fraction is on a linear-scale on the right axis. Both the total aerosol population and WIA exhibit a great deal of temporal structure with measured

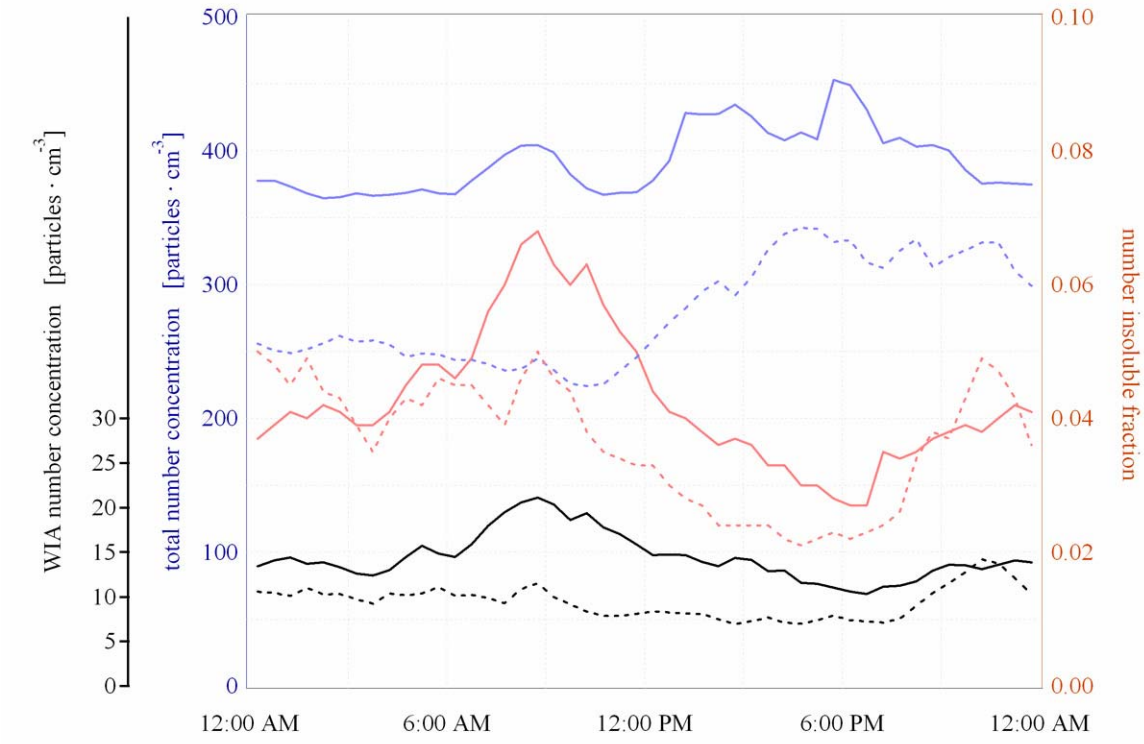

FIGURE 5.3. The diurnal pattern of the total aerosol (blue) and WIA (black) number concentration (two axes on left) and number insoluble fraction (red, right axis) averaged over the month of August 2004 as a function of time of day. Solid lines are the average of weekday values and dotted lines are the average of weekend values.

concentrations spanning an order of magnitude. The average insoluble fraction for the month was 4.1±2.5%.

Figure 5.3 illustrates the diurnal pattern of the average concentration and insoluble fraction values as a function of the time of day. Solid lines are for weekday values while dotted lines are for weekend values. Note that the WIA concentration is indicated by a second axis in order to clearly illustrate the temporal structure. The standard deviations of these values are not shown to maintain chart clarity, but are very close to 50±10%. The diurnal variation of the total aerosol concentration on weekdays displays a bi-modal pattern with both a mid-morning peak and a larger and broader peak in the afternoon. The diurnal pattern of the WIA concentration is uni-modal with peak concentration occurring in the mid-morning. This peak is likely related to the morning rush hour

increase in vehicle traffic. As the traffic flow tapers off and the mixing depth increases, this peak disappears. Since the afternoon peak in total concentration is not observed in the insoluble concentration, these particles are likely to either be secondary organic aerosol or an ionic species such as sulfate. Another major difference between the total aerosol and WIA diurnal patterns is the difference in magnitude between trough and peak. For the total aerosol population, this difference is 25% whereas for WIA, it is slightly over 100%. This may be explained by the hypothesis that the WIA sampled during this period was dominated by primary vehicular emissions. Since the mixing depth is much greater during the evening rush hour than the morning, primary emissions from vehicular traffic do not lead to as great of an increase in WIA concentration during the afternoon. The influence of the overnight descent of the mixing height is offset by a decrease in traffic such that the WIA concentration is relatively stable until the next morning's rush hour. On weekend evenings when there is more traffic at later times, the WIA concentration is observed to peak before midnight. The number insoluble fraction shows a pronounced peak in the morning when WIA concentration is greatest reaching an average weekday maximum of 6%. As is expected in an urban area heavily influenced by motor vehicles, particle concentrations are observed to be lower on weekends when there is less traffic. The number insoluble fraction also tends to be lower on weekends, although a secondary peak of 5% is observed before midnight on weekends that is absent on weekdays.

Figure 5.4 shows a time series of the absorption coefficient displayed concurrently with the WIA number concentration. Thirty minute averages have been displayed in order to facilitate visualization of the trends in this large data set. The temporal evolution of σ_{ap} closely followed the diurnal pattern of the WIA number concentration. The magnitude of σ_{ap} ranged from 0.62 to 46.8 Mm^{-1} and averaged 6.7 Mm^{-1} for the entire

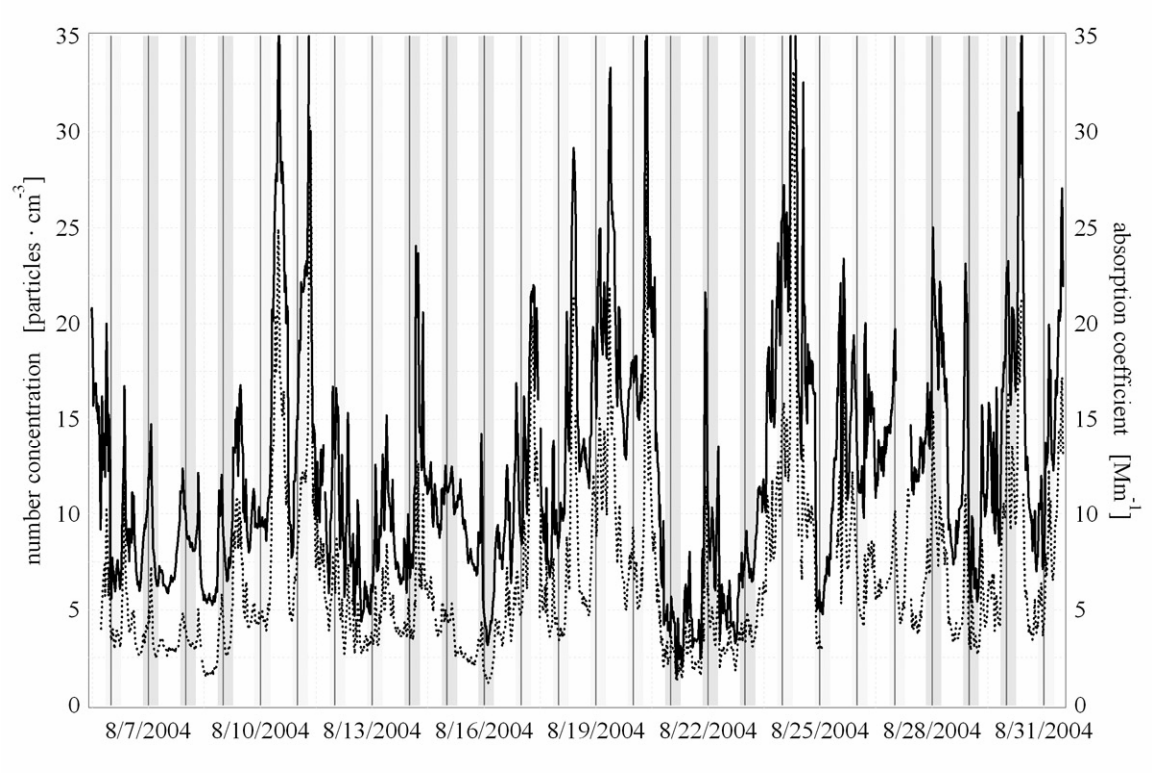

FIGURE 5.4. Time series of the absorption coefficient (dotted line) and the WIA number concentration (solid line) in the size range of 0.25-2.0 μm. These values are thirty minute averages. Weekday nighttime periods are shaded light gray and weekend nighttimes are shaded a darker gray.

month. Figure 5.5 shows the thirty minute average of f(RH) concurrently with the number insoluble fraction (i.e. the number of particles from 0.25-2.0 μm which are water-insoluble divided by the total number of particles from 0.25-2.0 μm). It is expected that as the fraction of aerosols which are water-insoluble becomes larger, the increase in light scattering due to hygroscopic growth will diminish and vice versa. However, since the insoluble fraction averages only 3% for the entire month, this effect may be easily overwhelmed by the 97% of the particles which are hygroscopic. Nonetheless, Figure 5.5 shows that the slopes of these two values tend to point in opposite directions. f(RH) therefore typically peaks in the late afternoon when the insoluble fraction is at a minimum and is lowest in the morning when the insoluble fraction peaks. A few time-periods were periodically observed throughout the month during which the slope of the

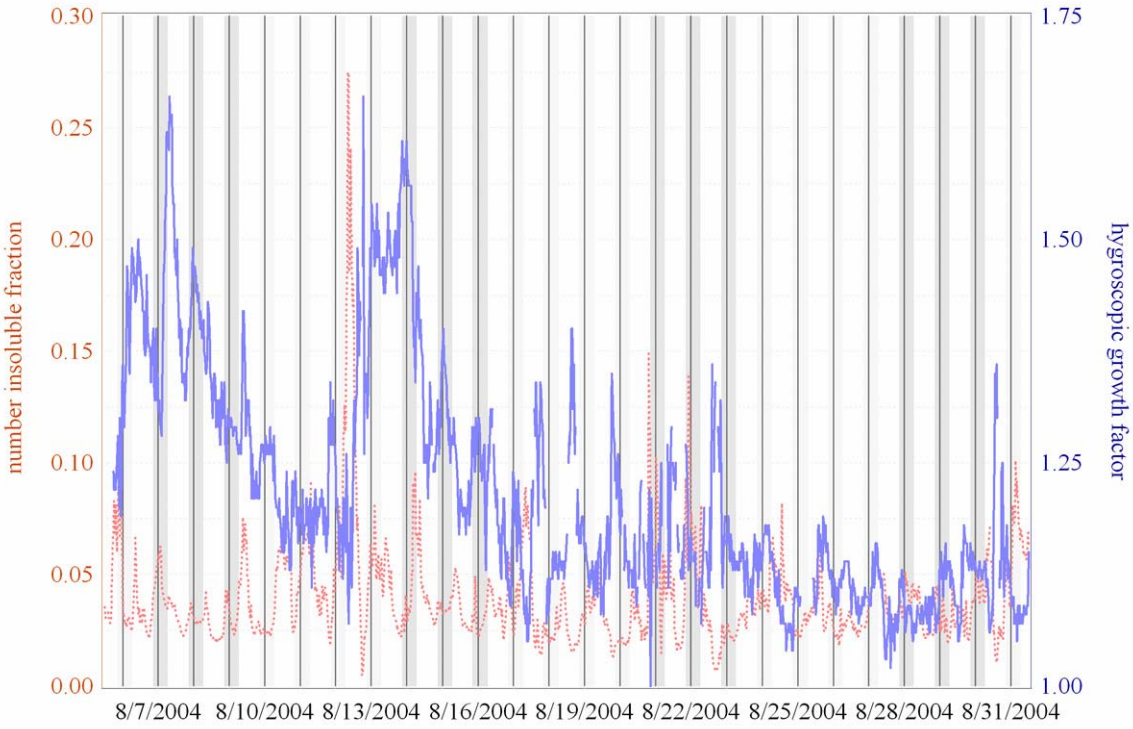

FIGURE 5.5. Thirty minute averaged time series of the hygroscopic growth factor, f(RH), (blue, right axis) and the number insoluble fraction (red, left axis) for particles in the size range 0.25-2.0 μm.

two curves were of the same rather than opposite sign, most notably on August 15, 16 and 24. Each time this occurred, it was also observed that the size distribution of WIA shifted toward larger sizes. As will be discussed in a later section, this is consistent with a dust incursion. Since crustal elements are not as hydrophobic as elemental carbon, it is possible that mineral aerosols are responsible for the increase in insoluble fraction during these periods while simultaneously experiencing hygroscopic growth.

Figure 5.6 shows a time series of the mass concentration of elemental and organic carbon. These values are 45-minute averages beginning at the top of every hour. Also shown on this chart is an estimate of WIA mass calculated from the measured number concentration averaged over the same time period as the EC/OC measurements. Conversion between number and mass concentration in the case of soot particles is not an exact process. However, these calculations provide a first-order approximation of

WIA mass and are useful for qualitatively comparing the trends in the evolution of EC and WIA concentration. WIA mass estimates are calculated by assuming that insoluble particles are spherical with a diameter equal to the log-average of the nominal upper and lower limits of the corresponding LiQuilaz channel and a density of 1.8 g · cm^{-3}. However, SEM analysis by many investigators has demonstrated that soot particles are fractal-like chain agglomerates of carbon spherules and are non-spherical to at least some extent. Analysis by *Hull et al.* [2004] suggests that the diameter inferred from light scattering approximately corresponds to the maximum distance between points on the chain agglomerate. Additional uncertainty in particle diameter arises from the disparity between the refractive index of soot particles and the PSL spheres used as a calibration standard. Another source of uncertainty in estimating particle mass is due to

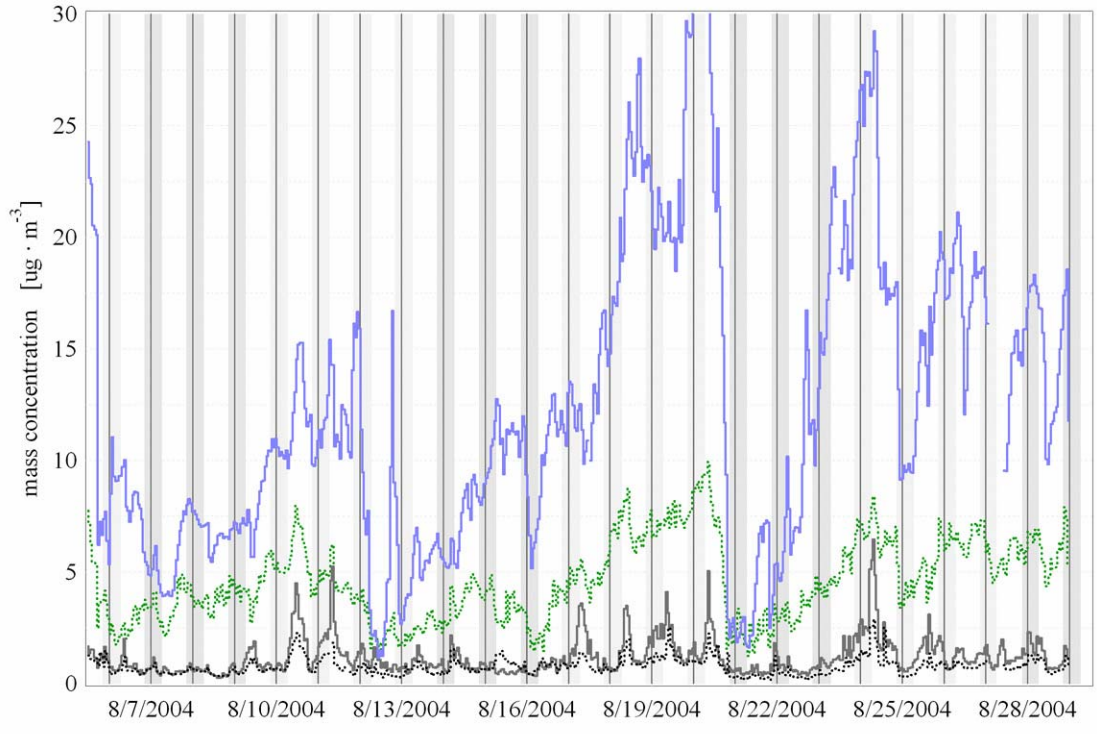

FIGURE 5.6. Time series of the measured mass concentration of elemental (solid gray) and organic (dotted green) carbon and the estimated total aerosol (solid blue) and WIA (dotted black) mass calculated from the measured number concentration. These values are 45 minute averages beginning at the top of every hour.

assumptions of the density of insoluble particles. The fractal-like structure of soot particles makes possible a wide range of values of particle density. Particles with a more open structure and a higher porosity will have a lower apparent density. The value of 1.8 $g \cdot cm^{-3}$ assumed for this study is consistent with values reported in the literature [*Fuller et al.*, 1999; *Janzen*, 1980], although this does not necessarily imply it is accurate.

With a few exceptions, the concentrations of EC and WIA closely parallel one another throughout the month with EC mass typically being 1.6 times larger than estimated WIA mass. Given that EC is completely insoluble in water, it is expected that WIA mass would be greater than or equal to EC mass. The discrepancy between observed and expected results may be explained by the uncertainty in converting WIA concentration from number to mass and by the fact that EC measurements cover the entire size range of particles with aerodynamic diameters less than 2.5 μm whereas the WIA measurements are only of the range of optical diameters 0.25-2.0 μm. It was frequently observed that in the period shortly following sunrise (particularly on August 9, 10, 24 and 26), the WIA mass estimate increased disproportionately to the measured EC mass concentration before returning to the monthly average after one or two hours. In addition, during the period of August 15-16, the estimated WIA mass exceeds EC mass by as much as a factor of two for a prolonged period. These discrepancies are apparently the result of a slight shift of the WIA size distribution toward larger sizes. Figure 5.7 clearly illustrates these shifts as a function of time. This chart displays the fraction of the WIA number concentration which was recorded in each LiQuilaz channel. Smaller diameter channels appear higher on the graph (*i.e*. compose a larger fraction of the concentration). When the smallest channels (corresponding to a nominal optical diameter of 0.25-0.35 μm) compose a smaller fraction of the concentration, the largest channels (optical diameter 0.4 μm and larger) compose a higher fraction. This

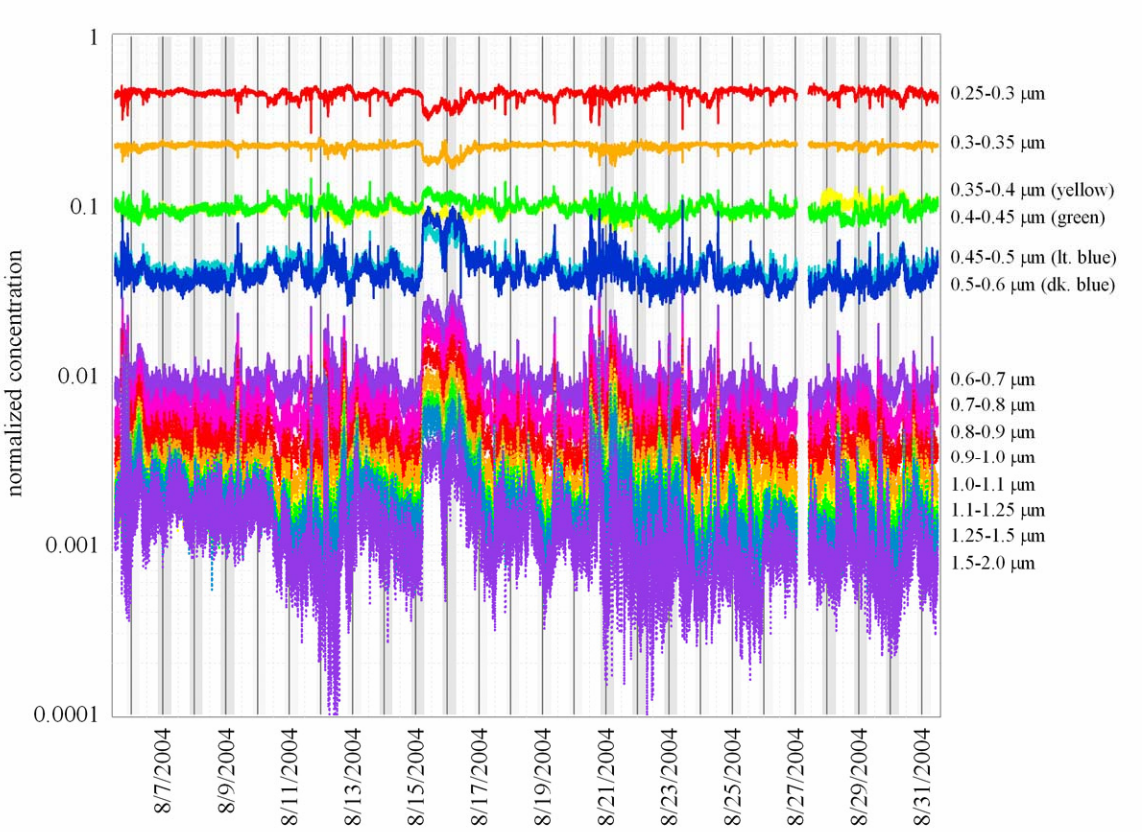

FIGURE 5.7. Fraction of the WIA number concentration which was recorded in each LiQuilaz channel. Channels which record smaller diameter particles appear higher on the graph.

phenomenon is especially pronounced on August 15-16 when the WIA mass estimate was observed to exceed measured EC mass. At this time, the fraction of the number concentration observed in the largest channels increased by a factor of four. A less-pronounced shift in size distribution is also frequently observed to occur in the morning hours at the same time that WIA mass was observed to increase disproportionately to EC mass and that the slope of the f(RH) time series is of the same sign as the number insoluble fraction. As previously mentioned, it is very unlikely that particles indicated by the LiQuilaz to be larger than 0.8 μm could be composed of elemental carbon. Possible sources for particle counts reported as greater than 0.8 μm are mineral aerosols, insoluble organic compounds and air bubbles generated by the impinger and entrained

in the sample flow. Of these possibilities, mineral aerosols of crustal origin are the most likely candidate. It is unlikely that entrained air bubbles are responsible for false counts at these sizes since these particles are not detected when a filter is installed at the inlet even though air is still drawn through the impinger. Large insoluble particles are considered more likely to be composed of crustal elements than insoluble organic carbon since the differing formation mechanisms of these particles results in the size distribution of mineral aerosols being skewed toward larger sizes relative to that of organic aerosols. This explanation is particularly compelling for the case of August 15-16 when the size distribution shift is especially pronounced. The SEARCH sampling program maintains a network of sampling sites throughout the Atlanta area including a site on Jefferson Street approximately 2 km from the Georgia Tech sampling site. Available data from this network includes 24 hour filter measurements of crustal

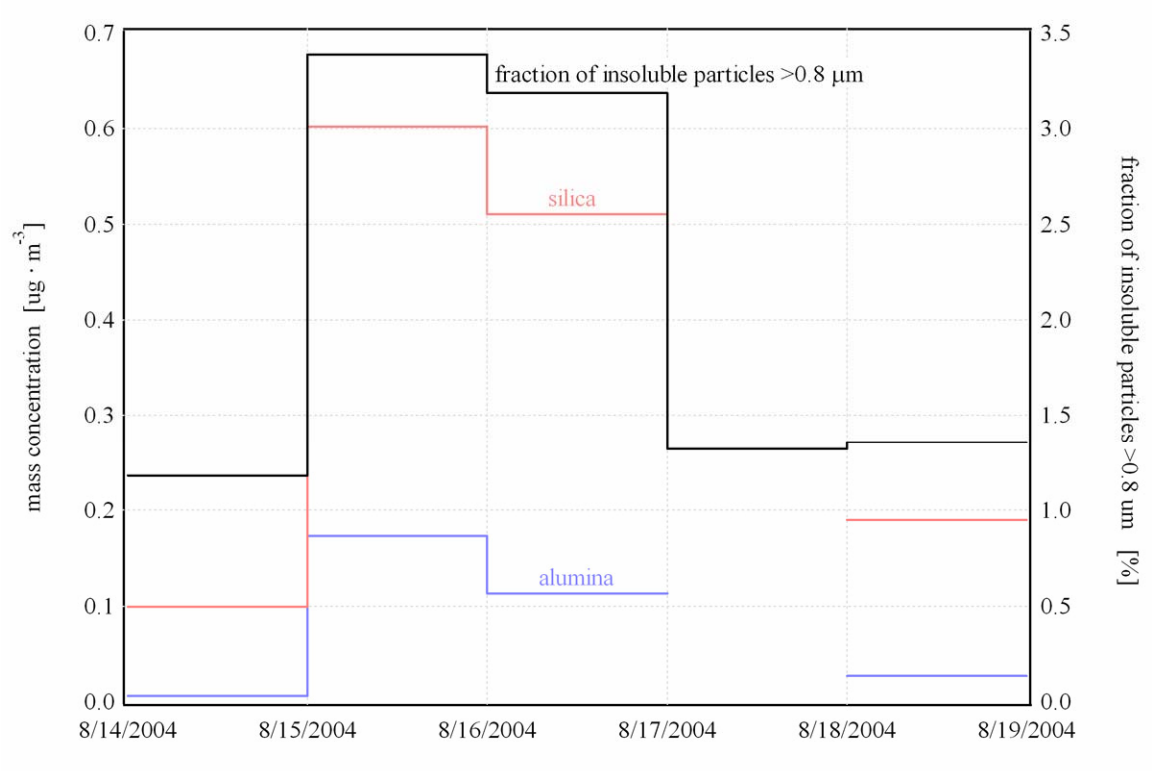

FIGURE 5.8. Mass concentration of silica (red) and alumina (blue) mineral aerosols at the Jefferson Street site in Atlanta (left axis) and the fraction of the WIA number concentration reported at particle sizes greater than 0.8 µm (right axis).

elements. Figure 5.8 shows the daily concentrations of alumina (Al_2O_3) and silica (SiO_2) for the period of August 14-19 at the Jefferson Street site in Atlanta [*B. Hartsell*, 2005, personal communication]. Also shown is the fraction of WIA number counts which were reported to be larger than 0.8 μm. This chart clearly illustrates an increase in the concentration of mineral aerosols at the same time as the WIA concentration shifts toward larger sizes. This suggests that the WIA instrumentation may be useful for detecting dust episodes and for distinguishing between soot particles and mineral aerosols.

5.3.2 Relationships between measured values

Figure 5.9 shows the linear regressions of several measured quantities. Figure 5.9(a) shows the linear regression of the thirty minute averages of the absorption coefficient with the measured WIA number concentration; Figure 5.9(b) shows the regression of EC mass with the estimated WIA mass; Figure 5.9(c) shows the regression of OC mass with estimated WIA mass and Figure 5.9(d) shows the regression of OC mass with EC mass. As is made clear in Figure 5.9(a), σ_{ap} is highly correlated with WIA number concentration with an r^2 value of 0.89. Since atmospheric absorption of visible wavelengths is dominated by a water-insoluble aerosol species, namely particulate soot, it is not surprising that WIA and absorption are highly correlated. Indeed, a linear regression of the two quantities is not needed to realize this. The time series analysis of these values which was discussed in the previous section reveals that with only a few exceptions (probably related to mineral aerosols), they co-vary almost perfectly. Although the regression and covariance of these quantities by itself is not proof of causation, the implication is striking.

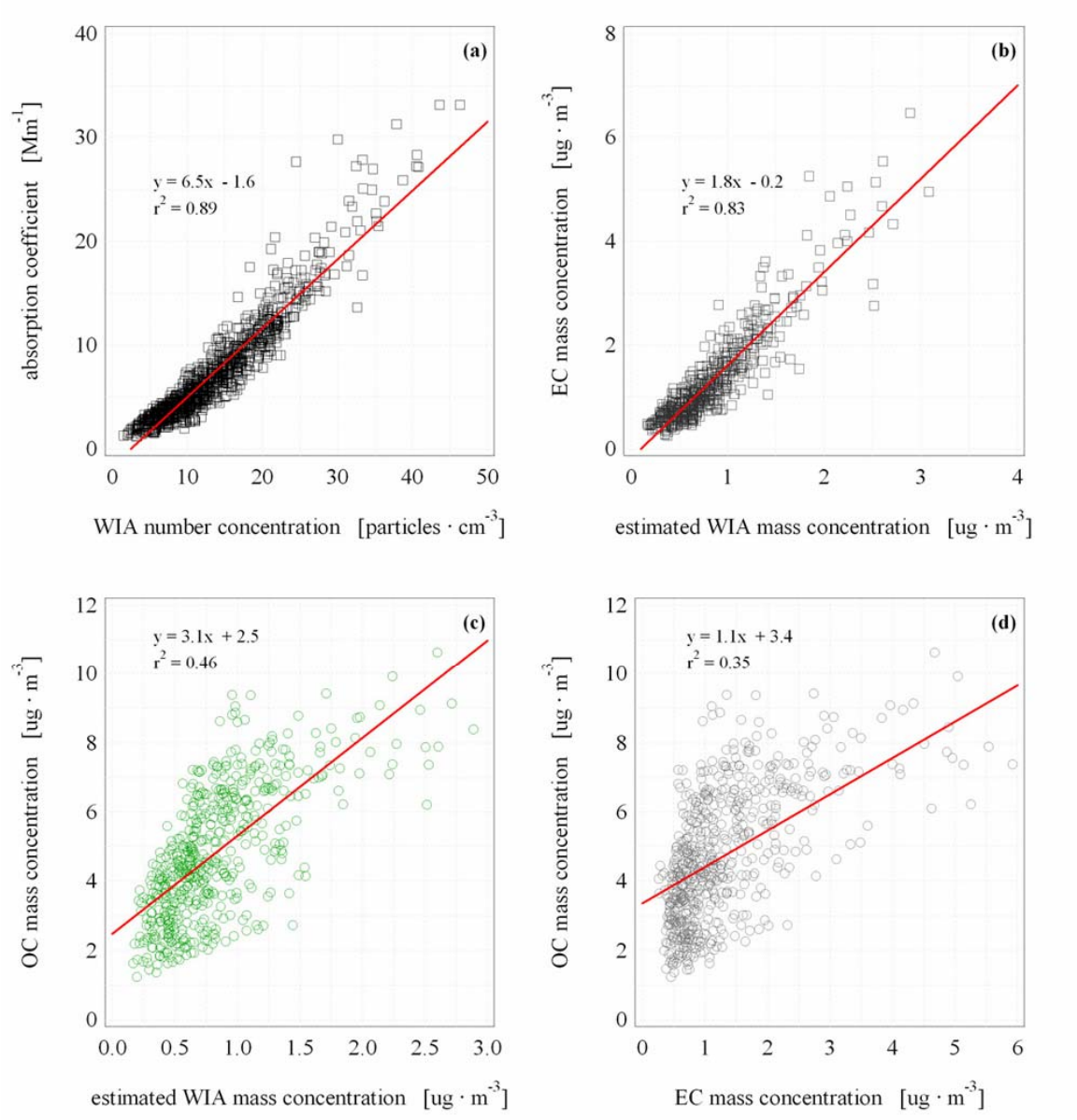

FIGURE 5.9. Linear regressions of several measured quantities. Figure 5.9(a) shows the linear regression of the thirty minute averages of the absorption coefficient with the measured WIA number concentration; Figure 5.9(b) shows the regression of EC mass with the estimated WIA mass; Figure 5.9(c) shows the regression of OC mass with estimated WIA mass and Figure 5.9(d) shows the regression of OC mass with EC mass.

Given the high correlation with σ_{ap}, it was expected that WIA would likewise be highly correlated with EC as is shown in Figure 5.9(b). The r^2 value for this regression is 0.83. Since EC is completely insoluble in water, the slope of the regression curve should theoretically be ≤ 1.0. However, this line suggests that on average, the measured mass

of elemental carbon is 1.7 times greater than the estimated mass of WIA. This discrepancy is likely the result of both the uncertainty in the conversion of WIA number concentration to mass and the fact that the EC filter measurements account for the mass of particles smaller than 0.25 μm while the LiQuilaz does not. Size-resolved measurements of the EC mass concentration at the Atlanta super site on Jefferson Street in August 1999 show that approximately 30% of the EC mass had an aerodynamic diameter less than 0.25 μm [*Carrico et al.*, 2001] Figure 9(c) shows that OC mass is not highly correlated with estimated WIA mass with an r^2 value of only 0.46. As is seen in Figure 5.9(d), the regression of OC mass with EC mass is virtually identical to the regression of OC mass with WIA mass. Given the large number of data points collected during this month of sampling, this regression strongly suggests that EC and WIA are not statistically independent variables and may in fact be different measurements of the same quantity. This observation combined with the high correlation of WIA and σ_{ap} provides convincing evidence that the particles measured by this technique during this sample period were most frequently composed of soot. This does not imply that insoluble OC aerosols are not present or are not detected, but rather that the signal from such particles was much less significant than that of EC particles. This observation may be explained by noting that the refractive index of insoluble organic carbon tends to be somewhat similar to that of the scattering medium of the LiQuilaz. This results in organic particles being undersized or not counted at all. In addition, organic aerosols determined to be insoluble by other techniques may have sufficient partial solubility to be dissolved in the nearly-infinitely dilute mixing chamber of the impinger used by this technique. It should be noted that this instrumentation does not provide information on the mixing state of aerosols such that soot particles counted by

the LiQuilaz may have existed in the atmosphere as the core of a larger particle containing significant quantities of water-soluble organic carbon or ionic mass.

5.4 Conclusion

The results of these measurements indicate that during the month of August 2004, approximately 4% (by number) of atmospheric particles in Atlanta with optical diameters 0.25-2.0 μm were water-insoluble aerosols as determined by our instrumentation. Since our technique counts particles optically in a water medium, particles with refractive indices similar to that of water are difficult to detect and are under-sized. Certain insoluble organic compounds fall into this category and may be present in atmospheric particles. Therefore, the actual insoluble fraction may have been greater than 4%. Particles which were detected by our instrumentation exhibit high correlations with elemental carbon mass and the absorption coefficient. Additionally, these particles also do not display independent correlation with organic carbon mass. These observations strongly suggest that the measured WIAs are dominated by particulate soot. This conclusion is strengthened by the additional observation that WIA concentration temporally co-varies with motor vehicle traffic (the predominate source of soot) on both weekdays and weekends. This does not imply that WIA is exclusively composed of elemental carbon. Indeed, several transient events were observed throughout the month that were consistent with an influx of mineral aerosols. At these times, the normally parallel temporal trend of WIA and EC concentration diverged while the size distribution of WIA simultaneously shifted toward larger sizes. Particles with diameters reported by the instrument to be larger than 0.8 μm are unlikely to be composed of elemental carbon due to their refractive properties. The fact that a few particles in this size range were

regularly detected suggests that mineral aerosols (and to some extent, large insoluble organics) were commonly present.

Time series analysis of both the total aerosol population and the water-insoluble subset reveals an interesting pattern. WIA concentration displayed a regular diurnal variability influenced by both normal traffic cycles and meteorological events such as precipitation and changes in the depth of the well-mixed boundary layer. The concentration of the total aerosol population displayed some diurnal regularity as well; however, it also experienced fluctuations of up to an order of magnitude which were not observed in the WIA concentration. This suggests that WIA are the result of local traffic emissions superimposed on a larger population of aerosols of more distant sources. This conclusion is consistent with a previous sampling campaign involving this instrument in the French Alps [*Greenwald et al*., 2005b]. In both cases, the sampling site was heavily influenced by motor vehicle traffic and displayed a repeated pattern of WIA concentration cycles against a larger backdrop of non-co-varying soluble aerosols. It may be interesting for future sampling campaigns to examine the concentration of WIA in areas not heavily influenced by direct motor vehicle emissions in order to gather information concerning the prevalence and lifetime of WIA in the atmosphere.

CONCLUSIONS AND FUTURE WORK

The atmospheric concentration of anthropogenic aerosols is significant in many important agricultural areas around the world. A study using the CERES crop model was conducted in order to estimate the possible range of the radiative influence of these aerosols on global crop yields. The presence of aerosols in the atmosphere simultaneously decreases total PAR and increases the fraction of PAR which is diffuse. Increasing the diffuse fraction increases the radiation use efficiency of a plant. The magnitude of this increase is not definitively known and most likely varies by species, cultivar, stage of development, irradiance level, LAI, and stress level. On clear sky days, aerosols both significantly decrease the amount of PAR reaching the surface and increase the diffuse fraction. On overcast days, aerosols decrease PAR without significantly changing the diffuse fraction. Therefore, the influence of aerosols on photosynthesis is more negative on overcast days than on clear days. Consequently, the more overcast days there are in a growing season, the more likely aerosols are to negatively influence agricultural production. Model results were found to be extremely sensitive to the initial assumption concerning the magnitude of the change in RUE with an increasing diffuse fraction. The relationship between the diffuse fraction and RUE is not well-known for most species of plant and needs to be determined in order to accurately predict the influence of aerosols on crop production. Using the most likely set of assumptions concerning AOD and ΔRUE, the influence of aerosols is predicted to reduce maize yields by approximately 10% at all examined sites, increase rice yields by 20% in California's central valley, slightly increase rice yields in Thailand, reduce rice

and wheat yields by 5-10% India, and cause essentially no change in wheat yield grown in the Midwestern United States. These model simulations were performed by stipulating that the plants experienced no water or nutrient stress. The results from these simulations strongly suggest the need for a more comprehensive study that will examine the influence of aerosols on temperature and evapotranspiration, the indirect effect of aerosols on clouds and precipitation, and the influence of water and nutrient stress.

A new technique to measure the size-resolved concentration of water-insoluble aerosols in near real-time has been developed and successfully implemented in field studies. Laboratory characterization has demonstrated that this instrumentation correctly measures the concentration and size distribution of polystyrene latex spheres. Analysis of the specific operating conditions of this instrumentation using a modified Mie theory algorithm suggests reasonable performance for the range of particle refractive indices likely to be found in the atmosphere. This analysis also suggests that insoluble particles reported by the instrument to be larger than 0.8 μm are unlikely to be composed of particulate soot and are instead likely to be composed of mineral aerosols of crustal origin. This does not imply that soot particles larger than 0.8 μm are not present in the atmosphere but rather that they are undersized by this instrumentation.

An initial field study consisting of four sampling campaigns in the Chamonix and Maurienne Valleys of the French Alps was conducted in 2003. Results of these sampling campaigns have shown that the concentration of insoluble particles is significant and that it fluctuates on time scales much too brief to be captured by filter samples, as short as a few minutes. In the alpine valleys examined in this study, the fraction (by number) of particles which are water-insoluble averages around 10% in both summer and winter. This is a factor of two higher than the insoluble fraction observed during a field test of

this instrumentation in a rural area near Atlanta, Georgia in August 2002 even though the total number concentrations at the two sites were comparable. Examination of the time evolution of particle concentrations shows a pattern of WIA being independently superimposed upon a larger background concentration of all types of aerosol. This pattern is especially pronounced during the summer when the daily evolution of mixing height draws in well-mixed air from outside the valley. In addition, the very rapid response of WIA concentration to local traffic patterns suggests that vehicular traffic is the primary source for insoluble aerosol in these valleys. Comparison of the time-series of WIA concentration with filter-based EC and OC measurements shows closer correlation with elemental carbon than organic carbon. Likewise, comparison of estimated size-resolved WIA mass concentration derived from optically-measured number concentration shows reasonable agreement with size-resolved elemental carbon measurements. The size-resolved insoluble fraction consistently exhibits a bi-modal distribution with peaks observed at 0.45 μm and 1.1 μm during all four campaigns in the French Alps. The size distribution of WIA appeaed to be relatively consistent with only a few exceptions. During the winter-phase of sampling in the Maurienne Valley, a snowfall event was observed to substantially increase the insoluble peak at 0.45 μm. It is possible that the increase in the fraction of insoluble particles of this size is the result of measurement of the insoluble nuclei of snowflakes being added to the concentration of ground-level WIA. It is also possible that this increase in insoluble fraction wais also influenced by an air mass change associated with the advance of a cold front through the valley. During the summer campaign in the Maurienne Valley, there was an extended time period during which the WIA concentration increased significantly with no corresponding increase in elemental carbon. At this time, the size distribution of the insoluble fraction was observed to shift larger sizes. Simultaneously, the fraction of

particles larger than 2.0 μm increased by a factor of four. Although it is not known if these large particles were insoluble, these observations are consistent with an increase in the concentration of wind-blown dust.

Another sampling campaign was conducted in an urban setting in Atlanta, Georgia during the month of August 2004. The results of these measurements indicate that approximately 4% (by number) of atmospheric particles with optical diameters 0.25-2.0 μm were water-insoluble during the month these measurements were being conducted. Since our technique counts particles optically in a water medium, particles with refractive indices similar to that of water are difficult to detect and are under-sized. Certain insoluble organic compounds fall into this category and may be present in atmospheric particles. Therefore, the actual insoluble fraction may have been greater than 4%. Particles which were detected by our instrumentation exhibit high correlations with elemental carbon mass and the absorption coefficient. Additionally, these particles also do not display independent correlation with organic carbon mass. These observations strongly suggest that the measured WIAs are dominated by particulate soot. This conclusion is strengthened by the additional observation that WIA concentration temporally co-varies with motor vehicle traffic (the predominate source of soot) on both weekdays and weekends. This does not imply that WIA is exclusively composed of elemental carbon. Indeed, several transient events were observed throughout the month that were consistent with an influx of mineral aerosols. At these times, the normally parallel temporal trend of WIA and EC concentration diverged while the size distribution of WIA simultaneously shifted toward larger sizes. Since particles with diameters reported by the instrument to be larger than 0.8 μm are unlikely to be composed of elemental carbon due to their refractive properties, the fact that a few particles in this

size range were regularly detected suggests that mineral aerosols (and to some extent, large insoluble organics) were commonly present.

Time series analysis of both the total aerosol population and the water-insoluble subset reveals an interesting pattern. WIA concentration displayed a regular diurnal variability influenced by both normal traffic cycles and meteorological events such as precipitation and changes in the depth of the well-mixed boundary layer. The concentration of the total aerosol population displayed some diurnal regularity as well; however, it also experienced fluctuations of up to an order of magnitude which were not observed in the WIA concentration. This suggests that WIAs are the result of local traffic emissions superimposed on a larger population of aerosols of more distant sources. This conclusion is consistent with the previous sampling campaigns in the French Alps. In both of these cases, the sampling sites are heavily influenced by motor vehicle traffic and display a repeated pattern of WIA concentration cycles against a larger backdrop of non-co-varying soluble aerosols. It may be interesting for future sampling campaigns to examine the concentration of WIA in areas not heavily influenced by direct motor vehicle emissions in order to gather information concerning the prevalence and lifetime of WIA in the atmosphere.

These field implementations have demonstrated the utility of this system to measure WIA and have suggested the importance of its continued use in order to characterize the prevalence and global distribution of WIA. In addition, several modifications of this technique may be useful for future studies. In each of the field campaigns discussed in this thesis, the solvent used in the impinging process was water; hence the measured particles are referred to as water-insoluble aerosols. However, it is possible to employ other solvents in order to further refine the target particle type. Many water-insoluble organic species are known to be present in atmospheric aerosols. Solvents such methanol or ethanol may be used to dissolve these compounds leaving only particulate

soot and mineral aerosols. The effect of evaporative cooling during the impinging process may make it difficult to use highly volatile solvents without freezing the impinger jets. Initial laboratory tests using hexane as the impinger solvent encountered this problem.

During each field campaign it was also observed that the insoluble number concentration was dominated by the smallest particles; however, the physics of the instrumentation prevents the detection of particles less than 0.25 μm using this technique. This limitation is largely the result of the wavelength of the laser used by the liquid particle counter. This wavelength is 780 nm or slightly longer than is visible. By using a shorter wavelength laser, it is theoretically possible to significantly reduce the lower limit of detectable particle sizes. A potential problem which may be encountered if this were to be attempted is the collection efficiency of the impinger for extremely small particles. The collection efficiency as currently operated is 80% for 0.3 μm particles. To efficiently capture particles smaller than this, novel techniques may need to be employed such as using more than one impinger in series or experimenting with both the liquid and air flow rates.

REFERENCES

Albrecht, B. A., 1989. Aerosols, cloud microphysics, and fractional cloudiness. *Science,* 245, 1227-1230.

Ångström, A., 1929. On the atmospheric transmission of sun radiation and on dust in the air. *Geografiska Annaler,* 11, 156-166.

Anquetin, S., C. Guilbaud and J.-P. Chollet, 1999. Thermal valley inversion impact on the dispersion of a passive pollutant in a complex mountainous area. *Atmospheric Environment,* 33, 3953-3959.

Batten, C. E., 1985. Spectral optical constants of soots from polarized angular reflectance measurements. *Applied Optics,* 24, 1193-1199.

Bergin, M. H., G. R. Cass, J. Xu, C. Fang, L. M. Zeng, T. Yu, L. G. Salmon, C. S. Kiang, X. Y. Tang, Y. H. Zhang and W. L. Chameides, 2001. Aerosol radiative, physical, and chemical properties in Beijing during June 1999. *Journal of Geophysical Research,* 106, 17969-17980.

Bergin, M. H., R. Greenwald, J. Xu and W. L. Chameides, 2001. Influence of aerosol dry deposition on photosynthetically active radiation available to plants: A case study in the Yangtze delta region of China. *Geophysical Research Letters,* 28, 3605-3608.

Birch, M. E. and R. A. Cary, 1996. Elemental carbon-based method for monitoring occupational exposures to particulate diesel exhaust. *Aerosol Science and Technology,* 25, 221-241.

Bond, T. C., T. L. Anderson and D. Campbell, 1999. Calibration and intercomparison of filter-based measurements of visible light absorption by aerosols. *Aerosol Science and Technology,* 30, 582-600.

Braga, R., 2000. Predicting the spatial pattern of grain yield under water limiting conditions. Agricultural and Biological Engineering Department

Brook, R. D., J. R. Brook, B. Urch, R. Vincent, S. Rajagopalan and F. Silverman, 2002. Inhalation of fine particulate air pollution and ozone causes acute arterial vasoconstriction in healthy adults. *Circulation,* 105, 1534-1536.

Carrico, C. M., M. H. Bergin, J. Xu, K. Baumann and H. Maring, 2003. Urban aerosol radiative properties: measurements during the 1999 Atlanta Supersite Experiment. *Journal of Geophysical Research,* 108, 8422.

Carrico, C. M., S. M. Kreidenweis, W. C. Malm, D. E. Day, T. Lee, J. Carrillo, G. R. McMeeking and J. L. Collett Jr., 2005. Hygroscopic growth behavior of a carbon-dominated aerosol in Yosemite National Park. *Atmospheric Environment,* 39, 1393-1404.

Castrignano, A., N. Katerji, F. Karam, M. Mastrorilli and A. Hamdy, 1998. A modified version of CERES-maize model for redicting crop response to salinity stress. *Ecological Modelling,* 111, 107-120.

Chameides, W. L., H. Yu, S. C. Liu, M. H. Bergin, X. Zhou, L. Mearns, G. Wang, C. S. Kiang, R. D. Saylor, C. Luo, Y. Huang, A. Steiner and F. Giorgi, 1999. Case Study of the effects of atmospheric aerosols and regional haze on agriculture: An opportunity to enhance crop yields in China through emission controls? *Proceedings of the National Academy of Sciences,* 96, 13626-13633.

Chang, H. and T. T. Charalampopoulos, 1990. Determination of the wavelength dependence of refractive indices of flame soot. *Proceedings: Mathematical and Physical Sciences,* 430, 577-591.

Charlson, R. J. and N. C. Ahlquist, 1969. Brown haze: NO_2 or aerosol? *Atmospheric Environment,* 3, 653-656.

Charlson, R. J., S. E. Schwartz, J. M. Hales, R. D. Cess, J. A. Coakley, J. R. Hansen and D. J. Hofman, 1992. Climate forcing by anthropogenic aerosols. *Science,* 255, 423-430.

Chen, S.-J., S.-H. Liao, W.-J. Jian and C.-C. Lin, 1997. Particle size distribution of aerosol carbons in ambient air. *Environment International,* 23, 475-488.

Cheyglinted, S., S. L. Ranamukhaarachchi and G. Singh, 2001. Assessment of the CERES-rice model for rice production in the central plain of Thailand. *Journal of Agricultural Science,* 137, 289-298.

Choudhury, B. J., 2001. Estimating gross photosynthesis using satellite and ancillary data. *Remote Sensing Environment,* 75, 1-2.

Chuang, P. Y., 2003. Measurement of the timescale of hygroscopic growth for atmospheric aerosols. *Journal of Geophysical Research,* 108, 5-1.

Chughtai, A. R., J. M. Kim and D. M. Smith, 2002. The effect of air/fuel ratio on properties and reactivities of combustion soots. *Journal of Atmospheric Chemistry,* 43, 21-43.

Chun, Y., J. Kim, J. Cheon Choi, K. On Boo, S. Nam Oh and M. Lee, 2001. Characteristic number size distribution of aerosol during Asian dust period in Korea. *Atmospheric Environment,* 35, 2715-2721.

Cohan, D. S., J. Xu, R. Greenwald, M. H. Bergin and W. L. Chameides, 2002. Impact of atmospheric aerosol light scattering and absorption on terrestrial net primary productivity. *Global Biogeochemical Cycles,* 16, 1090.

Dickerson, R. R., S. Kondragunta, G. Stenchikov, K. L. Civerolo, B. G. Doddridge and B. N. Holben, 1997. The impact of aerosols on solar ultraviolet radiation and photochemical smog. *Science,* 278, 827-830.

Ebert, M., S. Weinbruch, P. Hoffmann and H. M. Ortner, 2004. The chemical composition and complex refractive index of rural and urban influenced aerosols determined by individual particle analysis. *Atmospheric Environment,* 38, 6531-6545.

Fuller, K. A., W. C. Malm and S. M. Kreidenweis, 1999. Effects of mixing on extinction by carbonaceous particles. *Journal of Geophysical Research,* 104, 15941-15954.

Ghaffari, A., H. F. Cook and H. C. Lee, 2001. Simulating winter wheat yields under temperate conditions: exploring different management scenarios. *European Journal of Agronomy,* 15, 231-240.

Godwin, D. C. and U. Singh, 1998, Nitrogen balance and crop response to nitrogen in upland and lowland cropping systems, *in* Understanding Options for Agricultural Production, Kluwer Academic Publishers, Dordrecht, Netherlands.

Goetz, S. J. and S. D. Prince, 1996. Remote sensing of net primary production in boreal forest stands. *Agricultural and Forest Meteorology,* 78, 149-179.

Gomes, L. and D. A. Gillette, 1993. Comparison of characteristics of aerosol from dust storms in Central Asia with soil-derived dust from other regions. *Atmospheric Environment, Part A: General Topics,* 27A, 2539-2544.

Gorbunov, B., A. Baklanov, N. Kakutkina, H. L. Windsor and R. Toumi, 2001. Ice nucleation on soot particles. *Journal of Aerosol Science,* 32, 199-215.

Gorbunov, B., R. Hamilton, N. Clegg and R. Toumi, 1998. Water nucleation on aerosol particles containing both organic and soluble inorganic substances. *Atmospheric Research,* 48, 271-283.

Gray , H. A., G. R. Cass, J. J. Huntzicker, E. K. Heyerdahl and J. A. Rau, 1986. Characteristics of atmospheric organic and elemental carbon particle concentrations in Los Angeles. *Environmental Science and Technology,* 20, 580-590.

Greenfield, S., 1957. Rain scavenging of radioactive particulate matter from the atmosphere. *Journal of Meteorology,* 14, 115-125.

Greenwald, R., M. H. Bergin, C. M. Carrico and D. Grant, 2005a. A new real-time technique to measure the size-distribution of water-insoluble aerosols. *Environmental Science & Technology,*

Greenwald, R., M. H. Bergin, J.-L. Jaffrezo, J.-L. Besombes and G. Aymoz, 2005b. Size-resolved, real-time measurement of water-insoluble aerosols in the Chamonix and Maurienne Valleys of alpine France. *Journal of Geophysical Research,*

Gu, L., J. D. Fuentes, H. H. Shugart, R. M. Staebler and T. A. Black, 1999. Responses of net ecosystem exchanges of carbon dioxide to changes in cloudiness: Results from two North American deciduous forests. *Journal of Geophysical Research,* 104, 31421-31434.

Hanel, G., 1976. The properties of atmospheric aerosol particles as functions of the relative humidity at thermodynamic equlibrium with the surrounding moist air. *Advances in Geophysics,* 19, 73-188.

Heng, L. K., W. E. Baethgen and P. Moutonnet, 2000. The collection of a minimum dataset and the application of DSSAT (Decision Support System for Agrotechnology Transfer) for optimizing wheat yield in irrigated cropping systems. Optimizing nitrogen fertiliser application to irrigated wheat 7-17.

Hess, W. M. and C. R. Herd, 1993, Microstructure, morphology and general physical characteristics, *in* Carbon Black: Science and Technology, 89-173, Marcel Dekker, New York.

Hobbs, P. V., 1993, Aerosol-Cloud Interactions, *in* Aerosol-Cloud-Climate Interactions, 33-75, Academic Press, San Diego.

Hobbs, P. V., H. Harrison and E. Robinson, 1974. Atmospheric effects of pollutants. *Science,* 183, 909-915.

Hoogenboom, G., J. W. Jones, P. W. Wilkens, W. D. Batchelor, W. T. Bowen, L. A. Hunt, N. B. Pickering, U. Singh, D. C. Godwin, B. Baer, K. J. Boote, J. T. Ritchie and J. W. White, 1994, Crop models, *in* Decision Support System for Agrotechnology Transfer, Version 3, University of Hawaii, Honolulu, Hawaii.

Hoogenboom, G., P. W. Wilkens and G. Y. Tsuji, 1999. Decision Support System for Agrotechnology Transfer (DSSAT), Version 3. 4, 286.

Hull, P., I. Shepherd and A. Hunt, 2004. Modeling light scattering from diesel soot particles. *Applied Optics,* 43, 3433-3441.

Hunt, L. A., J. W. White and G. Hoogenboom, 2001. Agronomic data: Advances in documentation and protocols for exchange and use. *Agricultural Systems,* 70, 477-492.

Husar, R., J. Husar and S. Falke, 1995. Fine particle maps derived from regional $PM_{2.5}$ and visibility data.

Jaenicke, R., 1972. The optical particle counter: Cross-sensitivity and coincidence. *Journal of Aerosol Science,* 3, 95-111.

Jaenicke, R., 1993, Tropospheric aerosols, *in* Aerosol-Cloud-Climate Interactions, 1-31, Academic Press, San Diego.

Jaenicke, R., 2005. Abundance of cellular material and proteins in the atmosphere. *Science,* 308, 73.

Jaffrezo, J. L., G. Aymoz and J. Cozic, 2005a. Size distribution of EC and OC in the aerosol of Alpine valleys during summer and winter. *Atmospheric Chemistry and Physics Discussions,*

Jaffrezo, J.-L., G. Aymoz, J. Cozic, D. Chapuis and W. Maenhaut, 2005b. Seasonal variation of PM_{10} main constituents in two valleys of the French Alps. I: EC / OC fractions. *Atmospheric Chemistry and Physics Discussions,*

Jaffrezo, J.-L., G. Aymoz, C. Delaval and J. Cozic, 2005. Seasonal variations of the water-soluble organic carbon mass fraction of aerosol in two valleys of the French Alps. *Atmospheric Chemistry and Physics Discussions,*

Janzen, J., 1980. Extinction of light by highly nonspherical strongly absorbing colloidal particles: spectrophotometric determination of volume distributions for carbon blacks. *Applied Optics,* 19, 2977-2985.

Jones, J. W., G. Hoogenboom, C. H. Porter, K. J. Boote, W. D. Batchelor, L. A. Hunt, P. W. Wilkens, U. Singh, A. J. Gijsman and J. T. Ritchie, 2003. The DSSAT cropping system model. *European Journal of Agronomy,* 18, 235-265.

Kasim, K. and M. D. Dennett, 1986. Radiation absorption and growth of *Vicia faba* under shade at two densities. *Journal of Applied Biology,* 109, 639-650.

Kirchstetter, T., T. Novakov and P. V. Hobbs, 2004. Evidence that the spectral dependence of light absorption by aerosols is affected by organic carbon. *Journal of Geophysical Research,* 109.

Laakonsen, A., P. Korhonen, M. Kulmala and R. J. Charlson, 1998. Modification of the Köhler equation to include soluble trace gases and slightly soluble substances. *Journal of the Atmospheric Sciences,* 55, 853-862.

Le Tertre, A., S. Medina, E. Samoli, B. Forsberg, P. Michelozzi, A. Boumghar, J. M. Vonk, A. Bellini, R. Atkinson, J. G. Ayres, J. Sunyer, J. Schwartz and K. Katsouyanni, 2002. Short-term effects of particulate air pollution on cardiovascular diseases in eight European cities. *Journal of Epidemiology and Community Health,* 56, 773-779.

Lide, D. R., 2004. Handbook of Chemistry and Physics, 85th edition. CRC Press.

Lindberg, J. D., 1975. The composition and optical absorption coefficient of atmospheric particulate matter. *Optical and Quantum Electronics,* 7, 131-139.

Lorente, J., A. Redaño and X. de Cabo, 1994. Influence of urban aerosol on spectral solar irradiance. *Journal of Applied Meteorology,* 33, 406-415.

MacRobert, J. F. and M. J. Savage, 1998, The use of a crop simulation model for planning wheat irrigation in Zimbabwe, *in* Understanding Options for Agricultural Production, Kluwer Academic Publishers, Dordrecht, Netherlands.

Madronich, S., 1993, UV radiation in the natural and perturbed atmosphere, *in* Environmental Effects of UV (Ultraviolet) Radiation, Lewis Publisher, Boca Raton, Florida.

Mall, R. K. and P. K. Aggarwal, 2002. Climate change and rice yields in diverse agro-environments of India. I. Evaluation of impact assessment models. *Climatic Change,* 52, 315-330.

Malm, W. C., J. F. Sisler, D. Huffman, R. A. Eldred and T. A. Cahill, 1994. Spatial and seasonal trends in particle concentration and optical extinction in the United States. *Journal of Geophysical Research,* 99, 1347-1370.

Marchand, N., 2003. Etude de la composante organique de l'aérosol atmosphérique: cas de deux vallées alpines (Chamonix et Maurienne), et développement analytique. Laboratoire de Chimie Moléculaire et Environnement 262.

Martin, J. H., 1990. Glacial-interglacial CO_2 change: the iron hypothesis. *Paleoceanography,* 5, 1-13.

McInnes, L. M., M. H. Bergin, J. A. Ogren and S. E. Schwartz, 1998. Apportionment of light scattering and hygroscopic growth to aerosol composition. *Geophysical Research Letters,* 25, 513-516.

Mearns, L. O., C. Rosenzweig and R. Goldberg, 1996. The effect of changes in daily and interannual climatic variability of CERES-Wheat: a sensitivity study. *Climatic Change,* 32, 257-292.

Medalia, A. I. and L. W. Richards, 1972. Tinting strength of carbon black. *Journal of Colloid and Interface Science,* 40, 233-252.

Medalia, A. I. and D. Rivin, 1982. Particulate carbon and other components of soot and carbon black. *Carbon,* 20, 481-492.

Medalia, A. I., D. Rivin and D. R. Sanders, 1983. A comparison of carbon black with soot. *Science of the Total Environment,* 31, 1-22.

Metzger, K. B., P. E. Tolbert, M. Klein, J. L. Peel, W. D. Flanders, K. Todd, J. A. Mulholland, P. B. Ryan and H. Frumkin, 2004. Ambient air pollution and cardiovascular emergency department visits. *Epidemiology,* 15, 46-56.

Mie, G., 1908. Beiträge zur optik trüber medien, speziell kolloidaler metallösungen. *Annalen der Physik,* 25, 377-445.

Milford, J. B. and C. I. Davidson, 1987. The sizes of particulate sulfate and nitrate in the atmosphere - A review. *Journal of Air Pollution Control Association,* 37, 125-134.

Nobel, P. S., 1999, Leaves and Fluxes, *in* Physicochemical & Environmental Plant Physiology, Academic Press, San Diego, California.

Novakov, T., T. S. Bates and P. K. Quinn, 2000. Shipboard measurements of concentrations and properties of carbonaceous aerosols during ACE-2. *Tellus,* 52B, 228-238.

Park, K., D. B. Kittelson and M. P. H., 2004. Structural properties of diesel exhaust particles measured by transmission electron microscopy (TEM): relationships to particle mass and mobility. *Aerosol Science and Technology,* 38, 881-889.

Peel, J. L., P. E. Tolbert, M. Klein, K. B. Metzger, W. D. Flanders, K. Todd, J. A. Mulholland, P. B. Ryan and H. Frumkin, 2005. Ambient air pollution and respiratory emergency department visits. *Epidemiology,* 16, 164-174.

Peters, A., D. W. Dockery, J. E. Muller and M. A. Mittleman, 2001. Increased particulate air pollution and the triggering of myocardial infarction. *Circulation,* 103, 2810-2815.

Pluchino, A. B., S. S. Goldberg, J. M. Dowling and C. M. Randall, 1980. Refractive-index measurements of single micron-sized carbon particles. *Applied Optics,* 19, 3370-3372.

Pósfai, M., J. R. Anderson, P. R. Buseck and H. Sievering, 1999. Soot and sulfate aerosol particles in the remote marine troposphere. *Journal of Geophysical Research,* 104, 21685-21693.

Quenzel, H., 1969. Influence of refractive index on the accuracy of size determination of aerosol particles with light-scattering aerosol counters. *Applied Optics,* 8, 165-170.

Ritchie, J. T., 1991, Wheat phasic development, *in* Modeling Plant and Soil Systems, American Society of Agronomy, Crop Science Society of Agronomy, Soil Science Society of Agronomy, Madison, Wisconsin.

Ritchie, J. T., 1998, Soil water balance and plant stress, *in* Understanding Options for Agricultural Production, Kluwer Academic Publishers, Dordrecht, Netherlands.

Ritchie, J. T., U. Singh, D. C. Godwin and W. T. Bowen, 1998, Cereal growth, development and yield, *in* Understanding Options forAgricultural Production, Kluwer Academic Publishers, Dordrecht, Netherlands.

Rochette, P., R. L. Desjardins, E. Pattey and R. Lessard, 1996. Instantaneous measurement of radiation and water use efficiencies of a maize crop. *Agronomy Journal,* 88, 627-635.

Roderick, M. L., G. D. Farquhar, S. L. Berry and I. R. Noble, 2001. On the direct effect of clouds and atmospheric particles on the productivity and structure of vegetation. *Oecologia,* 129, 21-30.

Rood, M. J., D. S. Covert and T. V. Larson, 1987. Hygroscopic properties of atmospheric aerosol in Riverside, California. *Tellus,* 39B, 383-397.

Rosen, H., A. D. A. Hansen, L. Gundel and T. Novakov, 1978. Identification of the graphitic carbon component of source and ambient particulates by Raman spectroscopy and an optical attenuation technique. *Carbonaceous Particles in the Atmosphere*, 49-55.

Saarikko, R. A., 2000. Applying a site-based crop model to estimate regional yields under current and changed climates. *Ecological Modelling,* 131, 191-206.

Saxena, P. and L. M. Hildemann, 1996. Water-soluble organics in atmospheric particles: A critical review of the literature and application of thermodynamics to identify candidate compounds. *Journal of Atmospheric Chemistry,* 24, 57-109.

Saxena, P., L. M. Hildemann, P. H. McMurry and J. H. Seinfeld, 1995. Organics alter hygroscopic behavior of atmospheric particles. *Journal of Geophysical Research,* 100, 18755-18770.

Schwartz, S. E., 1996. The whitehouse effect-shortwave radiative forcing of climate by anthropogenic aerosols: an overview. *Journal of Aerosol Science,* 3, 359-382.

Seinfeld, J. H. and S. N. Pandis, 1998. Atmospheric Chemistry and Physics. 1326.

Sheridan, P. J. and J. A. Ogren, 1999. Observations of the vertical and regional variability of aerosol optical properties over central and eastern North America. *Journal of Geophysical Research,* 104, 16793-16805.

Sinclair, T. R., T. Shiraiwa and G. L. Hammer, 1992. Variation in crop radiation use efficiency with increased diffuse radiation. *Crop Science,* 32, 1281-1284.

Sloane, C. S., J. Watson, J. Chow, L. Pritchett and L. W. Richards, 1991. Size-segregated fine particle measurements by chemical species and their impact on visibility impairment in Denver. *Atmospheric Environment,* 25A, 1013-1024.

Sokolik, I. N. and O. B. Toon, 1999. Incorporation of mineralogical composition into models of the radiative properties of mineral aerosol from UV to IR wavelengths. *Journal of Geophysical Research,* 104, 9423-9444.

Sosnowski, T. R., L. Gradon and A. Podgórski, 2000. Influence of insoluble aerosol deposits on the surface activity of the pulmonary surfactant: a possible mechanism of alveolar clearance retardation? *Aerosol Science and Technology,* 32, 52-60.

Steele, D. D., E. C. Stegman and R. E. Knighton, 2000. Irrigation management for corn in the northern Great Plains, USA. *Irrigation Science,* 19, 107-114.

Tsuji, G. Y., G. Hoogenboom and P. K. Thornton, 1998. Understanding Options for Agricultural Production. Systems Approaches for Sustainable Agricultural Development, th Kluwer Academic Publishers, Dordrecht, Netherlands.

Tubiello, F. N., C. Rosenzweig, B. A. Kimball, P. J. Pinter Jr., G. W. Wall, D. J. Hunsaker, R. L. LaMorte and R. L. Garcia, 2001. Testing CERES-wheat with free-air carbon dioxide enrichment (FACE) experiment data: CO_2 and water interactions. *Agronomy Journal,* 91, 247-255.

Turpin, B. J., P. Saxena and E. Andrews, 2000. Measuring and simulating particulate organics in the atmosphere: problems and prospects. *Atmospheric Environment,* 34, 2983-3013.

Twomey, S., 1974. Pollution and the planetary albedo. *Atmospheric Environment,* 8, 1251-1256.

Twomey, S., 1991. Aerosols, clouds, and radiation. *Atmospheric Environment,* 25A, 2435-2442.

Venkataraman, C. and S. K. Friedlander, 1994. Size Distributions of Polycyclic Aromatic Hydrocarbons and Elemental Carbon. 2. Ambient Measurements and Effects of Atmospheric Processes. *Environmental Science & Technology,* 28, 563-572.

Venkataraman, C., J. M. Lyons and S. K. Friedlander, 1994. Size Distributions of Polycyclic Aromatic Hydrocarbons and Elemental Carbon. 1. Sampling, Measurement Methods, and Source Characterization. *Environmental Science & Technology,* 28, 555-562.

Whitby, K. T. and R. A. Vomela, 1967. Response of single particle optical counters to nonideal particles. *Environmental Science and Technology,* 1, 801-814.

Wiscombe, W. J., 1980. Improved Mie scattering algorithms. *Applied Optics,* 19, 1505-1509.

Xu, J., M. H. Bergin, R. Greenwald and P. B. Russell, 2003. Direct aerosol radiative forcing in the Yangtze delta region of China: Observation and model estimation. *Journal of Geophysical Research,* 108, 4060.

Xu, J., M. H. Bergin, X. Yu, G. Liu, J. Zhao, C. M. Carrico and K. Baumann, 2002. Measurement of aerosol chemical, physical and radiative properties in the Yangtze delta region of China. *Atmospheric Environment,* 36, 161-173.

Yu, J. Z., H. Yang, H. Zhang and A. K. H. Lau, 2004. Size distributions of water-soluble organic carbon in ambient aerosols and its size-resolved thermal characteristics. *Atmospheric Environment,* 38, 1061-1071.

Zappoli, S., A. Andracchio, S. Fuzzi, M. C. Facchini, A. Gelencser, G. Kiss, Z. Zrivacsy, A. Molnar, E. Meszaros, H. C. Hannson, K. Rosman and Y. Zebuhr, 1999. Inorganic, organic and macromolecular components of fine aerosol in different areas of Europe in relation to their water solubility. *Atmospheric Environment,* 33, 2733-2743.